BIOMASS AND ECO-FRIENDLY ADDITIVES BLENDS FOR STEEL PROTECTION IN ACIDIC MEDIA: EXPERIMENTAL AND COMPUTATIONAL STUDY.

BY

EZIUKA, JOHNGODSWILL EBUBE (B. ENG, FUTO)
ACE-FUELS/20/M.Sc./11000107

A THESIS SUBMITTED TO

THE POSTGRADUATE SCHOOL,
FEDERAL UNIVERSITY OF TECHNOLOGY, OWERRI.

IN PARTIAL FULFILMENT OF THE REQUIREMENTS FOR THE AWARD OF MASTER OF SCIENCE (M.Sc.) DEGREE IN CORROSION TECHNOLOGY

AUGUST, 2023

CERTIFICATION

This is to certify that this research was carried out by me, JohnGodswill Ebube Eziuka, (Reg. No: ACE-FUELS/20/M.Sc./11000107) a Master's Degree Student of the Department of Corrosion Technology at the Africa Centre of Excellence in Future Energies and Electrochemical Systems (ACE-FUELS), Federal University of Technology, Owerri (FUTO).

.....Ifeafegiyi..... Date 10/08/2023
Dr. D. I. Njoku
(Supervisor)

..... Date 10/08/2023
Engr. Dr. S. C. Nwanonenyi
(Co-supervisor)

..... Date 10/08/2023
Dr. C. O. Akalezi
(Program Coordinator)

..... Date 14/9/23
Prof. E. E. Oguzie
(Centre Leader)

..... Date .....
Prof. B. O. Esonu
(Dean, Postgraduate School)

..... Date 10/August, 2023
Prof. P. C. Okafor
(External Examiner)

DEDICATION

This research work is dedicated to God almighty.

ACKNOWLEDGMENTS

I would like to acknowledge God almighty for good health and divine grace.

My instructors and supervisors (Dr. Demian I. Njoku, Engr. Dr. Simeon C. Nwanonenyi, Dr. Chidiebere Arinzechukwu, Dr. B. I. Onyeachu) deserve appreciation for their tireless efforts during this study endeavor.

I wish to express my gratitude to the center leader (Prof. Emeka E. Oguzie), staffs at ACE-FUELS and my course mates for their kind provisions and supports throughout the study and research period.

Last but not least, I would want to express my gratitude to my parents (Mr. Raphael Eziuka & Mrs. Juliet Eziuka), my God mother (Rev. Debisi Akinde), my mentors (Engr. Mike Iwegbu, Engr. Eric Oguama, and Pastor Ugochukwu Ezeagwula) for their unwavering efforts that made this research project feasible.

TABLE OF CONTENTS

TITLE PAGE i

CERTIFICATION ii

DEDICATION iii

ACKNOWLEDGMENTS iv

ABSTRACT v

TABLE OF CONTENTS vi

LIST OF TABLES ix

LIST OF FIGURES xi

APPENDIX xiii

CHAPTER ONE

INTRODUCTION 1

1.1 Background of study 1

1.1.1 Corrosion Overview 2

1.1.2 Classification of Inhibitors 3

1.1.3 Biomass-based Inhibitors 3

1.2 Problem Statement 4

1.3 Aim of Study 5

1.4 Justification of Study 5

1.5 Scope of Study 6

CHAPTER TWO

LITERATURE REVIEW 8

2.1 Acid Corrosion of Metals and Inorganic Inhibitors 8

2.2 Acid Corrosion of Metals and Organic Inhibitors 9

2.3 Acid Corrosion of Metals and Plant Extracts 12
2.4 Synergism in Corrosion Inhibition of Metals in Acid Environment 16
2.5 Recent Advances on Inhibitor Blends for Acid Metal Corrosion 18

CHAPTER THREE

MATERIALS AND METHOD S 20
3.1 Materials: 20
3.1.1 Materials Preparation 20
3.2 Computational Simulation 21
3.3 Experimental Section 23
3.3.1 Gravimetric Technique 23
3.3.2 UV-Visible Spectrophotometer Measurements 24
3.3.3 Gas Chromatography - Mass Spectrometry (GC/MS) Analysis 24
3.3.4 Fourier Transform Infrared (FTIR) Spectroscopy Analysis 25
3.3.5 Adsorption Isotherm and Thermodynamic Parameters 26
3.3.6 Synergistic Index 26

CHAPTER FOUR

RESULTS AND DISCUSSION 28
4.1 RESULTS 28
4.1.1 Gravimetric Analysis 28
4.1a Gravimetric Results for *Pterocarpus santalinoides* (PS) 28
4.1b Gravimetric Results for *Piper guineense* (PG) 43
4.1c Gravimetric Results for *Picrilima nitida* (PN) 48
4.1.2 UV-Visible Spectrophotometry 53
4.1.3 Gas Chromatography Mass Spectrometry Results of *Pterocarpus santalinoides* (PS) 64

4.1.4 Theoretical (Computational) Studies 66
4.1.5 Fourier Transform Infrared (FTIR) Spectroscopy Analysis 72
4.1.6 Adsorption Isotherm and Thermodynamic Parameters 81
4.1.7 Synergistic Index (SI) 83
DISCUSSION 83
4.2.1 Gravimetric Data 83
4.2.2 Gas Chromatography Mass Spectrometry Results of *Pterocarpus santalinoides* 86
4.2.3 UV-Visible Spectra Results 86
4.2.4 Theoretical (Computational) Studies 88
4.2.5 Fourier Transform Infrared (FTIR) Spectroscopy Analysis 93
4.2.6 Adsorption Isotherm and Thermodynamic Parameters 94
4.2.7 Synergistic Index (SI) 96

CHAPTER FIVE

CONCLUSION AND RECOMMENDATIONS 97
5.1 Conclusion 97
5.2 Recommendations 98
5.3 Research Gap 98
5.4 Contribution to Knowledge 99

REFERENCES 100
APPENDIX 109

LIST OF TABLES

Table 4.1 Weight loss and inhibition efficiency values for mild steel corrosion 0.5 M HCl in the absence and presence of leaves extract of PS at different immersion time and ± 28ºC. 29

Table 4.2 Weight loss and inhibition efficiency values for mild steel corrosion in 0.25M H_2SO_4 in the absence and presence of leaves extract of PS at different immersion time and ± 28ºC. 30

Table 4.3 Weight loss and inhibition efficiency values for mild steel corrosion in 0.25M H_2SO_4in the absence and presence of Potassium iodide (KI) at different immersion time and ± 28ºC. 31

Table 4.4 Weight loss and inhibition efficiency values for mild steel corrosion in 0.25M H_2SO_4in the absence and presence of Sodium alginate at different immersion time and ± 28ºC 32

Table 4.5 Weight loss and inhibition efficiency values for mild steel corrosion in 0.25M H_2SO_4 in the absence and presence of blend of leave extracts of PS and sodium alginate at different immersion time and ± 28ºC 33

Table 4.6 Weight loss and inhibition efficiency values for mild steel corrosion in 0.25M H_2SO_4in the absence and presence of blend of leave extracts of PS and KI at different immersion time and ± 28ºC 34

Table 4.7 Weight loss and inhibition efficiency values for mild steel corrosion in 0.25M H_2SO_4in the absence and presence of blend of leave extracts of PS, sodium alginate and KI at different immersion time and ± 28ºC 35

Table 4.8 Weight loss and inhibition efficiency values for mild steel corrosion in 0.5 M HCl in the absence and presence of leave extracts of PG at different immersion time and ± 28ºC 44

Table 4.9 Weight loss and inhibition efficiency values for mild steel corrosion in 0.25M H_2SO_4in the absence and presence of leave extracts of PG at different immersion time and ± 28ºC 45

Table 4.10 Weight loss and inhibition efficiency values for mild

steel corrosion in 0.5 M HCl in the absence and presence of leave extracts of PN at different immersion time and ± 28ºC 49
Table 4.11 Weight loss and inhibition efficiency values for mild steel corrosion in 0.25 M H_2SO_4in the absence and presence of leave extracts of PN at different immersion time and ± 28ºC 50
Table 4.12 UV-Visible spectra result of aged and freshly prepared extract of PS 53
Table 4.13 UV-Visible spectra result of aged and freshly prepared extract of PG 55
Table 4.14 UV-Visible spectra result of aged and new extract of PN 57
Table 4.15 UV-Visible spectra result of PS in 0.25 M H_2SO_4 59
Table 4.16 UV-Visible spectra result of PS in 0.5 M HCl 61
Table 4.17 UV-Visible spectra result of blend of PS, KI and sodium alginate in 0.25 M H_2SO_4 63
Table 4.18 Selected compounds from the identified compounds from GC-MS analysis 66
Table 4.19 Calculated quantum chemical properties values 72
Table 4.20 Calculated Langmuir isotherm properties values 82
Table 4.21 Calculated thermodynamic parameters of ΔG^o_{ads} 81
Table 4.22 Calculated SI values 83
Table 4.23 Summary of FTIR Peak Values (cm^{-1}) and Possible Groups 94

LIST OF FIGURES

Fig 4.1 Variation of inhibition efficiency of ethanol extract of PS with time for mild steel corrosion in 0.5 M HCl solution 36
Fig 4.2 Variation of inhibition efficiency of ethanol extract of PS with time for mild steel corrosion in 0.25 M H_2SO_4 solution 37
Fig 4.3 Variation of inhibition efficiency of KI with time for mild steel corrosion in 0.25 M H_2SO_4 solution 38
Fig 4.4 Variation of inhibition efficiency of sodium alginate with time for mild steel corrosion in 0.25 M H_2SO_4 solution 39
Fig 4.5 Variation of inhibition efficiency of blend of ethanol extracts of PS and sodium alginate with time for mild steel corrosion in 0.25 M H_2SO_4 solution 40
Fig 4.6 Variation of inhibition efficiency of blend of ethanol extracts of PS and KI with time for mild steel corrosion in 0.25 M H_2SO_4 solution. 41
Fig 4.7 Variation of inhibition efficiency of blend of ethanol extracts of PS, sodium alginate and KI with time for mild steel corrosion in 0.25 M H_2SO_4 solution. 42
Fig 4.8 Variation of inhibition efficiency of ethanol extract of PG with time for mild steel corrosion in 0.5 M HCl solution 46
Fig 4.9 Variation of inhibition efficiency of ethanol extract of PG seeds with time for mild steel corrosion in 0.25 M H_2SO_4 solution 47
Fig 4.10 Variation of inhibition efficiency of ethanol extract of PN with time for mild steel corrosion in 0.5 M HCl solution 51
Fig 4.11 Variation of inhibition efficiency of ethanol extract of PN with time for mild steel corrosion in 0.25 M H_2SO_4 solution 52
Fig 4.12 UV-visible spectra graphical analysis of new (black) and one month old (blue) *Pterocarpus santalinoides* (PS). 54
Fig 4.13 UV-visible spectra graphical analysis of new (red) and one month old (old) *Piper guineense* (PG) 56
Fig 4.14 UV-visible spectra graphical analysis of new (black) and one month old (purple) *Picrilima nitida* (PN) 58
Fig 4.15 Day-1 (black) and Day-5 (blue) UV-visible spectra graph showing the peaks of PS in 0.25 M H_2SO_4 60
Fig 4.16 Day-1 (upper green) and Day-5 (lower green) UV-visible spectra graph showing the peaks of PS in 0.5 M HCl 62
Fig 4.17 Day-1 (upper) and Day-5 (lower) UV-visible spectra graph showing the peaks of blend of PS, KI and sodium

alginate in 0.25 M H_2SO_4 64
Fig 4.18 GC-MS Chromatogram of PS leaf extract 65
Fig 4.19a Electronic properties of Benzeneacetaldehyde (BA) from PS extract. 67
Fig 4.19b Benzene acetaldehyde (BA) adsorbed on Fe crystal surface 67
Fig 4.20a Electronic properties of 2(5H)-Furanone (FUR) from PS extract. 68
Fig 4.20b 2(5H)-Furanone (FUR) adsorbed on Fe crystal surface 68
Fig 4.21a Electronic properties of Ethyl 9, 12, 15-octadecatrienoate (EOD) from PS extract. 69
Fig 4.21b Ethyl 9, 12, 15-octadecatrienoate adsorbed on Fe crystal surface 69
Fig 4.22a. Electronic properties of Linoleic acid ethyl ester (LAEE) from PS extract. 70
Fig 4.22b Linoleic acid ethyl ester adsorbed on Fe crystal surface 70
Fig 4.23a Electronic properties of Squalene (SQU) from PS extract. 71
Fig 4.23b Squalene adsorbed on Fe crystal surface 71
Fig 4.24a FTIR spectrum of ethanol extract of PS 73
Fig 4.24b FTIR spectrum of mild steel in 0.25 MH_2SO_4 containing 1000 mg/l of PS 74
Fig 4.24c FTIR spectrum of mild steel in 0.25 MH_2SO_4 containing 500 mg/l of PS, 500mg/l of sodium alginate and 0.025 M of KI 75
Fig 4.24d FTIR spectrum of mild steel in 0.25 MH_2SO_4 containing 1000 mg/l of PS and 0.025 M of KI 76
Fig 4.24e FTIR spectrum of mild steel in 0.25 MH_2SO_4 containing 500 mg/l of PS and 500mg/l of sodium alginate 77
Fig 4.24f FTIR spectrum of mild steel in 0.25 MH_2SO_4 containing 0.025 M of KI 78
Fig 4.24g FTIR spectrum of mild steel in 0.25 MH_2SO_4 containing 1000mg/l of sodium alginate 79
Fig 4.24h FTIR spectrum of KI 80
Fig 4.24i FTIR spectrum of sodium alginate 81
Fig 4.25 Langmuir adsorption isotherm for the adsorption of PS on the surface of the mild steel at room temperature 82

ABSTRACT

The blends of ethanol extract of *Pterocarpus santalinoides,* PS (Nturukpa leaves), *Piper guineense,* PG (Uziza seeds), *Picrilima nitida,* PN (Akuama leaves) and potassium iodide, KI and sodium alginate, SA respectively were investigated as green corrosion inhibitors for the protection of mild steel in 0.5 M HCl and 0.25 M H_2SO_4 using experimental and computational approach. Results of gravimetric technique revealed corrosion inhibition efficiency (IE) of 63 % and 43 % at 120 h for mild steel in the presence of 1000 mg/L of PS concentration in 0.5 M HCl and 0.25 M H_2SO_4 respectively, 81 % and 86 % at 120 h for mild steel in the presence of 1000 mg/L of PG concentration in 0.5 M HCl and 0.25 M H_2SO_4 respectively, 77 % and 64 % at 120 h for mild steel in the presence of 1000 mg/L of PN concentration in 0.5 M HCl and 0.25 M H_2SO_4 respectively. progressively the corrosion inhibitor formed by optimal combination of PS, KI, and SA exhibited IE of 97 % at 120 h at room temperature in 0.25 M H_2SO_4. In addition, characterization studies done on the extracts using GC-MS and UV-Vis equipment revealed the phytochemical constituent's presence in the extracts, some were selected for theoretical computations based on their abundance. Furthermore, the density functional theory (DFT) calculations revealed the chemical indicators responsible for the adsorption and inhibition process within the inhibitor molecules and the binding energy of interaction (that is, adsorption strength) between the inhibitive molecules and Fe crystal (1 1 0) surface. FTIR spectra analysis revealed the possibility of adsorption and interaction of active elements heteroatoms on the mild steel surface. The Langmuir adsorption isotherm was also obeyed. Conclusively, SI shows a cooperative synergistic effect as the SI values are above unity.

Keywords: Ethanol extract; blends; inhibitor; corrosion; density functional theory

CHAPTER ONE
INTRODUCTION

1.1 Background of study

Oil and gas operators have used acid treatment (acidizing) to improve well productivity for many years. Apart from pumping acid into a wellbore or geologic formation that is capable of producing oil and/or gas, acid washing is most commonly performed with hydrochloric acid (HCl) mixtures to clean out scale such as calcium carbonate, rust, and other debris restricting flow in the well (Khadom & Farhan, 2018). Also, it is important to note that during pickling of the well tubing highly concentrated acids are used and this makes the environment corrosive to mild steels and other materials within the system (Njoku *et al*., 2021; Kausalya & Hazlina, 2020). Steel is widely used in many industries especially the oil and gas industry due to its excellent performance but it undergoes deterioration during its interaction with service environment involving mineral acids such as hydrochloric acid and sulphuric acid. The resultant effects of corrosion in the oil and gas sector are enormous including; economic loss due to replacement and maintenance of damaged structures over time, environmental pollution, reduction in the life span of equipment, etc. One of the methods to mitigate corrosion of steel in acidic environment is through the use of corrosion inhibitors (Sitz *et al*., 2012; Fouda *et al*., 2017). A good inhibitor is generally effective in small concentrations, stable, cheap and can extend the working life of industrial metallic surfaces (Khadom & Farhan, 2018). Many corrosion inhibiting formulations have been proposed to control corrosion in oil environment in recent time. However, the minimal protection efficacy, durability, stability, cost and toxicity shortcomings warrant the continuous search/demand for better formulations with better anticorrosion efficacy that are both cheap and less-toxic (Kausalya & Hazlina, 2020; Finšgar & Merl, 2014; Kokalj *et al*., 2011 and Finšgar

& Jackson, 2014). The use of environmental chemicals with low environmental impacts to control the deleterious effect of corrosion in industries aligns with the objectives/mandates world health organization (WHO). In other words, due to the toxicity of some corrosion inhibitors, there has been increasing search for green corrosion inhibitors (Znini *et al*., 2012). Furthermore, Several common sources of green inhibitors include plant extracts (Abdallah, 2018), pharmaceutical drugs (Abdallah, 2002), ionic liquids (Kobzar *et al*., 2021), and synthetic inhibitors (Khan *et al*., 2022; Wei *et al*., 2020). It is very important to note that the increased environmental consciousness and strict legislation over the past years led to the rise of the trend to use alternate green approaches characterized by minimum environmental burden (Wei *et al*., 2020). The prevention of metals used in industrial applications from corrosion is vital and must be properly given attention (Yadav *et al*., 2016; Finšgar & Jackson, 2014).

The most prevalent phytochemical elements in the extract were screened for their electronic characteristics and individual corrosion inhibition properties using computational modeling (molecular dynamics simulation and density functional theory) (Njoku *et al*., 2021).

1.1.1 Corrosion Overview

Corrosion is the destructive attack on the surface of material by reaction with its environment containing corrosives (Njoku *et al*., 2021; Oguzie *et al*., 2012). Thus, corrosive substance is any chemical that has the potential to dissolve or degrade the structure of member of a substrate in contact with it. They can be acids, oxidizers, or bases. Some factors such as water, oxygen, temperature etc. assist corrosive substances in executing their destruction actions. The formation of an oxide of iron due to the oxidation of iron atoms in solid solution is a well-known example of electrochemical corrosion commonly known as rust (Dillmann *et al*., 2004).

$$4Fe + 3O_2 + 2H_2O \rightarrow 4FeO.OH \quad (1.1)$$

1.1.2 Classification of Inhibitors

Inhibitors are materials (organic or inorganic) that are capable of reducing the corrosive effect of corrosion agents in a system (Njoku *et al*., 2021; Oguzie *et al*., 2012). It is important to note that organic inhibition mechanisms could differ for inhibitors with the same functional group due to molecular structure, electron density in the functional group, and size of the hydrocarbon chain (Camila, 2016). In addition, there are two major classes namely; inorganic (anodic and cathodic) and organic inhibitor.

(a) Inorganic corrosion inhibitors (passivators/anodic):

These are a type of inhibitors that cause large anodic shift of the corrosion potential, and force metal surface into the passivation range.

(b) Organic Inhibitors:

These are known as the film forming class of inhibitor. Typical examples of this class include; amines, amine salt, imidazolines (e.g., sodium benzoate mercaptans, esters, amines etc.)

1.1.3 Biomass-based Inhibitors

Acid and alkaline solutions are frequently employed in a variety of industrial applications to remove scales, oxides, and other contaminants from steel surfaces (Asadi *et al*., 2019). Hence, the use of corrosion inhibitors from biomass sources is essential because of their immense contributions in the reduction of toxic substances or materials that are discharged into our environments from chemical related industries (Verma *et al*., 2018; Popoola, 2019). Numerous studies have proved the value and effectiveness of plant extract, their role in the industry cannot be overestimated (Njoku *et al*., 2021; Oguzie *et al*., 2012). While some scientists

believe that medicines can function as a green corrosion inhibitors (Abdallah, 2002) others believe that plant extracts can effectively work as a good corrosion inhibitor (Matad *et al*., 2014; Wang *et al*., 2020; Hassannejad & Nouri, 2018; Alibakhshi *et al*., 2018 & Haldhar *et al*., 2019).

Biomass-based corrosion inhibitors are recently widely accepted because it is eco-friendly in nature (Abdallah *et al*., 2018). Another benefit of plant extract over other inhibitors (inorganic) is that it is widely available and renewable (Haldhar *et al*., 2018; Srivastava *et al*., 2017). They stand out and are preferred over other types of inhibitors because they contain an abundance of chemical components such flavonoids, polyphenols, and polysaccharides. Functional groups such as amide group (NH_2), carbonyl group (C=O), aldehydes group (CHO) and others are some of those sought after in plants. These functional groups enable a plant extract to function more effectively as a mild steel corrosion inhibitor (Saxena *et al*., 2018a; Saxena *et al*., 2018b).

1.2 Statement of Problems

The problems that necessitated the course of this research are outlined and discussed below;

i. Toxic nature of effective synthetic inhibitors:

Some synthetic inhibitors (especially the inorganic inhibitors) are toxic to the environment; this reason calls for research study to develop environmentally friendly organic-based corrosion inhibitors.

ii. Non availability and formulation details of corrosion inhibitors:

Non availability of corrosion inhibitors materials may directly result into high cost of corrosion inhibitors developed, also poor formulation of corrosion inhibitors may result to poor inhibitor's performance, hence, the need to develop cheaper with

readily available organic-based corrosion inhibitors materials with excellent formulation.

iii. Poor inhibitive performance of organic inhibitors on prolong exposure in harsh environment:

Review studies has shown that there is gradual drop in performance of some organic inhibitors after few hours of exposure to harsh environment; this reason also calls for research study to develop corrosion inhibitors with the capacity to protect mild steel from corrosion for days.

1.3 Aim of Study

The aim of the research is to investigate the *Pterocarpus santalinoides, Piper guineense* (Uziza seeds) and *Picrilima nitida* leaves and eco-friendly additives blends for steel protection in acidic media using gravitational and computational study.

Other specific objectives of study include the followings;

1. Characterization of the plant extracts using UV-vis and GC-MS
2. Gravimetric investigation of corrosion inhibition effects of the prepared extracts and eco-friendly additives.
3. Determination of corrosion parameters (weight loss, corrosion rate, inhibition efficiency and degree of surface coverage).
4. Computational investigation on the selected molecular inhibitor species on the extracts.
5. Analysis and discussion of experimental and theoretical results.

1.4 Justification of Study

Acids are used for several industrial processes such as in acid cleaning, pickling, and descaling and mostly in oil-well acidizing (Khadom & Farhan, 2018). These

processes aggravate the corrosion of steel structures and platforms leading to unexpected material failures, constant maintenance and replacements - which are costly gestures (Njoku *et al*., 2021). But, the motivation for the continued use of acid treatment processes lies on the development of corrosion inhibitors which ranged from in-organic-based and organic based (Kausalya & Hazlina, 2020). One of the most effective inorganic inhibitors are the chromate-based inhibitors, it is recently not very acceptable as its use is restricted by environmental and health regulations. For this reason, organic based inhibitors are the close alternative to the toxic inorganic chromate based for combating the corrosion menace (Njoku *et al*., 2021). Unfortunately, the low inhibition performance of most of these organic compound inhibitors in strong acidic conditions coupled with the cost and toxic nature of some synthetic species raise the calls by industrialists for the improvement of organic based acid (plants/leaves extract) corrosion inhibiting agents (Oguzie *et al*., 2012). One of the approaches being considered to unravel the shortcomings of cost, toxicity and efficiency is the blending (synergism) of non-toxic compounds, and/or naturally derived compounds. Thus, blending natural materials with some biopolymers (sodium alginate) and naturally derived inorganic salt (KI) is anticipated to improve efficiency and reduce cost and environmental/health concerns. Such products will benefit the inhibition of structures in acidic environments.

1.5 Scope of Study

The work done in the study is limited to the followings;

1. Sourcing and identification of plants and procuring of the reagents.
2. Preparation of plant extract and characterization
3. Preparation of metal coupons, corrodent and inhibited systems

4. Performing gravimetric measurement and determination of the corrosion parameters
5. Performing theoretical computational within the framework of density functional theory (DFT) using Material Studio software.
6. Analysis and discussion of the experimental and theoretical results.

CHAPTER TWO
LITERATURE REVIEW

2.1 Acid Corrosion of Metals and Inorganic Inhibitors

Corrosion inhibitor is an effective means to protect metal surfaces against corrosion menace (Raja *et al*., 2016). Many researchers have reported overtimes that the corrosion inhibitive potential of inorganic inhibitors in safe guarding metal surface exposed to harsh service environments are noticeably effective (Abuthahir *et al*., 2013; Ferraa *et al*., 2021; Moussa *et al*., 2018). Additionally, these researchers frequently provide justification for their intense efforts to create novel synthetic inorganic compounds that act as inhibitors. Thus, the risk of organic compounds degrading with time and temperature is the basis for the use of inorganic inhibitors as an alternative to organic chemicals. Hence, the need to look into the viability of using new inorganic chemicals (such as phosphites, chromates etc.) as inhibitors in corrosive solutions (Deyab *et al*., 2016).

Benabdellah *et al*. (2011) investigated the inhibitive efficiency of Triphenyltin2–thiophene carboxylate (TTC) on steel sample (with the following percentages 0.09% P, 0.38% Si, 0.01% Al, 0.05% Mn, 0.21% C, 0.05% S and the remainder being iron) in 1 M HCl acid solution. The techniques used are; polarization, weight loss, EIS and adsorption isotherm Hence, the percentage inhibition efficiency was found to increase with increasing concentration of inhibitor to reach 97% at 0.001 M.

Hemlata *et al*. (2013) investigated and evaluated (2-hydroxyethyl) triphenyl phosphonium bromide as corrosion inhibitor for mild steel in sulphuric acid. The team investigated the inhibition performance using electrochemical techniques like potentiodynamic polarization (PDP), potentiostatic polarization (PSP) and electrochemical impedance spectroscopy studies (EIS). PDP analytical study reveal that HETPB is an anodic type inhibitor with 98% efficiency at the concentration

range of (1× 10-2 to 4× 10-3) M for mild steel in 0.5 M sulfuric acid. PSP analytical study reveal that HETPB perform as passivating type of inhibitor at lower concentrations, hence, it acts as non-passivating type of inhibitor at higher concentrations.

AlBeladi *et al*. (2022) investigated Benzalkonium chloride/titanium dioxide as an effective corrosion inhibitor for steel in a sulfuric acid solution. The team investigated the inhibition performance using gravimetric measurements, cyclic and linear PDP, EIS, and hydrogen collection by water displacement evaluated inhibition performance. Finally, electronic properties were calculated using DFT method. Electrochemical analysis show that inhibitors enhanced corrosion protection with over 80% inhibition efficiency. Also, weight loss and hydrogen collection measurements revealed excellent inhibition performance. Finally, potentiodynamic polarization curves revealed that inhibitors exhibited dual behavior, but cathodic protection was more predominant.

Researchers have highlighted on the negative effects of most inorganic corrosion based inhibitors on the environment and human health and hence, suggested remedial replacement with eco-friendly materials (Saei *et al*., 2017; Njoku *et al*., 2021). Furthermore, Serdaroglu *et al*. (2021) extensively studied the toxicity of some inorganic materials used as corrosion inhibitors for metal protection. Hence, they pointed out that most inorganic inhibitors have toxic nature or characteristics and possess some negative effects on the environments. In addition, they suggested their total withdrawal as corrosion inhibitors despite their effectiveness due to ever increasing ecological awareness and strict environmental regulations.

2.2 Acid Corrosion of Metals and Organic Inhibitors

There has been many reports on the use of inhibitors from organic sources to retard the dissolution metallic surfaces in acidic medium. For instance,

Kamali *et al*. (2020) studied imidazolium-derived polymeric ionic liquid (PIL) as a green inhibitor for corrosion inhibition of mild steel in 1.0 M HCl using electrochemical impedance spectroscopy (EIS), scanning electron microscopy (SEM) measurements, and quantum chemical calculation. The results obtained revealed that corrosion inhibition efficiency of PIL exceeded 96% based on Tafel plot (Kamali *et al*., 2020).

Gao *et al*. (2008) concluded a study on preparing and corrosion inhibition behavior of quaternized polyethyleneimine for low carbon steel in sulfuric acid. The investigations were carried out using weight loss method, electrochemical technique (potentiodynamic polarization curves) and scanning electron microscopy (SEM). It was concluded that the inhibition efficiency of A3 steel can reach to 92% in 0.5 M H_2SO_4 solution for 72 h of immersing time.

Obot *et al*. (2017) investigated the potential of sodium alginate as a promising biopolymer for corrosion protection of API X60 (a high strength carbon steel) in saline medium. This study was carried out using gravimetric and electrochemical techniques (OCP, EIS and EFM). The inhibition efficiency of the SA increased with concentration (IE: 87.23%) but was lower at higher temperature (70 ^{o}C).

Li *et al*. (2017) investigated the influence of sodium alginate inhibitor addition on the corrosion protection performance of magnesium alloy (AZ91D) in NaCl solution using electrochemical tests, weight loss measurements, PDP, and SEM. It was recorded that inhibition efficiency increase with SA concentration, and then decreases. Note, taking the concentrations of sodium alginate, sodium silicate and sodium tungstate to be 0.03 mol/L, 0.015 mol/L, 0.02 mol/L, respectively, the inhibition efficiency of the inhibitor reached highest, that is 98%.

Dang *et al*. (2015) investigated the inhibition effect of sodium alginate on magnesium alloy in sodium chloride solution using weight loss test, PDP, EIS and FT-IR. It was recorded that with sodium alginate concentration increase, the

inhibition efficiency initially increased with time but later decreased. A maximum of 90.00% IE was recorded at 500 ppm concentration of sodium alginate concentration.

Ahanotu *et al*. (2020) investigated *Pterocarpus santalinoides* leaves extract as a sustainable and potent inhibitor for low carbon steel in a simulated pickling medium using electrochemical approaches at 25 ^{o}C and 60 ^{o}C. With 0.7 g/L PSLE, inhibition efficiency of >90% has been obtained at 60 ^{o}C. Based on calculated values of adsorption parameters, *Pterocarpus santalinoides* was confirmed as a potential inhibitor.

Ayoola *et al*. (2018) investigated data on inhibitive performance of chloramphenicol drug on A315 mild steel in acidic medium using weight loss method, open circuit potential (OCP) and linear polarization method. The team confirmed that chloramphenicol drug is an efficient corrosion inhibitor for Mild Steel in hydrochloric acid medium, also they showed that an inhibitor with high degree of surface coverage could be attributed to reason for high inhibition efficiency.

Keerthana and Ashraf, (2020) investigated carbon nanodots synthesized from chitosan and its application as a corrosion inhibitor in boat-building carbon steel BIS2062 using AFM, TEM, FTIR and UV-Vis. The UV-Vis spectroscopic analysis showed absorption peaks proving that unsaturated groups and heteroatoms are present. Also, Galvão *et al*., (2016) used computational UV-Vis spectroscopic study to investigate the chemical speciation of 2-mercaptobenzothiazole corrosion inhibitor in aqueous solution.

Matad *et al*. (2014) investigated ketosulfone drug as a green corrosion inhibitor for mild steel in acidic medium. The study showed that adsorption of the inhibitor on the mild steel surface in acid media obeyed Langmuir adsorption isotherm and calculated ΔG^{o}_{ads} value was negative which suggested a strong and stable interaction of the adsorbent layers on the surface of the steel.

Rouifi *et al*. (2019) investigated the performance of new soluble triazole as corrosion inhibitor for carbon steel in HCl, computational analysis was carried out to augment the study. The reactivity of the compound in view was quantum chemically analyzed by the DFT method to clarify the effectiveness of the soluble inhibitor, hence quantum chemical methods was used to elucidate the electronic structures also confirming that smaller energy gaps correspond to better stability.

2.3 Acid Corrosion of Metals and Plant Extracts

The extracts from many plants have created their own niche as reported by by many researchers in the corrosion studies due to the inhibitive performance in metal protection. For example, Ahanotu *et al*. (2020) investigated *Pterocarpus santalinoides* leaves extract as a sustainable and potent inhibitor for low carbon steel in a simulated pickling medium using UV-vis analysis, PDP test, SEM, EDAX, and AFM. The results showed that inhibition efficiency obtained was greater than 90% at 60 ^{o}C.

Ofoma *et al*. (2018) investigated the deterioration and inhibition of mild steel inhibition in 1.0 M and 5.0 M tetraoxosulphate (VI) acid respectively using leaf extract of *Pterocarpus santaliniodes* using weight loss and gasometric method respectively. Results of weight loss and gasometric measurement showed inhibition efficiency 88.70% and is 96% respectively in 1.0 M H_2SO_4, and an inhibition efficiency 71.76% and 79.66% respectively in 5.0 M H_2SO_4. It is clear indication that the gasometric method gave the optimum protection and confirmed that the extract is a good corrosion inhibitor for mild steel corrosion in the H_2SO_4 solutions. Oguzie *et al*. (2012) investigated the mechanism of corrosion inhibition of mild steel in HCl and H_2SO_4 acid solution respectively by acid extracts of *Piper guineense.* This study was carried out using gravimetric, potentiodynamic polarization and electrochemical impedance spectroscopy techniques as well as scanning electron

microscopy (SEM) and Fourier transform infrared spectroscopy (FTIR). The experimental result revealed that PG extract in HCl and H_2SO_4 recorded inhibition efficiency of above 88% and 91% in HCl and H_2SO_4 for EIS and PDP measurement respectively.

Oguzie *et al*. (2011) studied the corrosion and microbial (SRB) growth inhibiting effects of *Piper guineense* extract, this study was done using gravimetric, electrochemical techniques and computational studies. Gravimetric analysis recorded >90% IE, electrochemical studies revealed that the extract maintained reasonable inhibition efficiency with time, and the computational studies confirmed the inherent affinity towards adsorption on mild steel surface.

Njoku *et al*. (2021) investigated the corrosion protection of Q235 steel in acidic-chloride media using seed extracts of *Piper guineense* using gravimetric, EIS, electrochemical measurements, surface imaging (AFM, SEM) and characterization (XPS) technique. The extract recorded > 98% IE for prolonged time intervals of about 144 h. Furthermore, the adsorption strengths of some major phytoconstituents of the extract on steel were analysed using molecular dynamics simulations in the context of the density functional theory (DFT).

Nwosu *et al*. (2014) investigated the acidic corrosion inhibition of *Piper guineense* seed extract on Al alloy using gravimetric technique. The investigation recorded inhibition efficiency of about 95.34%.

Ezeugo and Onukwuli, (2017) investigated the optimization of corrosion inhibition of *Picralima nitida* leaves extract as green corrosion inhibitor for zinc in 1.0 M HCl using gravimetric, thermometric test and Fourier transform infrared (FTIR) analysis. Gravimetric method investigation recorded inhibition efficiency of about 86% while thermometric test investigation recorded inhibition efficiency of about 84%.

Ezeugo and Omotioma, (2018) investigated the adsorption kinetics of *Picrilima nitida* seed extract as a green corrosion inhibitor for zinc in 0.5 m H_2SO_4 using

gravimetric method and adsorption kinetic studies. Gravimetric method investigation recorded inhibition efficiency of about 84%.

Onukwuli *et al*. (2018) studied the potential of plant extract (*Picralima nitida*) as biodegradable inhibitor for zinc in dilute solution of sulfuric acid using gravimetric, thermometric test and Fourier transform infrared (FTIR) analysis. Increase in concentration resulted in inhibition efficiency (IE) increase. Gravimetric method investigation recorded inhibition efficiency of about 81.7%.

Rosli *et al*. (2019) investigated *Musa sapientum* (banana) peels as green corrosion inhibitor for mild steel using weight loss method and gas chromatography mass spectrometry (GC/MS) was used to characterize the peel extract, hence they detected the presence of bioactive compounds which are responsible for the corrosion inhibition and adsorption properties on mild steel surface. It was shown using the FTIR analysis that the presence of functional groups of alcohols, alkanes, carbonyls, aromatics, ethers, and esters that are responsible for corrosion by adsorption on steel surface.

Vasyliev and Vorobiova, (2019) investigated rape grist extract (*Brassica napus*) as a green corrosion inhibitor for water systems using weight loss and polarization techniques. GC-MS and FTIR techniques were used to analyze the composition of extract.

Karpagasundari and Kulothungan, (2014) investigated and analysed bioactive compounds in *Physalis minima* leaves using GC/MS, HPLC, UV-VIS and FTIR techniques, gas chromatography mass spectrometry (GC/MS) was used to investigated the chemical compositions of the extract of *Physalis minima* leaves and UV-Vis profile showed peaks proving the existence of chromophoric unit responsible for adsorption, hence, the appearance of one or more peaks in the graph in the UV-vis spectrum is a blatant sign that unsaturated groups and heteroatoms like S, N, and O are present.

Obi-Egbedi *et al*. (2012) investigated *Spondias mombin* as a green corrosion inhibitor for aluminium in sulphuric acid, correlation between inhibitive effect and electronic properties of extracts major constituents using density functional theory was also focused on. The study showed that organic compounds that offer electrons to empty orbitals of the metals and not only take free electrons from the metals make excellent corrosion inhibitors.

Mohammed *et al*. (2020) evaluated the corrosion inhibition efficacy of *Cola acuminata* extract for low carbon steel in simulated acid pickling environment. FTIR was used to examine the surface of the corroded carbon steel, FTIR revealed that the compound in view interacted with the carbon steel surface through the O and N heteroatoms of its phytoconstituents and also proved adsorption on the steel surface as reason for the corrosion inhibition.

Anbarasi and Vasudha, (2014) investigated corrosion inhibition potential of *Cucurbita maxima* plant extract on mild steel in acid media. The nature of the steel surface was analyzed using FTIR, hence FTIR analysis suggested the possibility of interaction of inhibitor constituents with the mild steel surface of study, finally adsorption mechanism was confirmed.

Golchinvafa *et al*. (2020) investigated the effect of natural inhibitor concentration of *Fumaria officinalis* and temperature on corrosion protection mechanism in API X80 pipeline steel in 1 M H_2SO_4 solution. ΔG^o_{ads} was calculated and it was shown that *Fumaria officinalis* caused the reduction of anodic and cathodic reactions through its physical-chemical adsorption, hence, mitigating corrosion of steel. It was revealed that a negative value will result in spontaneous adsorption of the *Fumaria officinalis* on the surface of the mild steel of study.

Finally, research findings revealed that plants are able to act as corrosion inhibitors for various metals in aggressive service environment due to presence of hetero atoms (such as N, S, and O), double bonds, π-bonds, etc. in the chemical structures

(Abuthahir *et al*., 2013). Thus, these functional groups form insoluble deposits on metal surface that act as blanket which reduces that rate at which corrosive ions access or penetrate the metal surface

2.4 Synergism in Corrosion Inhibition of Metals in Acid Environment

Many researchers have reported the impact of synergistic effects of inhibitors in retarding the dissolution of metal substrates in many harsh service environments. Typical examples are stated below;

Musa *et al*. (2011) investigated the synergistic effect of potassium iodide with phthalazone on the corrosion inhibition of mild steel in 1.0 M HCl. The study was carried out using electrochemical impedance spectroscopy (EIS) and potentiodynamic polarization measurements. The results showed inhibition efficiency of phthalazone increases with increase in concentration and increased further with the presence of 6.02 mM KI. PDP recorded 90% efficiency; EIS also recorded 87% efficiency.

Mohamad *et al*. (2014) investigated the synergistic effect of KI and coumarin derivative on the corrosion inhibition of aluminum alloy in 1.0 M H_2SO_4 acid solution using electrochemical measurements and density functional theory calculations. It was recorded that the inhibition efficiency increases with increasing inhibitor concentration and increases further in the presence of 6.02 mM KI but decreases significantly at higher temperature. PDP results recorded 87% efficiency whereas EIS recorded 83.3% efficiency.

Farag and Hegazy, (2013) investigated the synergistic inhibition effect of potassium iodide and novel Schiff bases on X65 steel corrosion in 0.5 M H_2SO_4 acid solution using potentiodynamic polarization, electrochemical impedance spectroscopy (EIS) techniques and scanning electron microscopy (SEM). It was recorded that the inhibition efficiency increases with the concentration of the Schiff bases and

increased further with the presence of KI. PDP and EIS recorded inhibition efficiency of 99.4% and 97.9% respectively.

Atmani *et al*. (2013) investigated synergistic corrosion inhibition effect between calcium lignosulfonate (CLS) and three kinds of inorganic inhibitors (Na_2MoO_4, Na_2SnO_3, and $NaWO_4$). They pointed out that inorganic compounds are usually not used alone recently due to their negative environmental impact rather they are blended in small amount or in synergy with other non-toxic compounds to improve corrosion inhibition efficiency of the new product.

Zhang *et al*. (2021) investigated the inhibition of mild steel corrosion in 1 M HCl by chondroit in sulfate and its synergistic effect with sodium alginate (a biopolymer). The study was carried out using weight loss test, electrochemical investigations, SEM, SECM and UV methods. The recorded results indicate that the mixtures of chondroitin sulfate and sodium alginate strongly inhibit the corrosion of mild steel compared to the inhibitors individually that is 95.18 % versus 72.78 %), hence, a proven synergistic inhibition effect.

Jeyaprabha *et al*. (2005) investigated synergistic influence of poly(aminoquinone) on corrosion inhibition of iron in acid media. The studies were carried out using potentiodynamic polarization and electrochemical impedance spectroscopy measurements. It was recorded that the inhibition efficiency of 80-90% was obtained.

Moses *et al*. (2021) studied synergistic corrosion inhibition of low carbon steel in 1.0 M HCl and H_2SO_4 media by 5-methyl-3-phenylisoxazole-4-carboxylic acid alone and with iodide ions combined. This was studied using weight loss, potentiodynamic polarization (PDP), electrochemical impedance spectroscopy (EIS), linear polarization resistance (LPR), ultraviolet–visible (UV–vis), spectrophotometer and surface observation methods. Inhibition efficiency of about

86 and 89% was observed at 25°C and inhibition efficiency of about 88 and 91% was observed at 60°C.

2.5 Recent Advances on Inhibitor Blends for Acid Metal Corrosion

Blending technique is a veritable tool for combining different (organic/organic, organic/inorganic or organic/inorganic) materials together through adjusting of quantity (amount) of material, pH levels, viscosity and homogenization to obtained multi-component material. Recently, some research works has been carried out to prove the potential of blending of materials to enhance corrosion inhibition in acidic environment. For instance;

Ituen *et al*. (2019) in the search for eco-friendly, inexpensive and efficient corrosion inhibitors used glutathione (GLT) and its blends for corrosion inhibition of X80 steel in simulated acid wash solution. Electrochemical and weight loss techniques were used to monitor corrosion process in-situ, while spectroscopic and microscopic methods were used to characterize corrosion products and surfaces. Experimental and theoretical findings realized from this study support in good agreement that glutathione and its blends effectively inhibit steel corrosion in simulated acid wash solution at 303 - 363 K.

The efficiency of tannin and calcium gluconate blends as corrosion inhibitors for carbon steel in near neutral water media was studied by (Kapor, 2002). In the experiment, the solutions of blends of tannin and calcium gluconate were prepared in a tap water and distilled water respectively and the synergistic behavior of two components or blends of different concentrations was investigated. The electrochemical potentiodynamic polarization study revealed the synergistic inhibition behavior of the blends.

Umoren *et al*. (2014) investigated effect of polyvinylpyrrolidone – polyethylene glycol blends on the corrosion inhibition of aluminium in HCl solution. The

inhibitive effect of the homopolymers and polymer blend was assessed using weight loss and hydrogen evolution methods at 30 °C and 60°C respectively. Results obtained show that inhibition efficiency increases with increase in concentration of the polymers but decreases with increase in temperature. The inhibition efficiency of the homopolymers and their blends decreased with rise in temperature. Inhibition efficiency was found to be synergistically enhanced on blending the two homopolymers with highest inhibition efficiency obtained for (PEG: PVP) blending ratio of 1:3

Qian and Cheng, (2019) investigated the inhibition performance of imidazoline (IM) and sodium dodecylbenzenesulphonate (SDBS) inhibitors on corrosion of X52 carbon steel in CO_2-saturated chloride solutions at 60 °C using surface characterization, weight-loss testing and electrochemical measurements. A synergism of the two inhibitors exists to enhance the corrosion inhibition performance compared to the inhibitors acting independently. The adsorption of both inhibitors on the steel is chemisorption, following the Temkin adsorption isotherm.

The inhibition of a quinolinium quaternary ammonium salt and a Gemini surfactant, 1,3-bis(dode-cyldimethylammonium chloride)-2-propanol, for mild steel in H_2S and CO_2 saturated brine solution was investigated by Zhao *et al*., (2015) using polarization test, EIS and XPS. Potentiodynamic polarization experiments shows that both the anodic and cathodic reactions are inhibited.

CHAPTER THREE

MATERIALS AND METHODS

3.1 Materials Preparation

(a) Metal coupon preparation

Mild steel (MS) specimen with composition of 0.179 % C, 0.165 % Si, 0.439 % Mn, 0.203 % Cu, 0.034 % S and Fe balance was obtained from the Metallurgical and Materials Engineering Department, Federal University of Technology, Owerri. Each sheet which was 0.1cm in thickness was mechanically pressed-cut into coupons of dimensions 3cm x 3cm and abraded with 800 and 1200 grades of emery papers. The samples were then washed thoroughly with distilled water degreased in absolute ethanol then dried in acetone and warm air.

(b) Preparation of extract from plants

The seeds of *Piper guineense*, leaves of *Pterocarpus santalinoides*, and leaves of *Picrilima nitida* were obtained locally and identified at the Department of Crop Science Technology, School of Agriculture and Agricultural Technology, Federal University of Technology Owerri. These materials were washed, dried to constant weight and ground into fine powder using an electric blender. The powdered material (15 g) was soaked in round bottom flask containing 300 ml of ethanol, thoroughly mixed by shaking and allowed to stand for 72 h. The resulting mixture was filtered; filtrate (extract) obtained was measured and stored in an air tight container at room temperature. In addition, the residue obtained was dried to constant weight and used to determine the amount of material dissolved in ethanol and estimate the concentration of the stock solution.

3.2 Computational Simulation

All theoretical calculations (quantum chemical reactivity and material dynamic simulation) were performed in the frame work of density functional theory (DFT) using DMol3 and Forcite module tools respectively as contained in Material Studio (BIOVIA) 2017 version.

(a) Quantum chemical reactivity

The effective phyto-chemical constituents of compounds present in the plant extract used which functioned as corrosion inhibitors were determined using GC-MS and their molecular structures were modeled together with the molecular structure of additives incorporated into the inhibited systems. The quantum chemical parameters determined from the quantum simulation include the followings; Geometrical optimized molecular structure, total electron density, frontier molecular orbitals, energies of molecular orbital, energy gap, Fukui functions, electron charge transfer, (ΔN), hardness, (η) and electronegativity (χ). The estimation of these parameters indicated in equations below using DFT program was done with a view to establish the active sites as well as local reactivity of the molecule responsible for the formation of metal-inhibitor complex ion and broaden simulative understanding of the corrosion inhibition and adsorption process (Njoku *et al*., 2021; Rouifi *et al*., 2019).

$$I = E_{HOMO} \quad (3.1)$$

$$A = E_{LUMO} \quad (3.2)$$

$$\Delta E = E_{LUMO\ -\ HOMO} \quad (3.3)$$

The HOMO (ev) and LUMO (ev) energies are related to the ionization potential (I) and the electron affinity (A) as they will be used in analysis to obtain corrosion inhibition efficiencies (Njoku *et al*., 2021). Electron charge transfer, (ΔN) from

Lewis-base (the inhibitor molecule) to Lewis-acid (metal surface) was quantified using the Equations below:

$$\Delta N = \frac{(\chi_m - \chi_i)}{2(\eta_m - \eta_i)} \quad (3.4)$$

$$\chi = \frac{I+A}{2} \quad (3.5)$$

$$\eta = \frac{I-A}{2} \quad (3.6)$$

Where, where χ_m and χ_i denote the absolute electronegativity of the metal and the inhibitor molecule, respectively; η_m and η_i denote the absolute hardness of the metal and the inhibitor (Njoku *et al*., 2021; Rouifi *et al*., 2019). The simulation studies will be performed by means of the DFT to support our findings experimentally.

(b) Molecular dynamic simulation

This was utilized to extensively evaluate the binding energy of interaction between the crystal metal surface and the inhibitor molecules and predict the inhibition efficacy of the molecule. This was achieved using molecular dynamics simulation via Forcite optimization and Quench module tool respectively as contained in the material studio (BIOVIA) 2017 version program. In performing the simulation, COMPASS forcefield was utilized to run calculations, the Fe crystal was cleaved along the (110) plane with thickness 2.39. The (110) plane is noted and preferred because of its geometry (densely packed) and also possess stabilization characteristics. The geometry of the bottom layers is constrained before optimizing the Fe (110) surface, which is subsequently enlarged into 13 x 10 supercell. The system is quenched every 250 steps. Forcite optimized structures of compounds and the Fe surface were used to sample the different interactions of the various compounds with the surface. The slab of Fe constructed for the docking process was significantly bigger than the organic molecules docked in order to avoid edge effects.

3.3 Experimental Section

The different experimental techniques used in course of this research include the followings;

3.3.1 Gravimetric Technique

The physical measurement used was weight loss measurement technique. The weight loss experiments were carried out with coupons immersed in 1.0 M HCl, and 0.25 M sulphuric acid solutions in the absence and presence of 100 mg/L, 250 mg/L, 500 mg/L and 1000 mg/L concentrations of extracts. The coupons were suspended in beakers containing 400 ml of test solutions maintained at room temperature with the aid of glass hooks and rods. All tests were carried out in aerated solutions. The weight loss with respect to time was determined by retrieving coupons from test solutions at 24 h, scrubbed with bristle brush under running water until it is clean, dried in acetone and warm air then reweighed. The coupons were subsequently re-immersed in their respective test solutions and the procedure repeated for 48 h, 72 h, 96 h, and 120 h. The experiments were run in duplicate and average weight loss recorded. The weight loss was taken to be the difference between the weight at a given time and the initial weight of the coupons. Hence, the weight loss (g) was calculated using Equation (3.7) (Njoku *et al*., 2021; Rouifi *et al*., 2019)

$$W = W_i - W_f \tag{3.7}$$

where W_i = initial weight (g), W_f = final weight (g)

The percentage inhibition efficiency IE (%) was calculated using Equation (3.8) as shown below:

$$IE = \left[1 - \frac{W_1}{W_2}\right] \text{ x } 100 \tag{3.8}$$

where W_1 and W_2 denotes weight loss of metal in the presence of extract and absence of extract respectively (Njoku *et al*., 2021; Rouifi *et al*., 2019).

The corrosion rate CR (mm/yr) was calculated using Equation (3.9) as shown below:

$$CR = \left[\frac{87600W}{DAT}\right] \quad (3.9)$$

where W= Weight loss (g), D= Density of steel sample (g/cm^3), A= Area of specimen exposed to corrosion (cm^2), T= Time of exposure (h) (Ayoola *et al*., 2018). The degree of surface coverage (**ϴ**) at each concentration of inhibitor was calculated using Equation (3.10)

$$\theta = \left[\frac{W_1 - W_2}{W_1}\right] \quad (3.10)$$

where W_1 and W_2 are the weight loss (g) in coupon without and with inhibitor respectively (Ayoola *et al*., 2018).

3.3.2 UV-Visible Spectrophotometer Measurements

The UV-visible measurements were taken using UV-VIS-NIR spectrophotometer, model UV-3600. The extracting solvents were used as blanks (control) and were first used to obtain the maximum absorption wavelength. The plots of absorbance of ethanolic extracts of seeds of *Piper guineense,* leaves of *Pterocarpus santalinoides*, and leaves of *Picrilima nitida* and the blends of *Pterocarpus santalinoides*, potassium iodide and sodium alginate at various wavelength was generated.

3.3.3 Gas Chromatography - Mass Spectrometry (GC-MS) Analysis

The leaves extract (10µL) of *Pterocarpus santalinoides* was analyzed using GC (Agilent 6890N) and MS (5973B MSD) with Restek capillary column (30 m x 0.25 mm; film thickness 1.4 µm). The temperature was programmed as follows: Initial temperature was 40 ^oC which increased to 150 ^oC at the rate of 10 ^oC/min. the temperature was again increased to 230 ^oC at the rate of 5 ^oC/min. The process continued till the temperature reached 280 ^oC at the rate of 20°C/min which was held for 8 minutes. The injector port temperature remained constant at 280°C and detector temperature was 250°C then. Helium was used as the carrier gas with a flow rate of

1 mL/min. Split ratio and ionization voltage were 110:1 and 70 eV respectively. To identify the unknown phytochemical components, present in the samples, their individual mass spectral peak value was compared with the database of National Institute of Science and Technology 2014. Then identification was done by comparing the unknown peak value and chromatogram from GC-MS against the known chromatogram peak value from the NIST Library database. Subsequently, the details about their molecular formula, molecular weight, retention time and percentage content were also obtained.

3.3.4 Fourier Transform Infrared (FTIR) Spectroscopy Analysis

The type of bonding for organic inhibitors adsorbed on the metal surface in 0.25 M H_2SO_4 environment can be identified using the Fourier Transform Infrared (FTIR) Spectroscopy instrument. The protective film that forms on a metal surface has been examined using FTIR spectra (Mohammed *et al*., 2020; Anbarasi & Vasudha, 2014). Hence, FTIR studies and analysis was carried out using Agilent Technology Cary 630 FTIR to understand the interaction between PS and the mild steel surface and blends of PS, sodium alginate, KI and the mild steel surface.

The power in the instrument was turned on and allowed to warm-up within 10-15 mins, then the computer attached to the system was turned on. Afterwards was initialization from the computer, i.e., the 'MicroLab PC window' icon was double clicked on and allowed to open, next was initiation of the sampling operation and method selection i.e., Absorbance or Transmittance. The crystal was cleaned with organic solvent, next was to check the crystal and the collecting background. Sample of about 10-15mg was placed (note: for solid samples, the sample is closed and pressed to make a pellet on top of the crystal or if it's liquid the sample will remain open to smear on top of the crystal). Next was sample alignment and sampling. Peaks

were picked and labeled by dragging to acquire the wave numbers as well as Transmittance or Absorbance.

3.3.5 Adsorption Isotherm and Thermodynamic Parameters

Langmuir isotherm, as widely accepted and most conventional model was employed, hence, it is defined as:

$$\left[\frac{1}{K_{ads}}\right] + C = \frac{C}{\theta} \quad (3.12)$$

where C is the inhibitor concentration (g/L), K_{ads} is the adsorption equilibrium constant and Θ is the degree of surface coverage (Golchinvafa *et al*., 2020).

Furthermore, to determine if the adsorption of PS as an inhibitor on the surface of the mild steel was of physical or chemical type, the thermodynamic parameter of ΔG^{o}_{ads} (KJ/mol) was evaluated and analyzed to reveal required information. Progressively, K_{ads}, was obtained from the inverse interception of Langmuir adsorption curve. With K_{ads} value and using equation 3.12, ΔG^{o}_{ads} can be calculated (Golchinvafa *et al*., 2020)

$$(\Delta G^{o}_{ads}) = - RT \ln (1\times10^{6} K_{ads}) \quad (3.13)$$

where 1×10^{6} is the water molecules concentration, R is Gibbs free energy (KJ), T (^{o}C)is the temperature, K_{ads} is the adsorption equilibrium constant (which can be taken from the inverse interception of Langmuir adsorption curve).

3.3.6 Synergistic Index (SI)

The synergism value for the blends was evaluated using equation (3.14) below

$$SI = \frac{1 - I_{1+2}}{1 - I\prime_{1+2}} \quad (3.14)$$

where I_{1+2} is equivalent to I_1 + I_2; I_1 is the inhibition efficiency of KI or SA; I_2 is the inhibition efficiency of the PS; and I'_{1+2} is the measured inhibition efficiency for combination of PS and KI or SA (Chidiebere *et al*., 2014).

CHAPTER FOUR

RESULTS AND DISCUSSION

4.1 RESULTS

4.1.1 Gravimetric Analysis

The extract from *Pterocarpus santalinoides* (PS), *Piper guineense* (PG) and *Picrilima nitida* (PN) were applied to mitigate corrosion of mild steel in 0.5 M HCl and 0.25 M H_2SO_4 environments respectively via gravimetric measurement technique. The corresponding weight loss, corrosion rate, inhibition efficiency and degree of surface coverage data obtained are presented in Tables 4.1 to 4.11.

4.1a Gravimetric Results for *Pterocarpus santalinoides* (PS)

(i) Weight loss (WL)

The WL results from Tables 4.1 and 4.2 demonstrate that the addition of PS as a mild steel corrosion inhibitor significantly decreased the WL of mild steel in settings containing 0.5 M HCl and 0.25 M H_2SO_4.

(ii) Corrosion rate (CR)

The CR data from Table 4.1 and Table 4.2 also show that the introduction of PS as mild steel corrosion inhibitor greatly reduced the CR of mild steel in 0.5 M HCl and 0.25 M H_2SO_4 environments. Increase in PS concentration from 100 mg/L to 1000 mg/L reduced the mild steel CR

(iii) Inhibition efficiency (IE)

The IE data from Table 4.1 and Table 4.2 revealed that the introduction of PS as mild steel corrosion inhibitor had great effect as IE of PS on mild steel is observed to increase with increasing PS concentration (from 100 mg/L to 1000 mg/L) in 0.5 M HCl and 0.25 M H_2SO_4 environments.

(iv) Degree of surface coverage

Data presented in Table 4.1 and Table 4.2 demonstrate that the addition of PS as a mild steel corrosion inhibitor had a significant impact on the degree of surface coverage because it is seen on mild steel to increase with increasing PS concentrations (from 100 mg/L to 1000 mg/L) in 0.5 M HCl and 0.25 M H_2SO_4 environments.

Table 4.1 Weight loss and inhibition efficiency values for mild steel corrosion 0.5 M HCl in the absence and presence of leaves extract of PS at different immersion time and ± 28ºC.

Time(h)	Conc. (mg/L)	Initial weight (g)	Final weight (g)	Weight loss (g)	Corrosion rate (mm/yr)	I.E. (%)	Degree of surface coverage (Θ)
24	Blank	7.9679	7.8103	0.1576	3.8166	–	–
	100	8.5080	8.4589	0.0491	1.1891	68.8769	0.6890
	250	8.4826	8.4476	0.0350	0.8476	77.7602	0.7780
	500	8.3927	8.3547	0.0380	0.9203	75.8883	0.7590
	1000	8.3394	8.3071	0.0323	0.7822	79.5368	0.7950
48	Blank	7.9679	7.7819	0.1860	2.2522	–	–
	100	8.5080	8.4427	0.0652	0.7895	64.9194	0.6500
	250	8.4826	8.4274	0.0553	0.6696	70.2957	0.7030
	500	8.3927	8.3250	0.0677	0.8198	63.6022	0.6360
	1000	8.3394	8.2842	0.0552	0.6684	70.3495	0.7030
72	Blank	7.9679	7.7430	0.2249	1.8155	–	–
	100	8.5080	8.4267	0.0813	0.6563	63.8506	0.6390
	250	8.4826	8.4114	0.0712	0.5748	68.3415	0.6830
	500	8.3927	8.3047	0.0881	0.7112	60.8493	0.6080
	1000	8.3394	8.2679	0.0715	0.5772	68.2303	0.6820
96	Blank	7.9679	7.7155	0.2524	1.5281	–	–
	100	8.5080	8.4106	0.0974	0.5897	61.4105	0.6140
	250	8.4826	8.3958	0.0869	0.5261	65.5903	0.6560
	500	8.3927	8.2856	0.1072	0.6490	57.5475	0.5750
	1000	8.3394	8.2504	0.0890	0.5388	64.7583	0.6470
120	Blank	7.9679	7.6846	0.2834	1.3726	–	–
	100	8.5080	8.3964	0.1116	0.5405	60.6317	0.6060
	250	8.4826	8.3835	0.0992	0.4805	65.0079	0.6500
	500	8.3927	8.2678	0.1249	0.6049	55.9202	0.5590
	1000	8.3394	8.2371	0.1023	0.4955	63.9139	0.6390

The PS leave extract applied to mitigate corrosion of mild steel in 0.5 M HCl environment is shown to be promising, but the inhibition efficiency reduced with

prolonged coupon immersion time. It is important to note that high inhibition efficiency is recorded with 1000 mg/L of PS.

Table 4.2 Weight loss and inhibition efficiency values for mild steel corrosion in 0.25 M H_2SO_4 in the absence and presence of leaves extract of PS at different immersion time and ± 28ºC.

Time(h)	Conc. (mg/L)	Initial weight (g)	Final weight (g)	Weight loss (g)	Corrosion rate (mm/yr)	I.E (%)	Degree of surface coverage (Ɵ)
24	Blank	6.6964	5.9836	0.7128	17.2619	–	–
	100	7.2635	6.9750	0.2886	6.9891	59.5160	0.5950
	250	6.9384	6.7898	0.1486	3.5987	79.1512	0.7920
	500	7.8435	7.7526	0.0909	2.2013	87.2466	0.8730
	1000	7.6900	7.6072	0.0828	2.0052	88.3830	0.8840
48	Blank	6.6964	5.8020	0.8944	10.8299	–	–
	100	7.2635	6.8093	0.4542	5.4997	49.2145	0.4920
	250	6.9384	6.7210	0.2174	2.6324	75.6918	0.7570
	500	7.8435	7.6494	0.1941	2.3503	78.2971	0.7830
	1000	7.6900	7.5071	0.1830	2.2159	79.5438	0.7950
72	Blank	6.6964	5.7804	0.9160	7.3943	–	–
	100	7.2635	6.6646	0.5990	4.8354	34.6089	0.3460
	250	6.9384	6.6098	0.3286	2.6526	64.1301	0.6410
	500	7.8435	7.5298	0.3137	2.5323	65.7569	0.6580
	1000	7.6900	7.3863	0.3037	2.4516	66.8432	0.6690
96	Blank	6.6964	5.7283	0.9681	5.8611	–	–
	100	7.2635	6.5358	0.7277	4.4057	24.8283	0.2480
	250	6.9384	6.4787	0.4597	2.7832	52.5179	0.5250
	500	7.8435	7.3932	0.4503	2.7262	53.4890	0.5350
	1000	7.6900	7.2615	0.4286	2.5949	55.7306	0.5570
120	Blank	6.6964	5.6728	1.0236	4.9577	–	–
	100	7.2635	6.4172	0.8463	4.0990	17.3212	0.1730
	250	6.9384	6.3142	0.6242	3.0233	39.0191	0.3900
	500	7.8435	7.2305	0.6130	2.9690	40.1182	0.4010
	1000	7.6900	7.1152	0.5748	2.7840	43.8453	0.4390

With 1000 mg/L of PS, inhibition efficiency is noticeably high. It has been demonstrated that using PS leaves extract to prevent mild steel from corroding in an atmosphere with 0.25 M H_2SO_4 is promising but efficiency reduces over time

Table 4.3 Weight loss and inhibition efficiency values for mild steel corrosion in 0.25 M H_2SO_4 in the absence and presence of Potassium iodide (KI) at different immersion time and ± 28°C.

Time(h)	Conc(mole)	Initial weight (g)	Final weight (g)	Weight loss (g)	I.E (%)
	Blank	5.6780	4.2891	1.3889	–
	0.0010	6.9510	6.0602	0.8909	35.8593
24	0.0250	6.8320	6.2526	0.5794	58.2850
	0.0500	4.6039	3.9680	0.6360	54.2120
	Blank	5.6780	4.1220	1.5560	–
	0.0010	6.9510	5.9386	1.0125	34.9304
48	0.0250	6.8320	6.1710	0.6611	57.5147
	0.0500	4.6039	3.8534	0.7506	51.7626
	Blank	5.6780	3.9404	1.7376	–
	0.0010	6.9510	5.7946	1.1565	33.4436
72	0.0250	6.8320	5.9998	0.8322	52.1050
	0.0500	4.6039	3.7298	0.8741	49.6935
	Blank	5.6780	3.7933	1.8847	–
	0.0010	6.9510	5.6658	1.2852	31.8070
96	0.0250	6.8320	5.8687	0.9633	48.8871
	0.0500	4.6039	3.6057	0.9982	47.0353
	Blank	5.6780	3.6578	2.0202	–
	0.0010	6.9510	5.5372	1.4138	30.0168
120	0.0250	6.8320	5.7380	1.0940	45.8447
	0.0500	4.6039	3.4605	1.1434	43.4016

Inhibition efficiency reduced with prolonged coupon immersion time and it is more pronounced with 0.05 M of KI.

Table 4.4 Weight loss and inhibition efficiency values for mild steel corrosion in 0.25 M H_2SO_4 in the absence and presence of Sodium alginate at different immersion time and ± 28ºC

Time(h)	Conc(mg/L)	Initial weight (g)	Final weight (g)	Weight loss (g)	I.E (%)
	Blank	7.1346	6.9668	0.1678	–
	100	7.7039	7.0775	0.6265	-273.3313
24	500	7.7739	7.3362	0.4377	-160.8462
	1000	7.8089	7.6527	0.1562	6.9428
	Blank	7.1346	6.9532	0.1815	–
	100	7.7039	6.6542	1.0497	-478.5065
48	500	7.7739	6.9673	0.8066	-344.5302
	1000	7.8089	7.6070	0.2019	-11.2428
	Blank	7.1346	6.9511	0.1835	–
	100	7.7039	6.3054	1.3985	-662.1253
72	500	7.7739	6.7036	1.0704	-483.2970
	1000	7.8089	7.5792	0.2297	-25.1771
	Blank	7.1346	6.9486	0.1861	–
	100	7.7039	6.0019	1.7021	-814.8347
96	500	7.7739	6.4437	1.3303	-614.9960
	1000	7.8089	7.5577	0.2512	-34.9906
	Blank	7.1346	6.9461	0.1885	–
	100	7.7039	5.7547	1.9492	-934.0584
120	500	7.7739	6.1972	1.5767	-736.4456
	1000	7.8089	7.5353	0.2736	-45.1459

The biopolymer inhibitor promotes corrosion with prolonged coupon immersion time. From Table 4.4, it is shown that in 24 h with 1000 mg/L, a certain inhibitive activity was noticed (that is 7%), which dropped below 0% after 48 h.

Table 4.5 Weight loss and inhibition efficiency values for mild steel corrosion in 0.25 M H_2SO_4 in the absence and presence of blend of leave extracts of PS and sodium alginate at different immersion time and ± 28ºC

Time (h)	Conc (mg/L)	Initial weight (g)	Final weight (g)	Weight loss (g)	I.E (%)
24	Blank	6.8505	6.3175	0.5331	–
	500(PS) + 500(SA)	6.1318	6.0260	0.1059	80.1426
48	Blank	6.8505	5.9601	0.8905	–
	500(PS) + 500(SA)	6.1318	5.8838	0.2481	72.1433
72	Blank	6.8505	5.6376	1.2130	–
	500(PS) + 500(SA)	6.1318	5.7073	0.4246	64.9986
96	Blank	6.8505	5.2073	1.6433	–
	500(PS) + 500(SA)	6.1318	5.5625	0.5693	65.3552
120	Blank	6.8505	4.8233	2.0272	–
	500(PS) + 500(SA)	6.1318	5.1899	0.9419	53.5369

IE reduced with prolonged coupon immersion time, the blend of PS leaves extract and sodium alginate applied to mitigate corrosion of mild steel in 0.25 M H_2SO_4 environment is observed to be effective.

Table 4.6 Weight loss and inhibition efficiency values for mild steel corrosion in 0.25 M H_2SO_4 in the absence and presence of blend of leave extracts of PS and KI at different immersion time and ± 28ºC

Time (h)	Conc (PS: mg/L), (KI: mole)	Initial weight (g)	Final weight (g)	Weight loss (g)	I.E (%)
24	Blank	5.7537	5.2018	0.5519	–
	1000(PS) + 0.0250(KI)	5.4409	5.3505	0.0904	83.6187
48	Blank	5.7537	4.7754	0.9783	–
	1000(PS) + 0.0250(KI)	5.4409	5.2593	0.1816	81.4423
72	Blank	5.7537	4.3510	1.4027	–
	1000(PS) + 0.0250(KI)	5.4409	5.1700	0.2709	80.6872
96	Blank	5.7537	3.9277	1.8260	–
	1000(PS) + 0.0250(KI)	5.4409	5.0726	0.3683	79.8324
120	Blank	5.7537	3.6524	2.1013	–
	1000(PS) + 0.0250(KI)	5.4409	4.9800	0.4609	78.0660

The combination of PS leaves extract and KI applied to prevent mild steel from corroding in an environment with 0.25 M H_2SO_4 appears to be a potential formulation because IE was reduced with prolonged coupon immersion time.

Table 4.7 Weight loss and inhibition efficiency values for mild steel corrosion in 0.25 M H_2SO_4 in the absence and presence of blend of leave extracts of PS, sodium alginate and KI at different immersion time and ± 28°C

Time (h)	Conc. (PS:mg/L), (KI:mole), (SA:mg/L),	Initial weight (g)	Final weight (g)	Weight loss (g)	Corrosion rate (mm/yr)	I.E (%)	Degree of surface coverage (Ɵ)
24	Blank 500(PS)+ 0.0250(KI)+ 500(SA)	7.6941 7.5491	6.9441 7.5260	0.7500 0.0231	18.1628 0.5594	– 96.9200	– 0.9690
48	Blank 500(PS)+ 0.0250(KI)+ 500(SA)	7.6941 7.5491	6.0255 7.5220	1.6686 0.0272	20.2043 0.3294	– 98.3728	– 0.9840
72	Blank 500(PS)+ 0.0250(KI)+ 500(SA)	7.6941 7.5491	5.5405 7.5166	2.1536 0.0325	17.3846 0.2624	– 98.4909	– 0.9850
96	Blank 500(PS)+ 0.0250(KI)+ 500(SA)	7.6941 7.5491	5.3050 7.5089	2.3891 0.0403	14.4643 0.2440	– 98.3153	– 0.9830
120	Blank 500(PS)+ 0.0250(KI)+ 500(SA)	7.6941 7.5491	5.1193 7.5004	2.5748 0.0488	12.4708 0.2364	– 98.1066	– 0.9810

IE in 24 h was 97%, after 48 h, IE increased to 98% and was maintained up to 120 h. The blend of PS leaves extract, sodium alginate and KI applied to mitigate corrosion of mild steel in 0.25 M H_2SO_4 environment is shown to be effective as inhibition efficiency was prolonged and maintained.

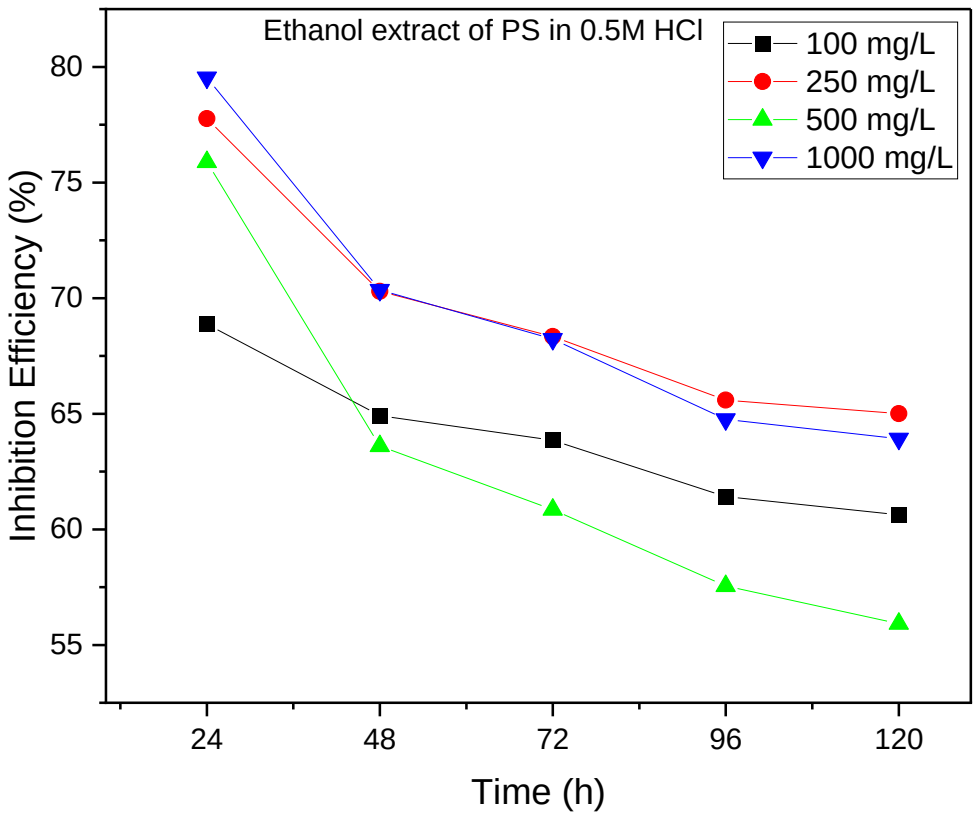

Fig 4.1 Variation of inhibition efficiency of ethanol extract of PS with time for mild steel corrosion in 0.5 M HCl solution

The corrosion inhibition efficiency of PS leaves extract (from Figure 4.1) in 0.5 M HCl solution increased with increase in concentration but there is notably a gradual reduction of inhibition efficiency with prolonged coupon immersion time.

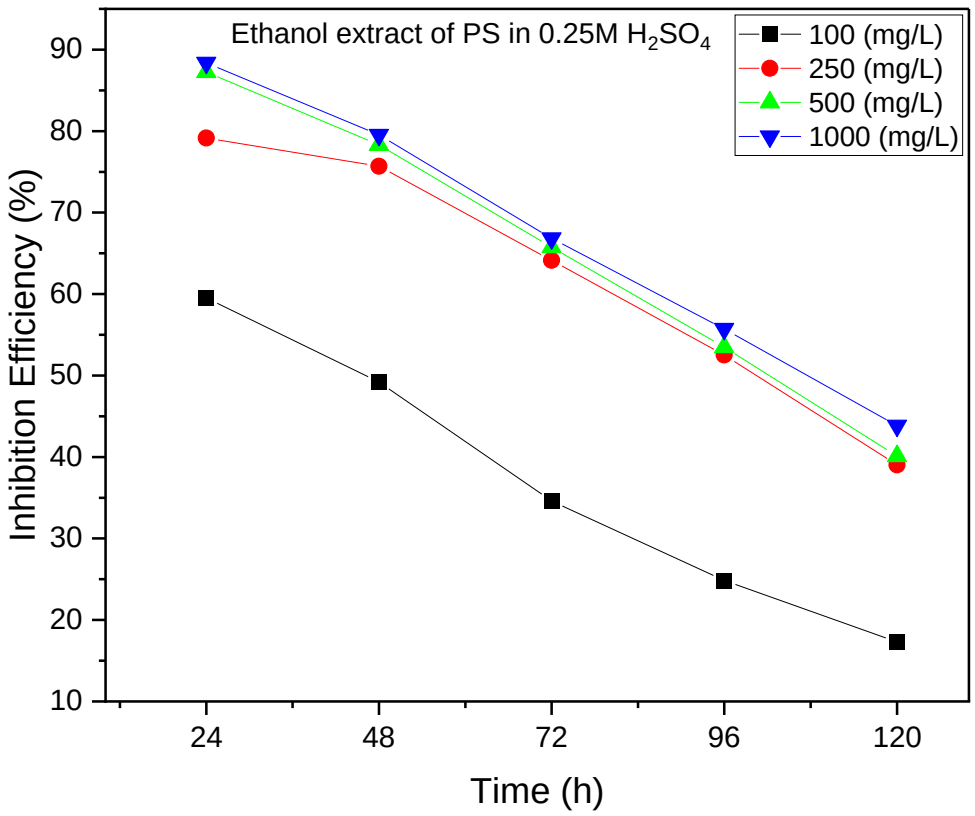

Fig 4.2 Variation of inhibition efficiency of ethanol extract of PS with time for mild steel corrosion in 0.25 M H_2SO_4 solution

The corrosion inhibition efficiency of PS leaves extract (from Figure 4.2) in 0.25 M H_2SO_4 solution increased with increase in concentration but there is a gradual reduction of inhibition efficiency with prolonged coupon immersion time.

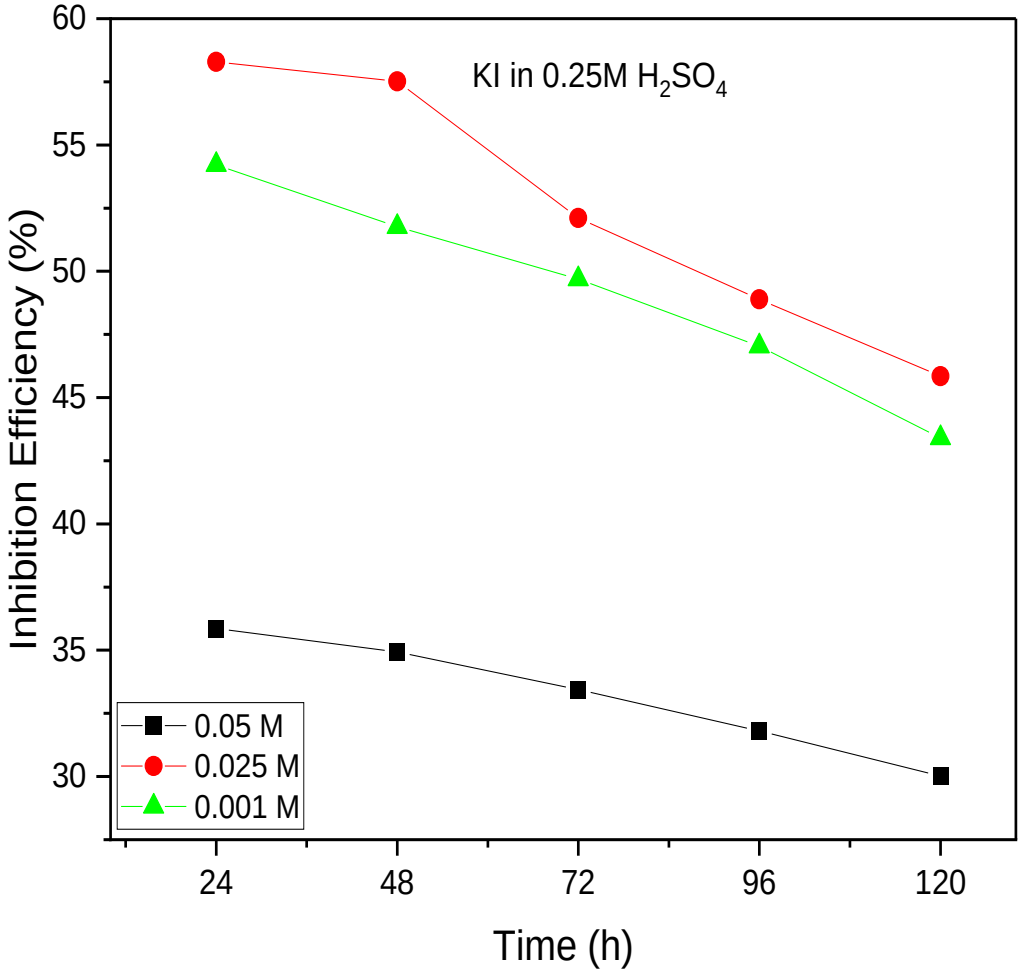

Fig 4.3 Variation of inhibition efficiency of KI with time for mild steel corrosion in 0.25 M H_2SO_4 solution

The corrosion inhibition efficiency of KI (from Figure 4.3) in 0.25 M H_2SO_4 solution increased with increase in concentration but there is notably a reduction of inhibition efficiency with increase from 0.025M to 0.05 M. Conclusively, there is notably a gradual reduction of inhibition efficiency with prolonged coupon immersion time.

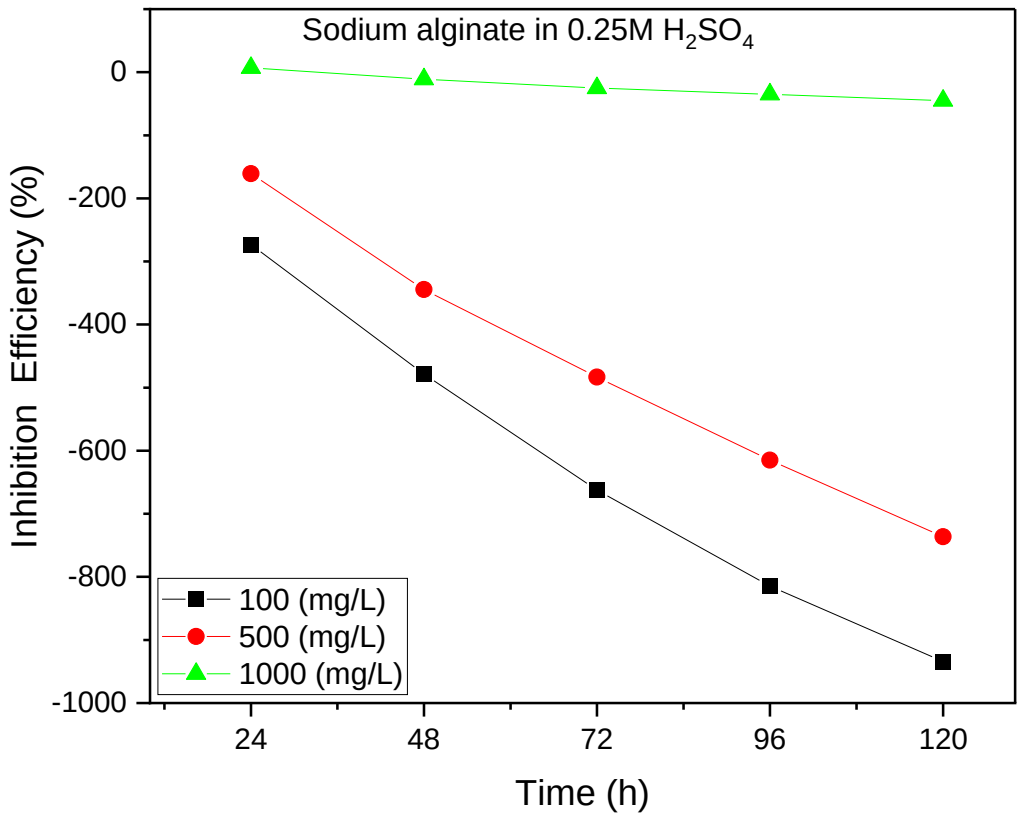

Fig 4.4 Variation of inhibition efficiency of sodium alginate with time for mild steel corrosion in 0.25 M H_2SO_4 solution

The corrosion inhibition efficiency of sodium alginate (from Figure 4.4) in 0.25 M H_2SO_4 solution is seen not to be promising as sodium alginate facilitated corrosion rate with time. This could be attributed to the poor adsorption characteristics of sodium alginate molecules on the surface of the mild steel.

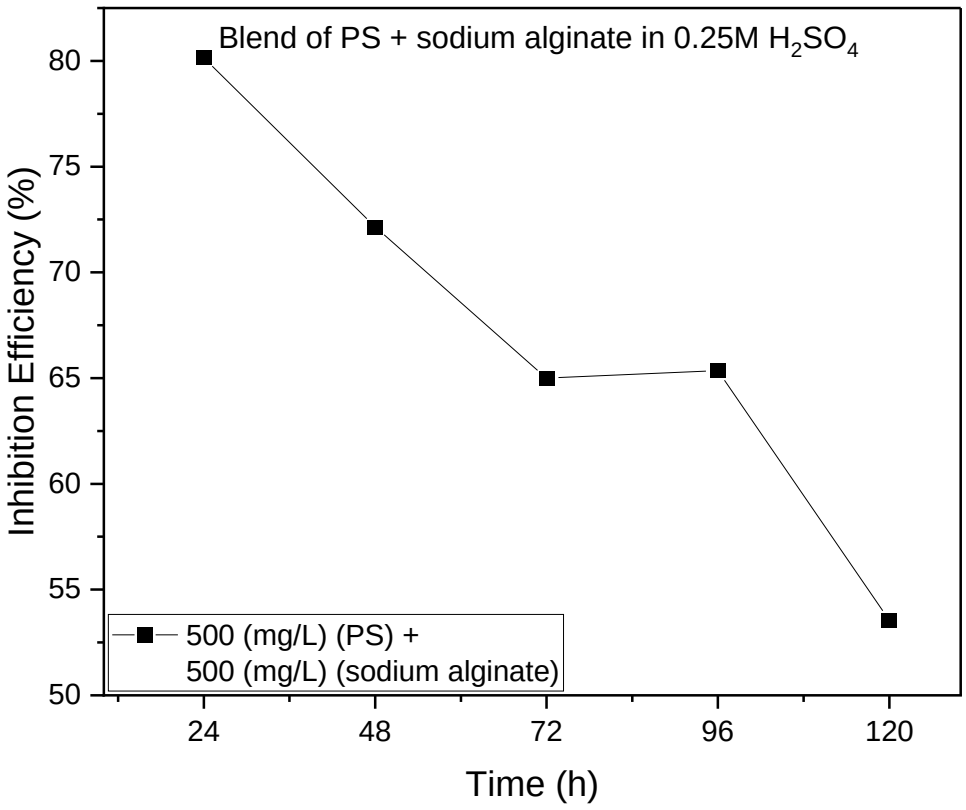

Fig 4.5 Variation of inhibition efficiency of blend of ethanol extract of PS and sodium alginate with time for mild steel corrosion in 0.25 M H_2SO_4 solution

The corrosion inhibition efficiency of blend of ethanol extracts of PS and sodium alginate (from Figure 4.5) in 0.25 M H_2SO_4 solution is notably decreasing gradually with prolonged coupon immersion time.

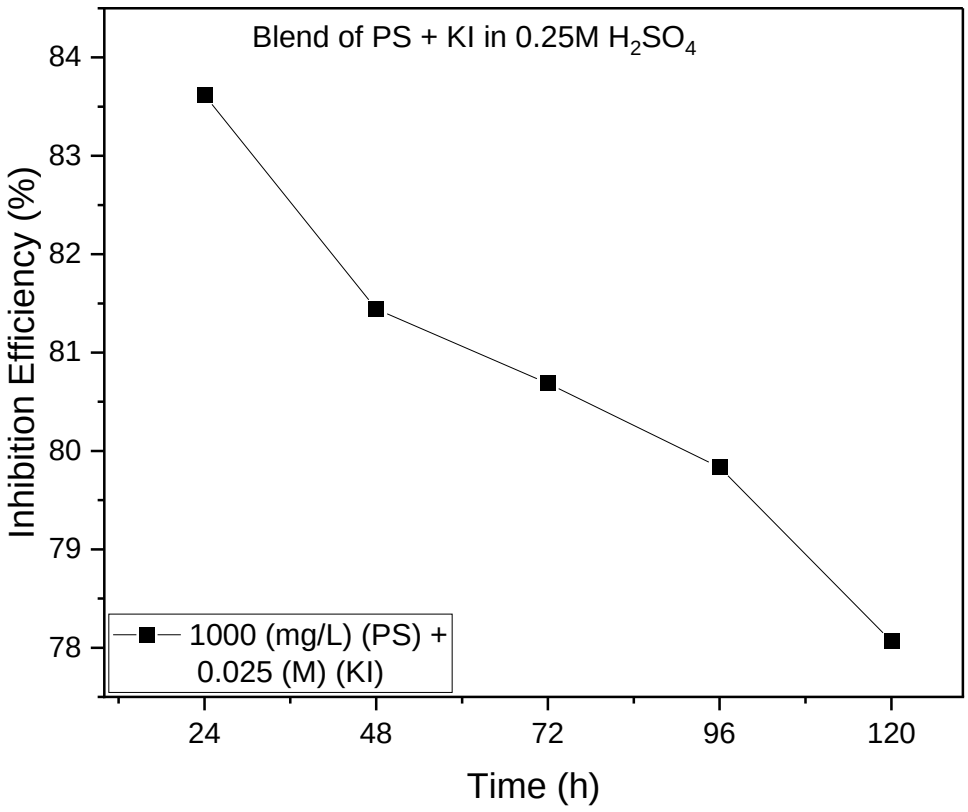

Fig 4.6 Variation of inhibition efficiency of blend of ethanol extract of PS and KI with time for mild steel corrosion in 0.25 M H_2SO_4 solution.

The corrosion inhibition efficiency of blend of ethanol extracts of PS and KI (from Figure 4.6) in 0.25 M H_2SO_4 solution is notably decreasing gradually with prolonged coupon immersion time.

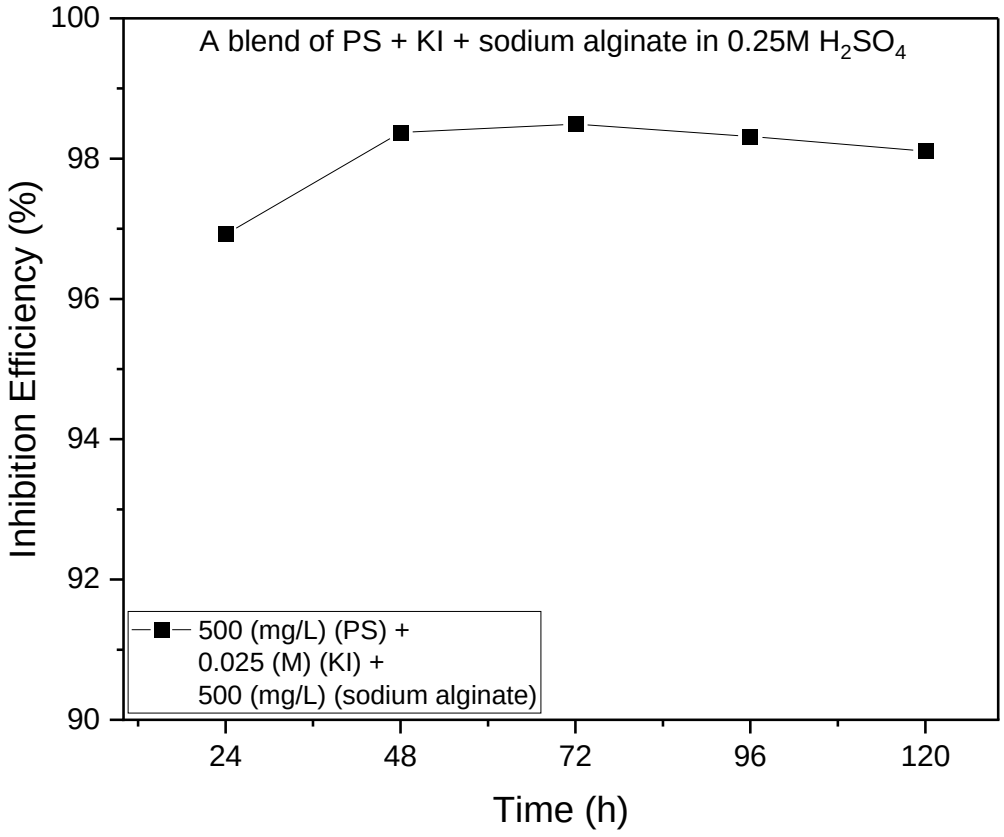

Fig 4.7 Variation of inhibition efficiency of blend of ethanol extracts of PS, sodium alginate and KI with time for mild steel corrosion in 0.25 M H_2SO_4 solution.

The corrosion inhibition efficiency of blend of ethanol extracts of PS, sodium alginate and KI (from Figure 4.7) in 0.25 M H_2SO_4 solution is very pronounced with prolonged coupon immersion time (up to 120 h).

4.1b Gravimetric Results for *Piper guineense* (PG)

(i) Weight loss (WL)

The WL results from Tables 4.8 and 4.9 demonstrate that the addition of PG as a mild steel corrosion inhibitor significantly decreased the WL of mild steel in settings containing 0.5 M HCl and 0.25 M H_2SO_4.

(ii) Corrosion rate (CR)

The CR data from Table 4.8 and Table 4.9 show that the presence of PG as mild steel corrosion inhibitor greatly reduced the CR of mild steel in 0.5 M HCl and 0.25 M H_2SO_4 environments. Increase in PG concentration from 100 mg/L to 1000 mg/L reduced the mild steel CR

(iii) Inhibition efficiency (IE)

The recorded IE results presented in Table 4.8 and Table 4.9 revealed that the addition of PG as mild steel corrosion inhibitor had great effect as the performance of PG on mild steel protection is observed to increase with increasing PG concentration (from 100 mg/L to 1000 mg/L) in 0.5 M HCl and 0.25 M H_2SO_4 environments.

(iv) Degree of surface coverage

Data presented in Table 4.8 and Table 4.9 demonstrate that the addition of PG as a mild steel corrosion inhibitor had a significant impact on the degree of surface coverage because it is seen on mild steel to increase with increasing PG concentrations (from 100 mg/L to 1000 mg/L) in 0.5 M HCl and 0.25 M H_2SO_4 environments.

Table 4.8 Weight loss and inhibition efficiency values for mild steel corrosion in 0.5 M HCl in the absence and presence of leave extracts of PG at different immersion time and ± 28ºC

Time (h)	Conc. (mg/L)	Initial weight (g)	Final weight (g)	Weight loss (g)	Corrosion rate (mm/yr)	I.E (%)	Degree of surface coverage (Ɵ)
24	Blank	7.7773	7.6531	0.1242	3.0078	–	–
	100	8.2021	8.1686	0.0335	0.8113	73.0568	0.7300
	250	7.8004	7.7721	0.0283	0.6853	77.2453	0.7720
	500	8.1168	8.0931	0.0237	0.5740	80.9102	0.8090
	1000	8.0484	8.0361	0.0123	0.2979	90.0926	0.9010
48	Blank	7.7773	7.5972	0.1801	2.1808	–	–
	100	8.2021	8.1509	0.0512	0.6200	71.5991	0.7160
	250	7.8004	7.7583	0.0421	0.5098	76.6519	0.7660
	500	8.1168	8.0800	0.0368	0.4456	79.5669	0.7960
	1000	8.0484	8.0265	0.0219	0.2652	87.8401	0.8780
72	Blank	7.7773	7.5695	0.2078	1.6774	–	–
	100	8.2021	8.1409	0.0612	0.4940	70.5486	0.7060
	250	7.8004	7.7500	0.0504	0.4069	75.7459	0.7580
	500	8.1168	8.0712	0.0456	0.3681	78.0558	0.7810
	1000	8.0484	8.0192	0.0292	0.2357	85.9240	0.8600
96	Blank	7.7773	7.5512	0.2261	1.3689	–	–
	100	8.2021	8.1277	0.0744	0.4504	67.1090	0.6710
	250	7.8004	7.7391	0.0613	0.3711	72.9042	0.7290
	500	8.1168	8.0641	0.0527	0.3191	76.6866	0.7670
	1000	8.0484	8.0115	0.0370	0.2240	83.6541	0.8360
120	Blank	7.7773	7.5352	0.2421	1.1726	–	–
	100	8.2021	8.1122	0.0899	0.4354	62.8796	0.6290
	250	7.8004	7.7283	0.0721	0.3492	70.2128	0.7020
	500	8.1168	8.0562	0.0606	0.2935	74.9432	0.7500
	1000	8.0484	8.0031	0.0453	0.2194	81.2849	0.8130

The PG seed extract applied to mitigate corrosion of mild steel in 0.5 M HCl environment is shown to be promising, but the inhibition efficiency reduced with time. It is important to note that high inhibition efficiency is recorded with 1000 mg/L of PG.

Table 4.9 Weight loss and inhibition efficiency values for mild steel corrosion in 0.25M H_2SO_4in the absence and presence of leave extracts of PG at different immersion time and ± 28ºC

Time(h)	Conc(mg/L)	Initial weight (g)	Final weight (g)	Weight loss (g)	Corrosion rate (mm/yr)	I.E (%)	Degree of surface coverage (Ɵ)
	Blank	6.5707	5.6178	0.9529	23.0765	–	–
	100	6.9880	6.6555	0.3326	8.0546	65.0994	0.6510
24	250	7.7155	7.5207	0.1948	4.7175	79.5613	0.7960
	500	7.2175	7.0923	0.1252	3.0320	86.8605	0.8690
	1000	7.9337	7.8675	0.0662	1.6032	93.0472	0.9310
	Blank	6.5707	4.7395	1.8312	22.1732	–	–
	100	6.9880	6.3441	0.6439	7.7967	64.8373	0.6480
48	250	7.7155	7.3285	0.3870	4.6860	78.8663	0.7890
	500	7.2175	6.9663	0.2512	3.0417	86.2822	0.8630
	1000	7.9337	7.7847	0.1490	1.8042	91.8633	0.9190
	Blank	6.5707	4.1232	2.4475	19.7571	–	–
	100	6.9880	6.0216	0.9665	7.8019	60.5120	0.6050
72	250	7.7155	7.1550	0.5605	4.5246	77.0986	0.7710
	500	7.2175	6.8529	0.3646	2.9432	85.1049	0.8510
	1000	7.9337	7.6903	0.2434	1.9648	90.0550	0.9010
	Blank	6.5707	3.7799	2.7908	16.8963	–	–
	100	6.9880	5.7782	1.2098	7.3245	56.6496	0.5670
96	250	7.7155	7.0010	0.7145	4.3258	74.3976	0.7440
	500	7.2175	6.7462	0.4713	2.8534	83.1139	0.8310
	1000	7.9337	7.6010	0.3327	2.0143	88.0785	0.8810
	Blank	6.5707	3.5597	3.0110	14.5835	–	–
	100	6.9880	5.5507	1.4374	6.9619	52.2626	0.5230
120	250	7.7155	6.8588	0.8567	4.1494	71.5488	0.7160
	500	7.2175	6.6465	0.5710	2.7656	81.0375	0.8100
	1000	7.9337	7.5154	0.4183	2.0260	86.1074	0.8610

With 1000 mg/L of PG, inhibition efficiency is noticeably high. It has been demonstrated that using PG seed extract to prevent mild steel from corroding in an atmosphere with 0.25 M H_2SO_4 is promising but efficiency reduces over time.

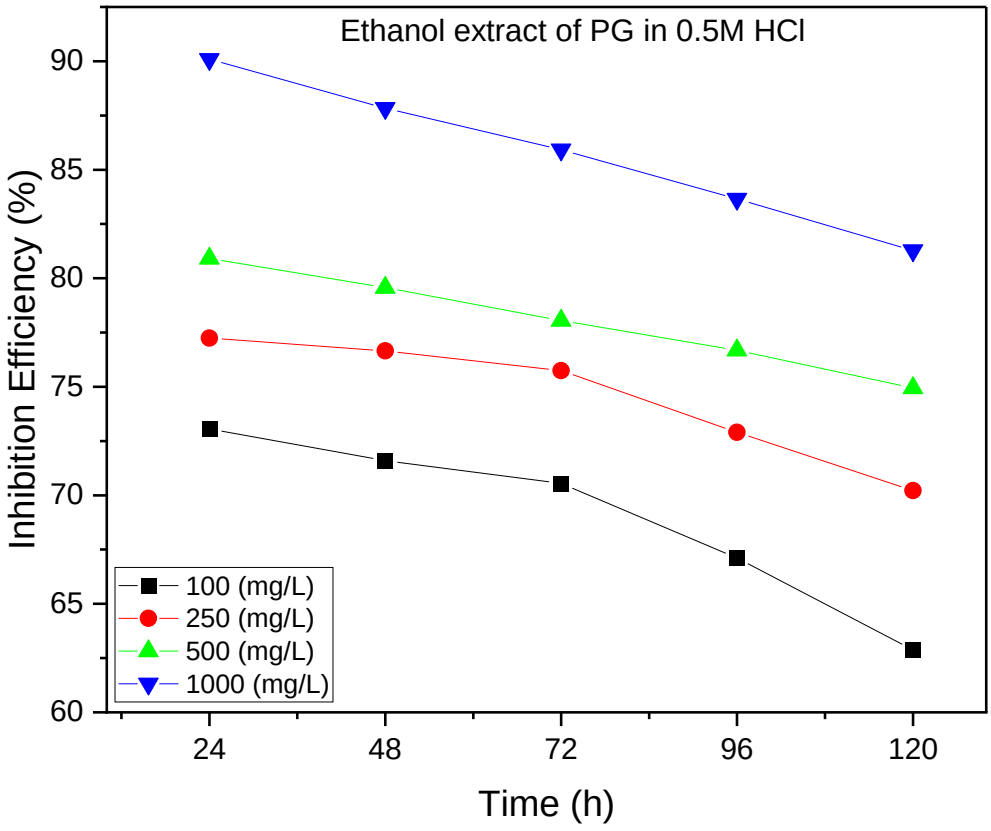

Fig 4.8 Variation of inhibition efficiency of ethanol extract of PG with time for mild steel corrosion in 0.5 M HCl solution

The corrosion inhibition efficiency of PG seed extract (from Figure 4.8) in 0.5 M HCl solution increased with increase in concentration but there is notably a gradual reduction of inhibition efficiency with prolonged coupon immersion time.

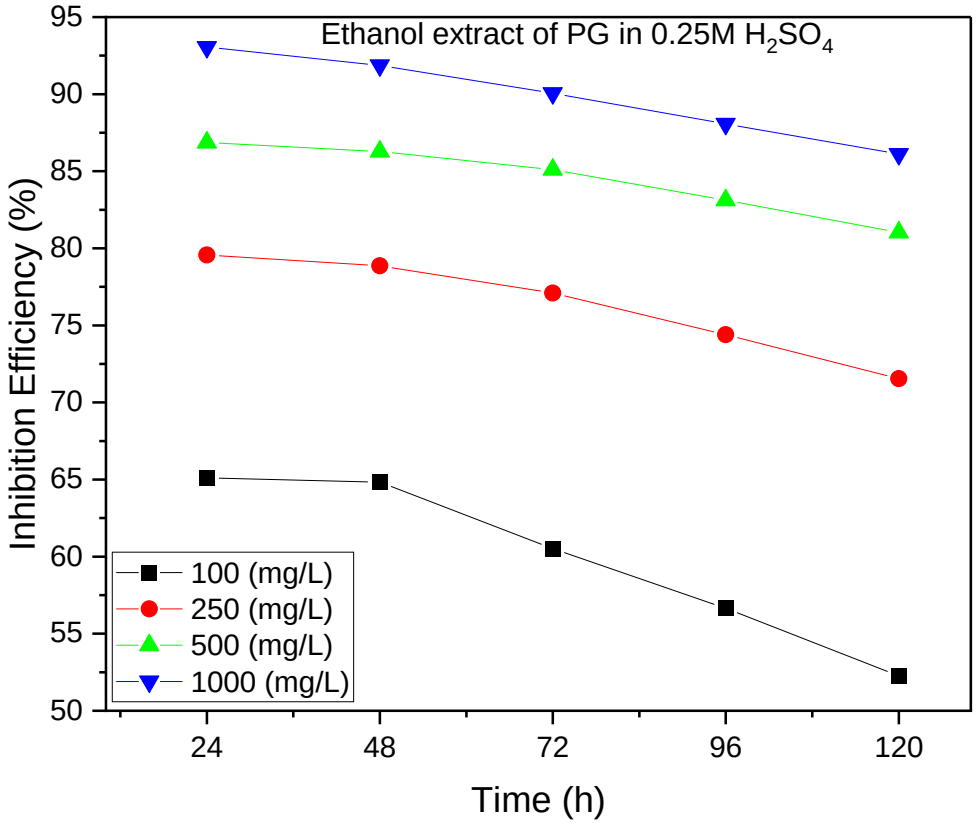

Fig 4.9 Variation of inhibition efficiency of ethanol extract of PG seeds with time for mild steel corrosion in 0.25 M H_2SO_4 solution

The corrosion inhibition efficiency of PG seed extract (from Figure 4.9) in 0.25 M H_2SO_4 solution increased with increase in concentration but there is notably a gradual reduction of inhibition efficiency with prolonged coupon immersion time.

4.1c Gravimetric Results for *Picrilima nitida* (PN)

(i) Weight loss (WL)

The WL results from Tables 4.10 and 4.11 demonstrate that the addition of PN as a mild steel corrosion inhibitor significantly decreased the WL of mild steel in settings containing 0.5 M HCl and 0.25 M H_2SO_4.

(ii) Corrosion rate (CR)

The CR data from Table 4.10 and Table 4.11 show that the presence of PN as mild steel corrosion inhibitor greatly reduced the CR of mild steel in 0.5 M HCl and 0.25 M H_2SO_4 environments. Increase in PN concentration from 100 mg/L to 1000 mg/L further reduced the mild steel CR

(iii) Inhibition efficiency (IE)

The recorded IE results presented in Table 4.10 and Table 4.11 revealed that the addition of PN as mild steel corrosion inhibitor had great effect as the performance of PN on mild steel protection is observed to increase with increasing PN concentration (from 100 mg/L to 1000 mg/L) in 0.5 M HCl and 0.25 M H_2SO_4 environments.

(iv) Degree of surface coverage

Data presented in Table 4.10 and Table 4.11 demonstrate that the addition of PN as mild steel corrosion inhibitor had a significant impact on the degree of surface coverage because it is seen on mild steel to increase with increasing PN concentrations (from 100 mg/L to 1000 mg/L) in 0.5 M HCl and 0.25 M H_2SO_4 environments.

Table 4.10 Weight loss and inhibition efficiency values for mild steel corrosion in 0.5 M HCl in the absence and presence of leave extracts of PN at different immersion time and ± 28ºC

Time(h)	Conc(mg/L)	Initial weight (g)	Final weight (g)	Weight loss (g)	Corrosion rate (mm/yr)	I.E (%)	Degree of surface coverage (Ɵ)
24	Blank	7.9640	7.8060	0.1580	3.8263	–	–
	100	6.8197	6.7780	0.0417	1.0099	73.5992	0.7360
	250	7.7295	7.6896	0.0399	0.9663	74.7072	0.7480
	500	8.2596	8.2348	0.0248	0.6006	84.3305	0.8430
	1000	5.8957	5.8683	0.0275	0.6660	82.6211	0.8260
48	Blank	7.9640	7.7409	0.2231	2.7014	–	–
	100	6.8197	6.7635	0.0562	0.6805	74.8095	0.7480
	250	7.7295	7.6731	0.0564	0.6829	74.7199	0.7470
	500	8.2596	8.2238	0.0358	0.4335	83.9534	0.8400
	1000	5.8957	5.8593	0.0364	0.4408	83.6844	0.8370
72	Blank	7.9640	7.7218	0.2422	1.9551	–	–
	100	6.8197	6.7484	0.0713	0.5756	70.5761	0.7060
	250	7.7295	7.6581	0.0714	0.5764	70.4935	0.7050
	500	8.2596	8.2117	0.0479	0.3867	80.2189	0.8020
	1000	5.8957	5.8491	0.0466	0.3762	80.7557	0.8080
96	Blank	7.9640	7.7057	0.2583	1.5638	–	–
	100	6.8197	6.7353	0.0844	0.5110	67.3379	0.6730
	250	7.7295	7.6445	0.0850	0.5146	67.0668	0.6710
	500	8.2596	8.2009	0.0587	0.3554	77.2701	0.7730
	1000	5.8957	5.8400	0.0558	0.3378	78.4124	0.7840
120	Blank	7.9640	7.6944	0.2696	1.3058	–	–
	100	6.8197	6.7271	0.0926	0.4485	65.6650	0.6570
	250	7.7295	7.6345	0.0950	0.4601	64.7561	0.6480
	500	8.2596	8.1924	0.0672	0.3255	75.0696	0.7510
	1000	5.8957	5.8341	0.0616	0.2984	77.1471	0.7720

The PN leaves extract applied to mitigate corrosion of mild steel in 0.5 M HCl environment is shown to be promising, but the inhibition efficiency reduced with time.

Table 4.11 Weight loss and inhibition efficiency values for mild steel corrosion in 0.25 M H_2SO_4in the absence and presence of leave extracts of PN at different immersion time and ± 28ºC

Time (h)	Conc (mg/L)	Initial weight (g)	Final weight (g)	Weight loss (g)	Corrosion rate (mm/yr)	I.E (%)	Degree of surface coverage (Ɵ)
24	Blank	5.1742	3.9785	1.1958	28.9588	–	–
	100	5.6977	5.0497	0.6480	15.6927	45.8081	0.4580
	250	6.6507	6.2663	0.3844	9.3091	67.8528	0.6790
	500	5.6827	5.4011	0.2816	6.8195	76.4499	0.7650
	1000	5.4107	5.2761	0.1346	3.2596	88.7476	0.8870
48	Blank	5.1742	3.2069	1.9674	23.8224	–	–
	100	5.6977	4.5601	1.1377	13.7759	42.1735	0.4220
	250	6.6507	5.9868	0.6640	8.0401	66.2516	0.6630
	500	5.6827	5.1572	0.5255	6.3631	73.2889	0.7330
	1000	5.4107	5.1076	0.3031	3.6701	84.5960	0.8460
72	Blank	5.1742	3.0702	2.1041	16.9851	–	–
	100	5.6977	4.0236	1.6742	13.5148	20.4320	0.2040
	250	6.6507	5.6697	0.9811	7.9198	53.3733	0.5340
	500	5.6827	4.8590	0.8237	6.6492	60.8517	0.6090
	1000	5.4107	4.9386	0.4721	3.8110	77.5623	0.7760
96	Blank	5.1742	2.9526	2.2216	13.4502	–	–
	100	5.6977	3.4267	2.2711	13.7499	-2.2259	-0.0220
	250	6.6507	5.3003	1.3505	8.1763	39.2127	0.3920
	500	5.6827	4.5125	1.1703	7.0853	47.3240	0.4730
	1000	5.4107	4.7642	0.6465	3.9141	70.9016	0.7090
120	Blank	5.1742	2.8374	2.3369	11.3186	–	–
	100	5.6977	2.8032	2.8945	14.0192	-23.8633	-0.2390
	250	6.6507	4.9065	1.7442	8.4479	25.3611	0.2540
	500	5.6827	4.1288	1.5539	7.5262	33.5045	0.3350
	1000	5.4107	4.5798	0.8309	4.0244	64.4457	0.6440

With 1000 mg/L of PN, inhibition efficiency is noticeably high. It has been demonstrated that using PN leaves extract to prevent mild steel from corroding in an atmosphere with 0.25 M H_2SO_4 is promising but efficiency reduces over time.

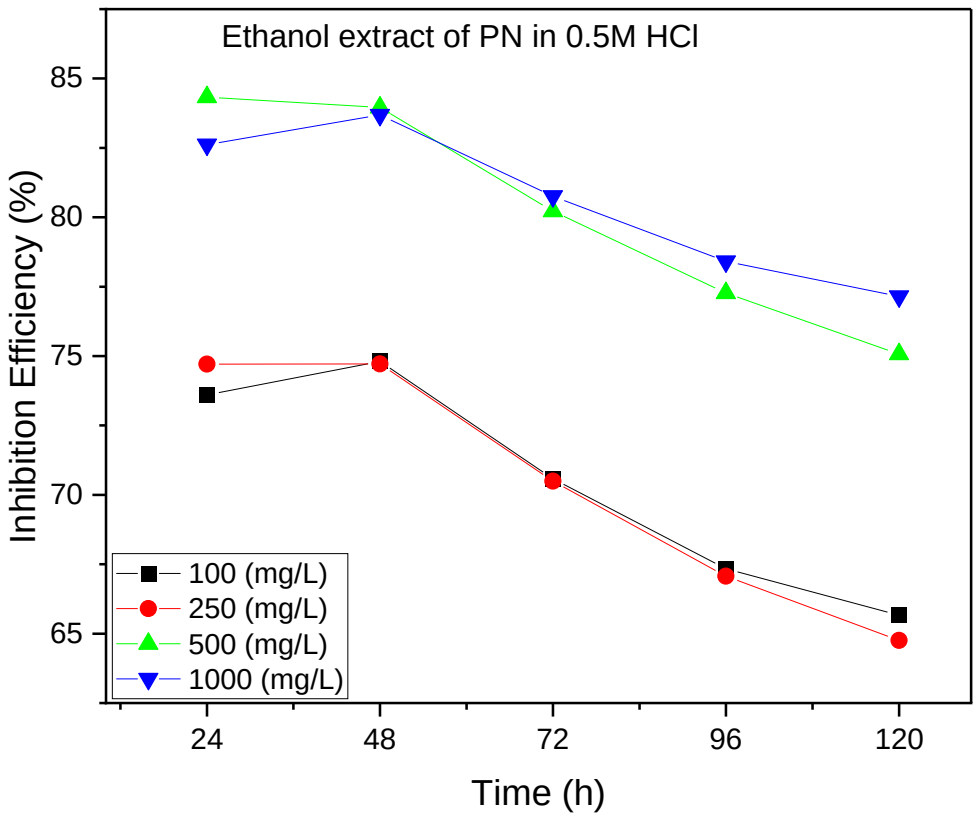

Fig 4.10 Variation of inhibition efficiency of ethanol extract of PN with time for mild steel corrosion in 0.5 M HCl solution

The presence of 1000 mg/L of the PN leaves extract (from Figure 4.10) in the 0.5 M HCl solution boosted its ability to stop mild steel corrosion, although there is noticeably a steady decline in that ability with increasing coupon immersion duration.

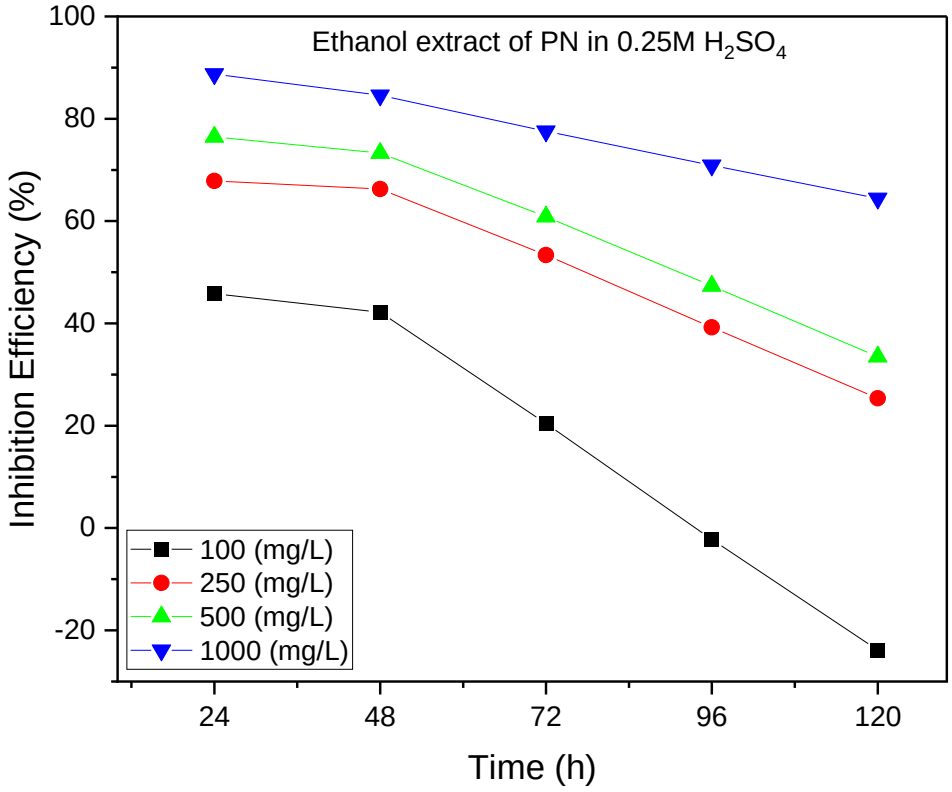

Fig 4.11 Variation of inhibition efficiency of ethanol extract of PN with time for mild steel corrosion in 0.25 M H_2SO_4 solution

With increasing concentration, the PN leaves extract's ability to mitigate corrosion in a 0.25 M H_2SO_4 solution increased, but there is noticeably a steady decline in that ability with increasing coupon immersion duration.

4.1.2 UV-Visible Spectrophotometry

(i) UV-Visible spectra result of PS, PG and PN

The UV-Visible spectra result of freshly and aged ethanol extract of *Pterocarpus santalinoides* (PS), *Piper guineense* (PG) and *Picrilima nitida* (PN) are presented in Figure 4.12 to 4.14.

(a) UV-Visible spectra result of PS

UV-Visible spectra result of aged and new extracts of PS presenting wavelength and absorbance values in Table 4.12

Table 4.12 UV-Visible spectra result of aged and freshly prepared extract of PS

AGED EXTRACT		
S/N	Wavelength (nm)	Absorbance (abs)
1	666.0000	1.6000
2	611.5000	0.4000
3	535.0000	0.4000
FRESH PREPARED EXTRACT		
1	666.5000	6.0000
2	608.5000	1.1000
3	537.0000	1.1000

Table 4.12 shows three values of wavelength for aged and new extract with varying values of both wavelength and absorbance, it is clearly shown that the absorbance value of new extract is higher than that of aged extract. Below is a graphical representation of the values given in Table 4.12

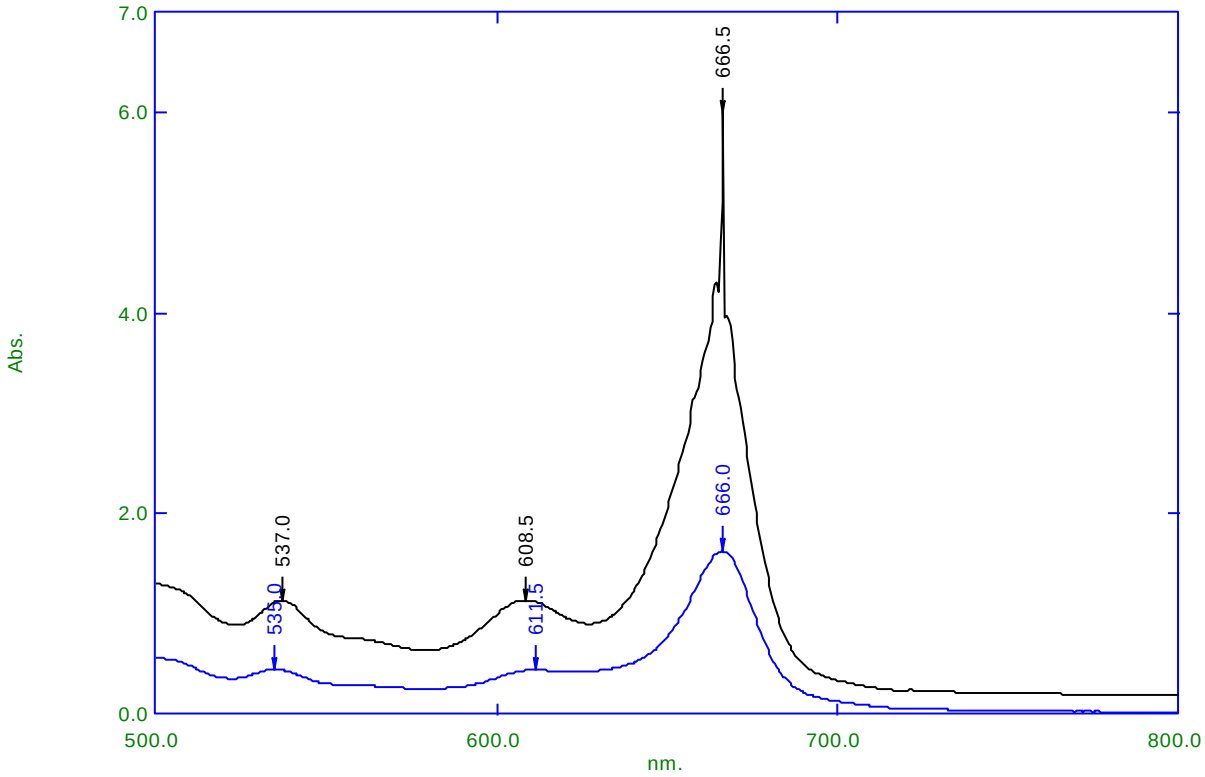

Fig 4.12 UV-visible spectra graphical analysis of new (black) and one month old (blue) *Pterocarpus santalinoides* (PS).

The absorbance of new PS leaves extract is observed to be higher than that of old extract, this could be related to the loss of the functional phytoconstituent with time resulting in loss of concentration. This could also be attributed to the cause of loss of PS leaves extract efficiency with prolonged time of immersion.

(b) UV-Visible spectra result of PG

UV-Visible spectra result of aged and new extract of PG presenting wavelength and absorbance values in Table 4.13

Table 4.13 UV-Visible spectra result of aged and freshly prepared extract of PG

AGED EXTRACT		
S/N	Wavelength (nm)	Absorbance (abs)
1	758.0000	0.0000
2	665.0000	0.1000
3	606.0000	0.0000
FRESH PREPARED EXTRACT		
1	796.0000	0.9000
2	784.5000	0.9000
3	725.0000	1.0000
4	665.5000	1.2000
5	606.5000	1.0000

Table 4.13 above present varying values of both wavelength and absorbance, it is notably revealed that the absorbance value of new extract is higher than that of old extract at some corresponding wavelength values. Below is a graphical representation of the values given in Table 4.13

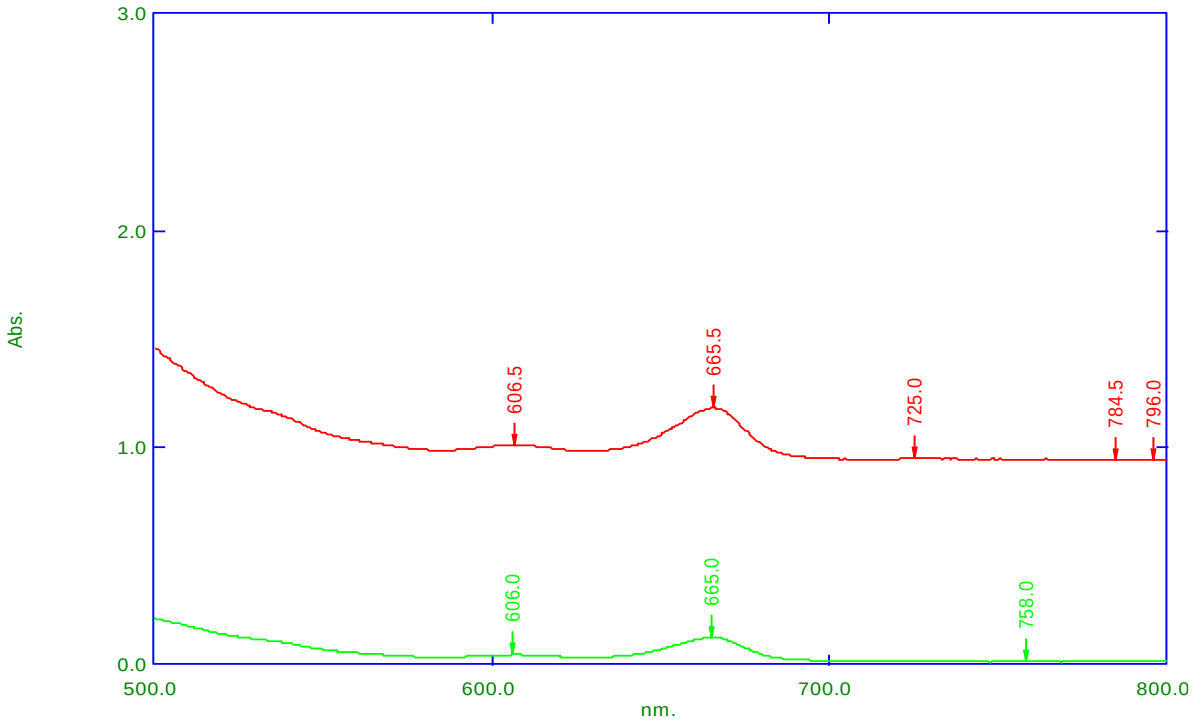

Fig 4.13 UV-visible spectra graphical analysis of new (red) and one month old (old) *Piper guineense* (PG)

The absorbance of new PG leaves extract is observed to be higher than that of old extract, this could be related to the loss of the functional phytoconstituent with time resulting in loss of concentration. This could also be attributed to the cause of loss of PG leaves extract efficiency with prolonged time of immersion.

(c) UV-Visible spectra result of PN

UV-Visible spectra result of aged and new extract of PN presenting wavelength and absorbance values in Table 4.14

Table 4.14 UV-Visible spectra result of aged and new extract of PN

AGED EXTRACT		
S/N	Wavelength (nm)	Absorbance (abs)
1	793.0000	0.0000
2	664.0000	0.6000
3	609.5000	0.2000
4	532.0000	0.3000
5	404.5000	2.5000
FRESH PREPARED EXTRACT		
1	663.5000	3.1000
2	536.5000	0.5000

Table 4.14 above present varying values of both wavelength and absorbance, it is clearly shown that the absorbance value of new extract is higher than that of old extract at some corresponding wavelength values.

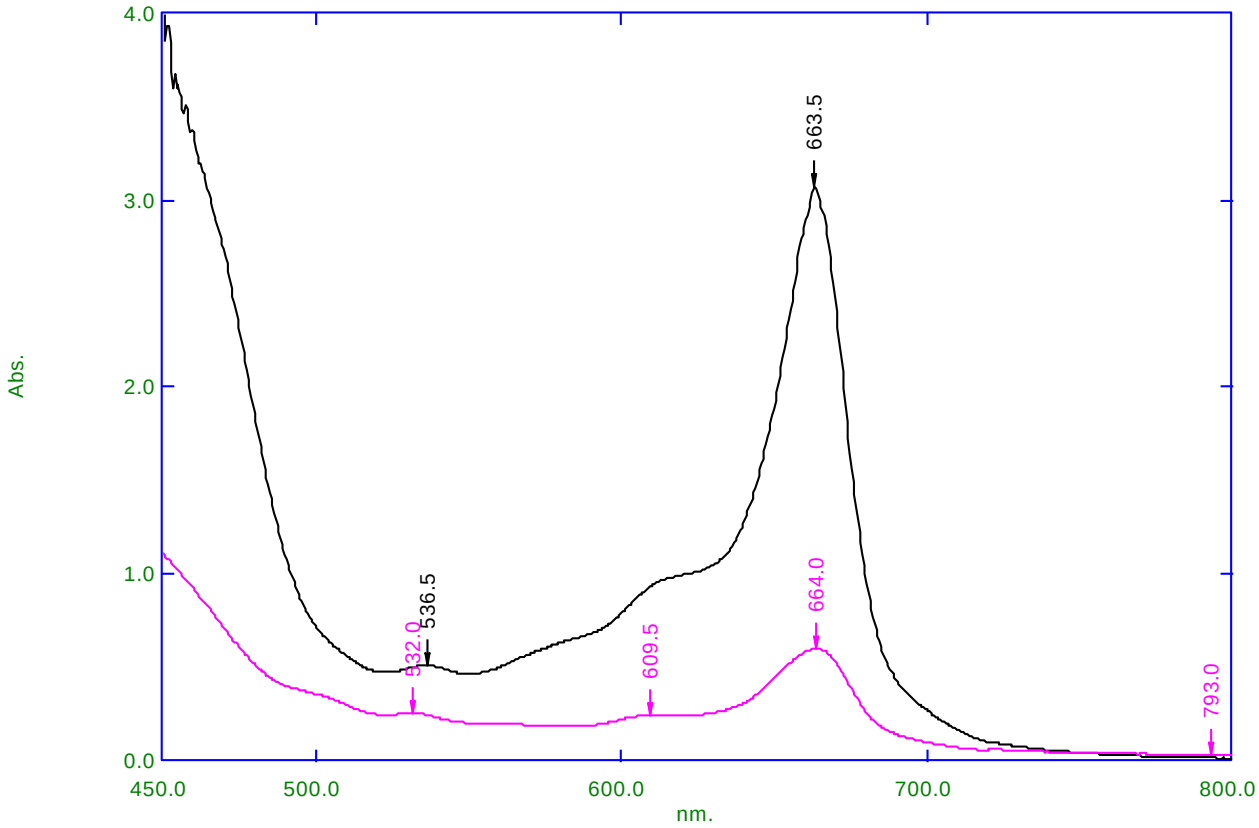

Fig 4.14 UV-visible spectra graphical analysis of new (black) and one month old (purple) *Picrilima nitida* (PN)

The absorbance of new PN leaves extract is observed to be higher than that of old extract, this could be related to the loss of the functional phytoconstituent with time resulting in loss of concentration. This could also be attributed to the cause of loss of PN leaves extract efficiency with prolonged time of immersion.

(ii) UV-Visible spectra result of PS in 0.25 M H_2SO_4, 0.5 M HCl and blend of PS, KI and Sodium alginate

Day-1 and Day-5 UV-Visible spectra result of PS in 0.25 M H_2SO_4, 0.5 M Cl and blend of PS, KI and sodium alginate are presented in Figure 4.15 to 4.20.

(a) UV-Visible spectra result of PS in 0.25 M H_2SO_4

UV-Visible spectra result of PS in 0.25 M H_2SO_4 presenting wavelength and absorbance values in Table 4.15

Table 4.15 UV-Visible spectra result of PS in 0.25 M H_2SO_4

DAY-1		
S/N	Wavelength (nm)	Absorbance (abs)
1	763.5000	0.2000
2	723.5000	0.2000
3	706.0000	0.2000
4	657.0000	0.2000
5	624.5000	0.2000
6	607.5000	0.2000
7	571.5000	0.2000
8	530.5000	0.2000
9	467.5000	0.2000
10	446.5000	0.2000
11	409.0000	0.2000
DAY-5		
1	752.0000	0.1000
2	706.5000	0.2000
3	674.0000	0.2000
4	667.0000	0.2000
5	496.0000	0.2000

Table 4.15 present varying number of peaks values when PS is present in 0.25 M H_2SO_4 in Day-1 and Day-5. It is clearly shown that the number of PS peaks reduced with time which could be attributed to loss of the active phytoconstituents in 0.25 M H_2SO_4 environment. Below is a graphical representation of the values given in Table 4.15

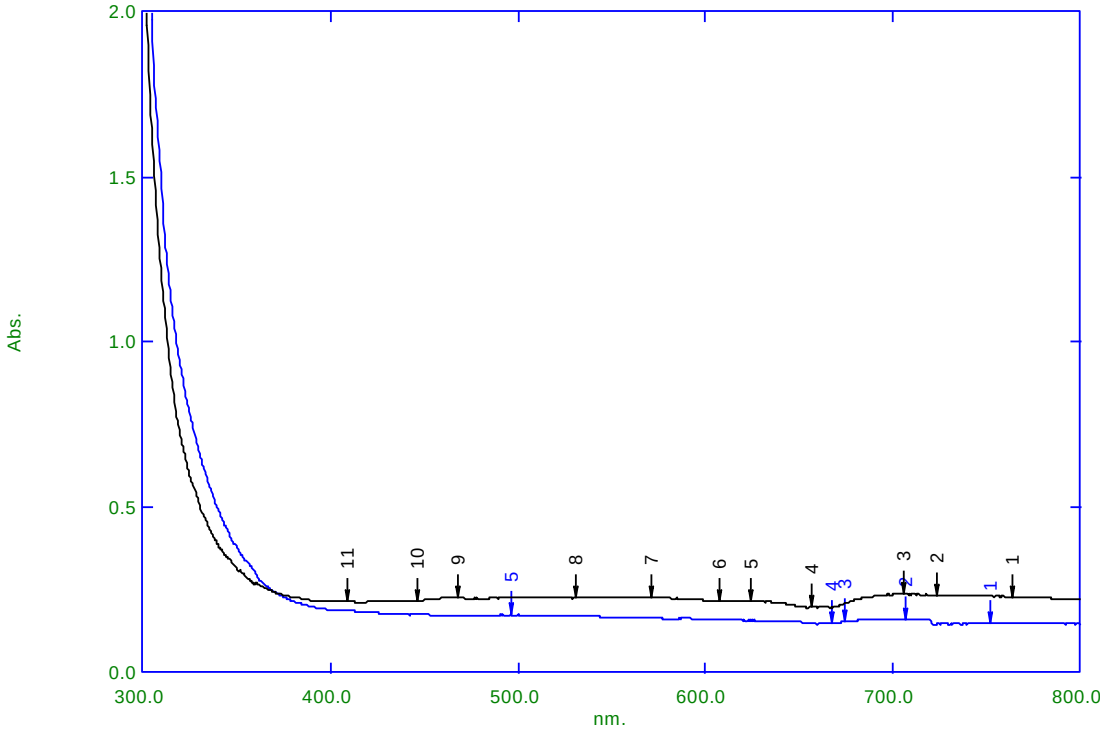

Fig 4.15 Day-1 (black) and Day-5 (blue) UV-visible spectra graph showing the peaks of PS in 0.25 M H_2SO_4

Figure 4.15 is a UV-Vis graph showing the peaks of PS in 0.25 M H_2SO_4 for day-1 and day-5. There is clearly a reduction of peaks with time, this is clearly indicating that PS is losing the functional phytoconstituents which could be attributed to the loss of inhibition efficiency in the environment.

(b) UV-Visible spectra result of PS in 0.5 M HCl

UV-Visible spectra result of PS in 0.5 M HCl presenting wavelength and absorbance values in Table 4.16

Table 4.16 UV-Visible spectra result of PS in 0.5 M HCl

DAY-1		
S/N	Wavelength (nm)	Absorbance (abs)
1	692.5000	0.6000
2	613.5000	0.5000
3	547.5000	0.6000
4	514.5000	0.6000
5	466.5000	0.6000
DAY-5		
1	734.5000	0.2000
2	727.5000	0.2000
3	711.0000	0.3000
4	588.0000	0.3000
5	420.0000	0.3000

Table 4.16 shows same number of peaks values when PS is present in 0.5 M HCl in Day-1 and Day-5. While the number of peaks remain the same, it is clearly shown that the absorbance values of PS differ with respect to time.

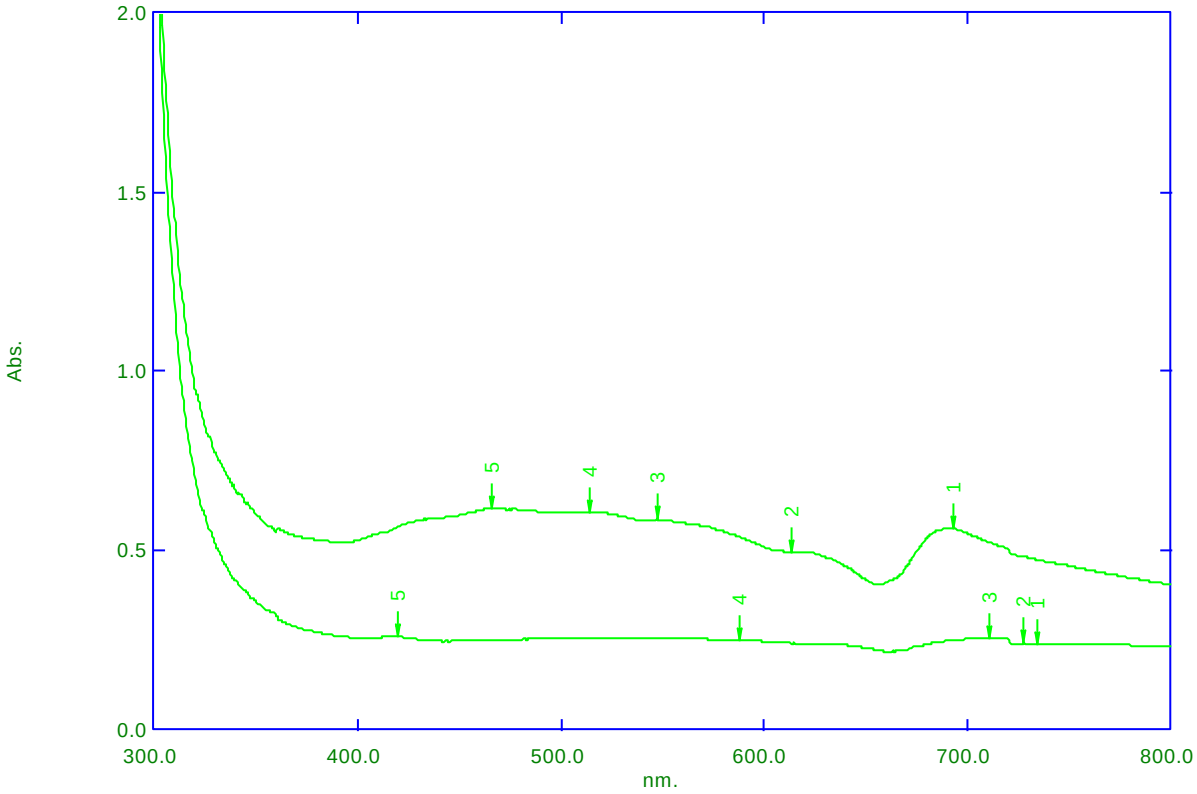

Fig 4.16 Day-1 (upper green) and Day-5 (lower green) UV-visible spectra graph showing the peaks of PS in 0.5 M HCl

Figure 4.16 is a UV-Vis graph showing the peaks of PS in 0.5 M HCl for day-1 and day-5. There are clearly varying values of absorbance which may be a function of the reduced chromophoric units of PS with time in 0.5 M HCl environment, this could also be attributed to the cause of loss of inhibition efficiency in the environment.

(c) UV-Visible spectra result of blend of PS, KI and sodium alginate in 0.25 M H_2SO_4

UV-Visible spectra result of blend of PS, KI and sodium alginate in 0.25 M H_2SO_4 presenting wavelength and absorbance values in Table 4.17

Table 4.17 UV-Visible spectra result of blend of PS, KI and sodium alginate in 0.25 M H_2SO_4

DAY-1		
S/N	Wavelength (nm)	Absorbance (abs)
1	767.5000	1.0000
2	693.5000	1.0000
3	331.5000	2.5000
4	317.0000	3.1000
DAY-5		
1	756.5000	1.1000
2	737.5000	1.1000
3	697.5000	1.1000
4	690.0000	1.1000

Table 4.17 present the same number of peaks values when blend of PS, KI and sodium alginate is present in 0.25 M H_2SO_4 in Day-1 and Day-5. While the number of peaks remain the same, it is notably revealed that the absorbance values of the blend differ with little value difference with respect to time.

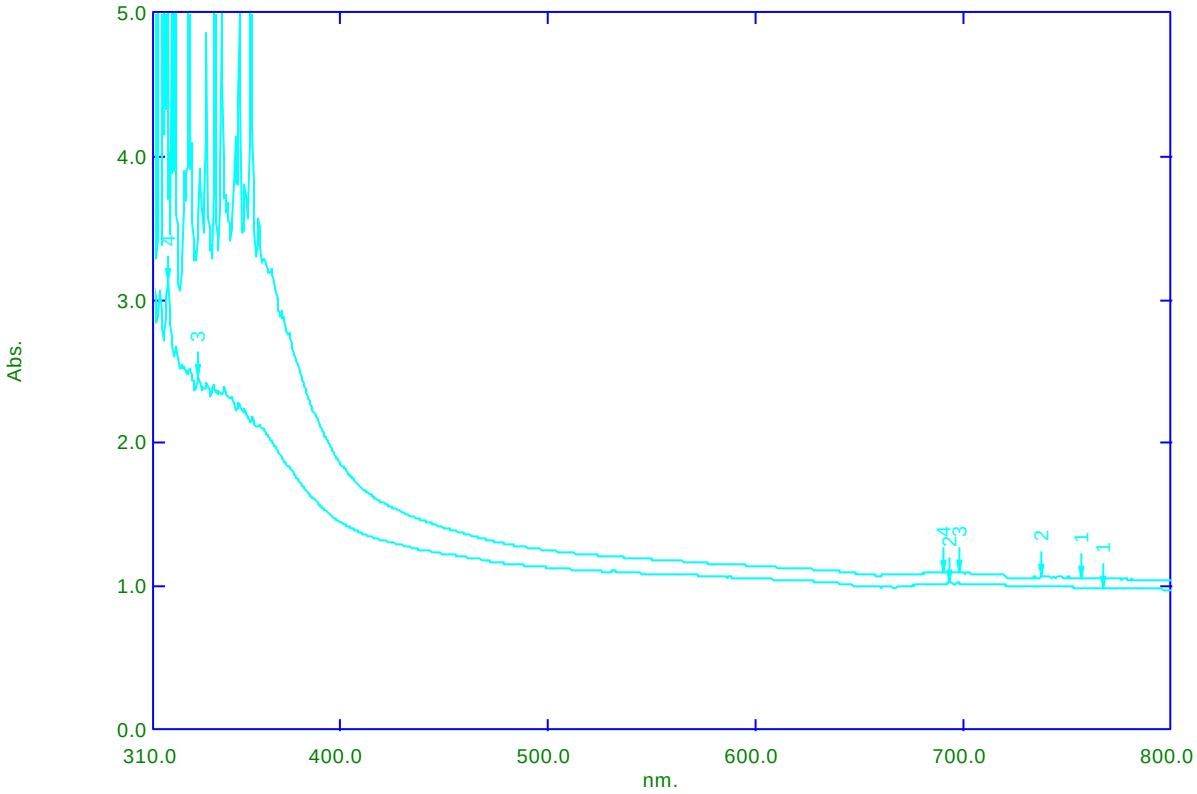

Fig 4.17 Day-1 (upper) and Day-5 (lower) UV-visible spectra graph showing the peaks of blend of PS, KI and sodium alginate in 0.25 M H_2SO_4

Figure 4.17 is a UV-Vis graph showing the peaks of blend of PS, KI and sodium alginate in 0.25 M$H_2SO_4$for day-1 and day-5. There are clearly insignificant varying values of absorbance which may be a function of the retained chromophoric units of PS with time in 0.25 M H_2SO_4 environment, this could also be attributed to the good inhibition efficiency of the blend in 0.25 M H_2SO_4 environment.

4.1.3 Gas Chromatography Mass Spectrometry Results of *Pterocarpus santalinoides* (PS)

The identified peaks of the unknown phytochemical components of ethanol leaves extract of *Pterocarpus santalinoides* analyzed using GC (Agilent 6890N) and MS (5973B MSD) are presented in Figure 4.18

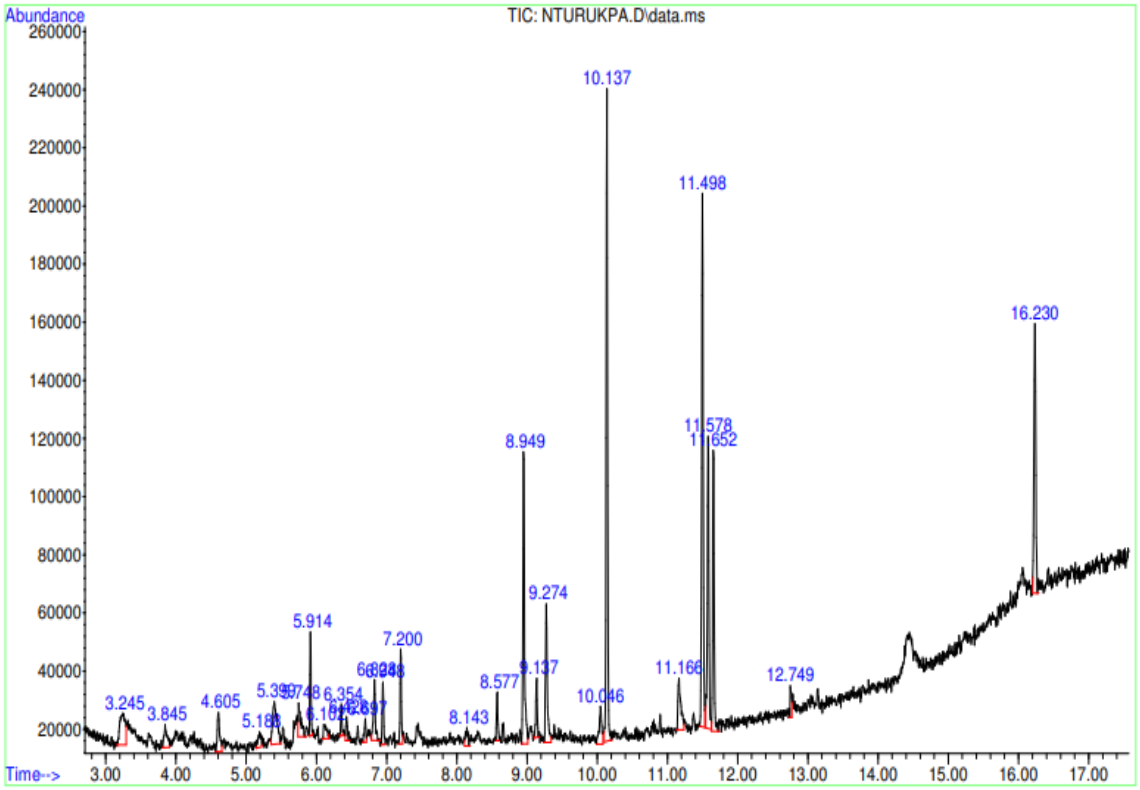

Fig 4.18 GC-MS Chromatogram of PS leaf extract

The identification of the unknown phytochemical components present in ethanol extract of PS was analyzed using GC-MS. Their individual mass spectral peak value was compared with the database of National Institute of Science and Technology 2014. Then identification was done by comparing the unknown peak value and chromatogram from GC-MS against the known chromatogram peak value from the NIST Library database. The obtained molecular formula, molecular weight, retention time and percentage content were obtained alongside as presented in Appendix (1).

The selected phytochemical constituents observed from result with high percentage composition are presented in Table 4.18

Table 4.18 Selected compounds from the identified compounds from GC-MS analysis

S/N	Structure	Retention time	% Composition	MW (g/mol)
1	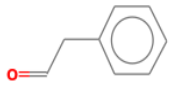 Benzeneacetaldehyde	3.8450	0.6800	120.1500
2	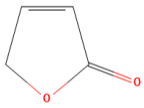 2(5H)-Furanone	3.2450	1.7300	84.0700
3	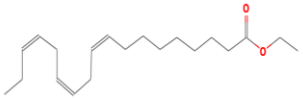 Ethyl 9,12,15-octadecatrienoate	11.5780	4.7200	306.4800
4	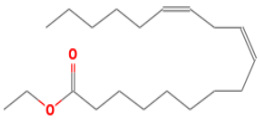 Linoleic acid ethyl ester	11.4980	8.1900	308.5000
5	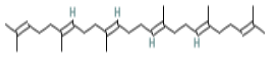 Squalene	16.2300	4.8600	410.7300

GC-MS was employed to extensively and further characterize the leaf extract of PS. Hence, the Tables above are the corresponding phytocompounds and their properties identified from GC-MS analysis. The full detail of all identified compounds and their properties are detailed in Appendix (1).

4.1.4 Theoretical (Computational) Studies

Computational studies carried out to augment the experimental analysis in the laboratory were done using the DFT program, Forcite optimization and Quench

module tool respectively. The pictorial illustrations for PS are presented in Figure 4.19(a & b) to 4.23(a & b).

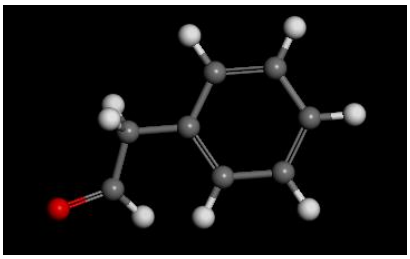

Benzeneacetaldehyde

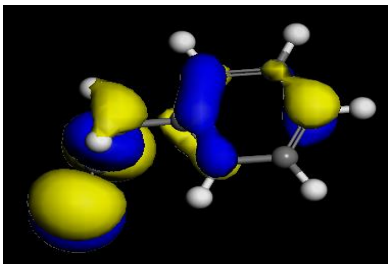

HOMO

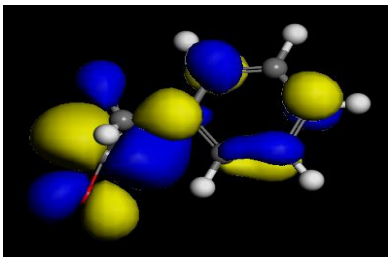

LUMO

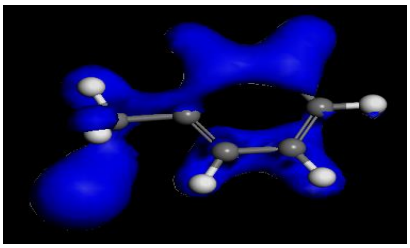

(Electrophilic (f^-))

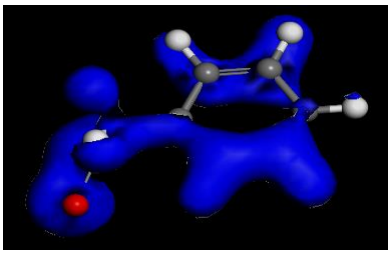

(Nucleophilic (f^+))

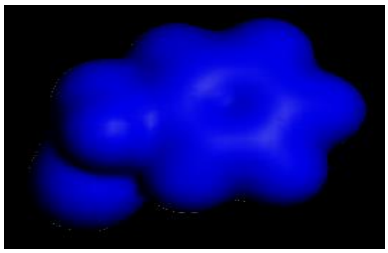

Total electron density

Fig 4.19a Electronic properties of Benzeneacetaldehyde (BA) from PS extract. **(Atomic legend: white= H; gray = C; red = O; blue = N. The blue and yellow isosurfaces depict the electron density difference: The blue regions show electron accumulation while the yellow regions show electron loss).**

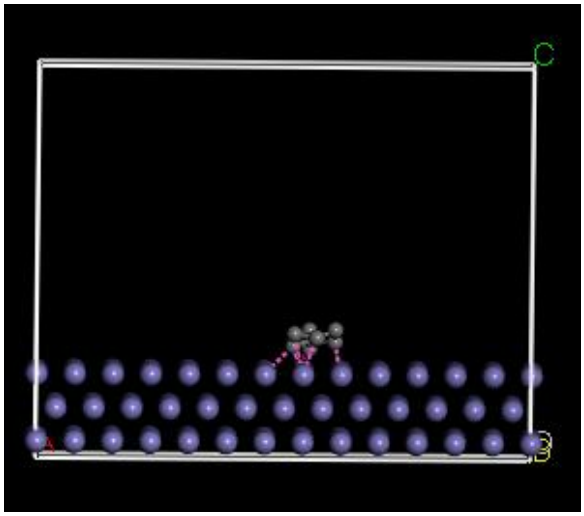

Fe-inh interaction

Fig 4.19b Benzene acetaldehyde (BA) adsorbed on Fe crystal surface

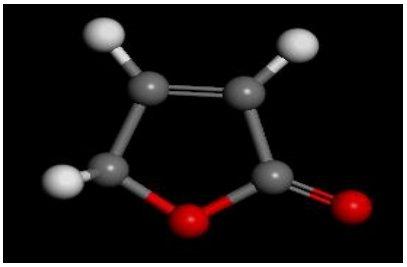

2(5H)-Furanone

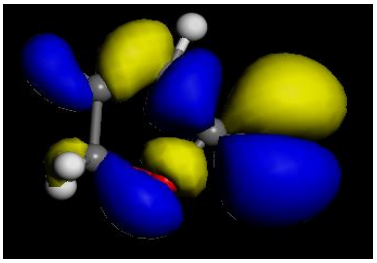

HOMO

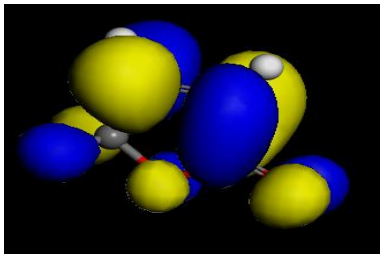

LUMO

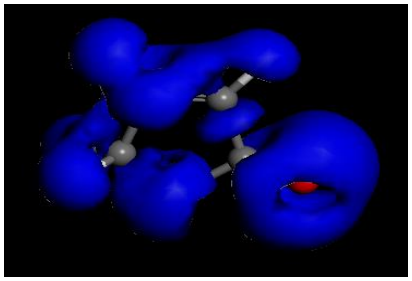

(Electrophilic (f^-))

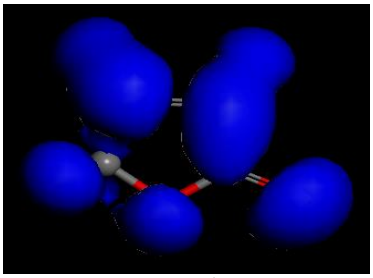

(Nucleophilic (f^+))

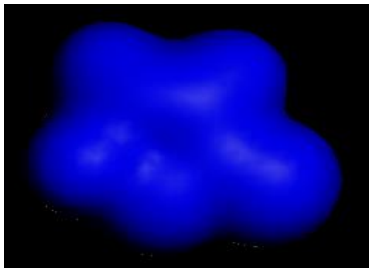

Total electron density

Fig 4.20a Electronic properties of 2(5H)-Furanone (FUR) from PS extract.
(Atomic legend: white= H; gray = C; red = O; blue = N. The blue and yellow isosurfaces depict the electron density difference: The blue regions show electron accumulation while the yellow regions show electron loss).

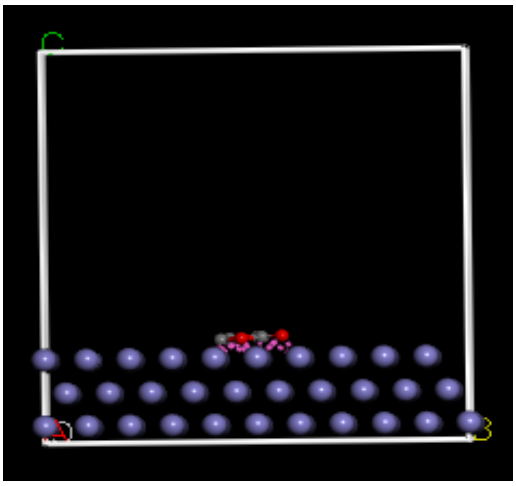

Fe-inh interaction

Fig 4.20b 2(5H)-Furanone (FUR) adsorbed on Fe crystal surface

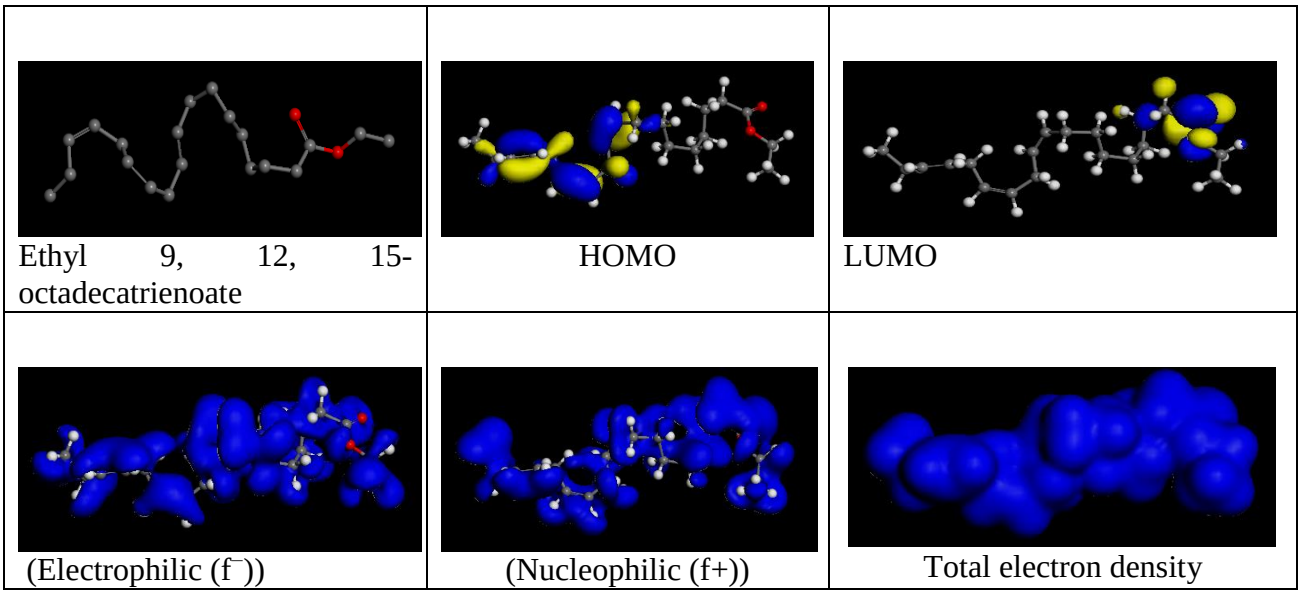

Fig 4.21a Electronic properties of Ethyl 9, 12, 15-octadecatrienoate (EOD) from PS extract. **(Atomic legend: white= H; gray = C; red = O; blue = N. The blue and yellow isosurfaces depict the electron density difference: The blue regions show electron accumulation while the yellow regions show electron loss).**

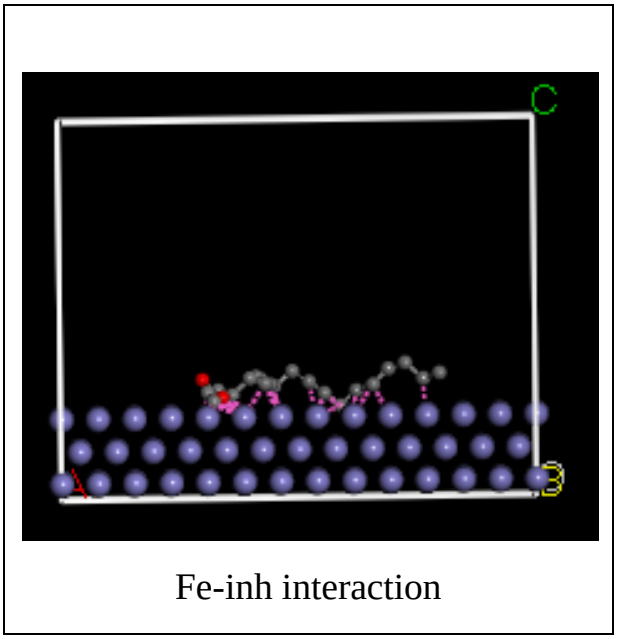

Fig 4.21b Ethyl 9, 12, 15-octadecatrienoate adsorbed on Fe crystal surface

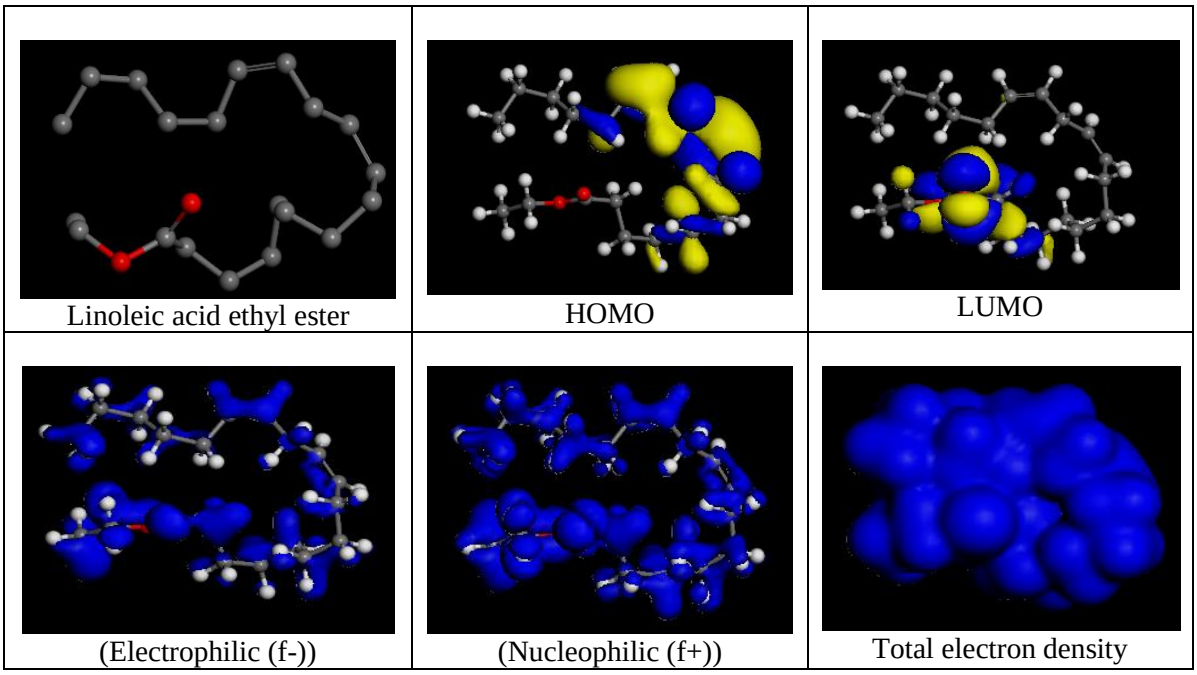

Fig 4.22a. Electronic properties of Linoleic acid ethyl ester (LAEE) from PS extract. **(Atomic legend: white= H; gray = C; red = O; blue = N. The blue and yellow isosurfaces depict the electron density difference: The blue regions show electron accumulation while the yellow regions show electron loss).**

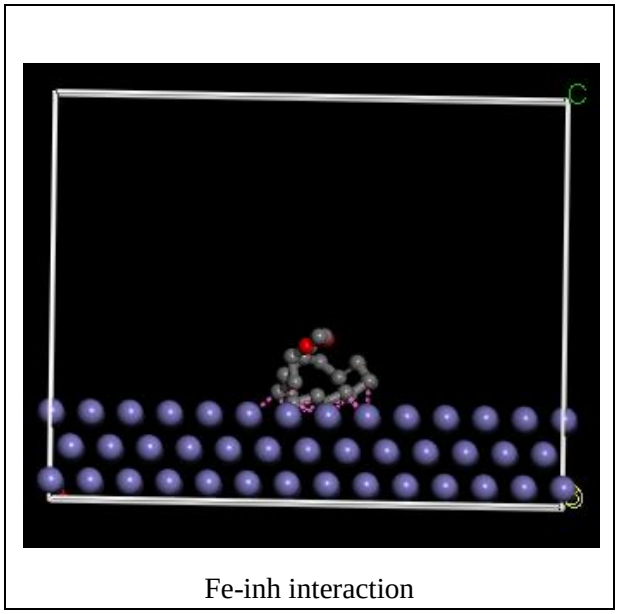

Fig 4.22b Linoleic acid ethyl ester adsorbed on Fe crystal surface

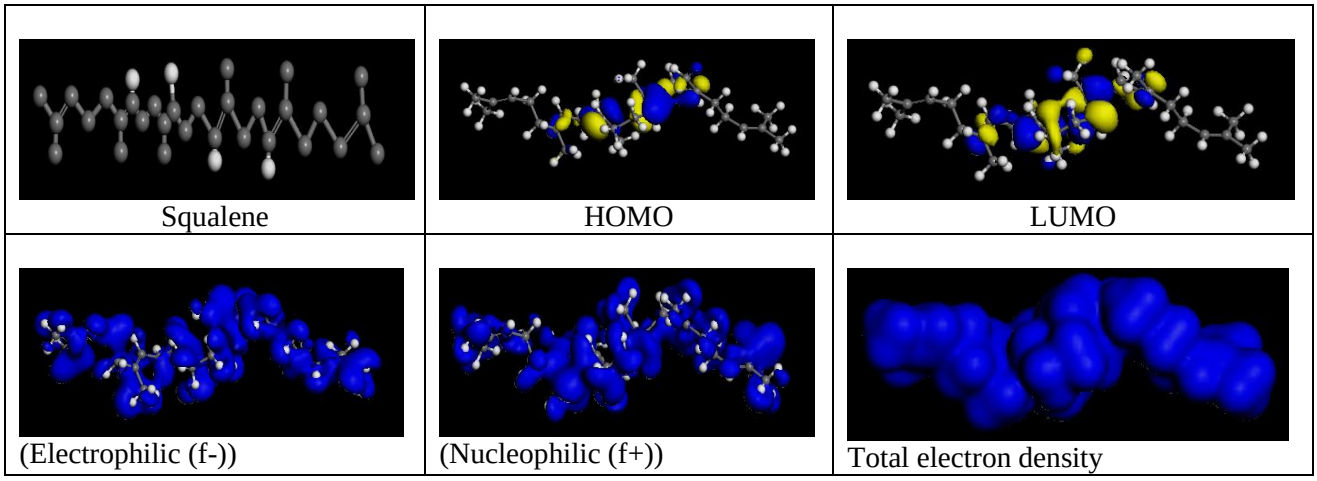

Fig 4.23a Electronic properties of Squalene (SQU) from PS extract.
(Atomic legend: white= H; gray = C; red = O; blue = N. The blue and yellow isosurfaces depict the electron density difference: The blue regions show electron accumulation while the yellow regions show electron loss).

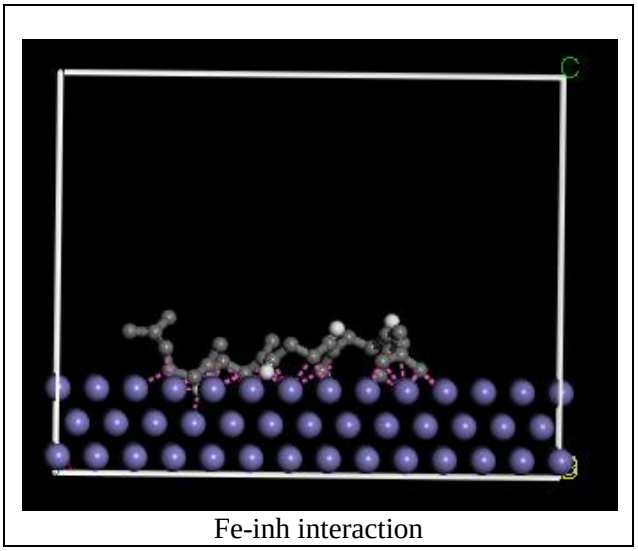

Fig 4.23b Squalene adsorbed on Fe crystal surface

Values obtained and calculated from optimized structures, calculated quantum chemical properties and interaction energies of the selected and major phytoconstituents of PS using DFT model (computational) are presented in Table 4.19.

Table 4.19 Calculated quantum chemical properties values

S/N	Compounds	E_{HOMO} (ev)	E_{LUMO} (eV)	ΔE (eV)	X	η	ΔN	Binding Energy (kJ/mol)
1	Benzene acetaldehyde	-5.7075	-2.0858	3.6217	3.9000	3.6200	0.4280	-83.9000
2	2(5H)-Furanone	-6.3536	-2.4001	3.9535	4.3800	1.9800	0.6620	-74.7000
3	Ethyl 9,12,15-octadecatrienoate	-5.3669	-0.8421	4.5248	3.1100	2.2600	0.8610	-192.2000
4	Linoleic acid ethyl ester	-5.4445	-0.8680	4.5765	3.1600	2.2900	0.8380	-230.3000
5	Squalene	-5.0135	-0.3930	4.6205	2.7000	2.3100	0.9310	-321.2000

Table 4.19 above is presenting the functional and abundance phytoconstituents identified by GC-MS analysis. The compounds were optimized and calculations were possible with the use of Material Studio (DFT Model, DMol3 and Forcite Quench Tools) to obtain the quantum chemical properties and interaction energies of the major phytoconstituents of PS.

4.1.5 Fourier Transform Infrared (FTIR) Spectroscopy Analysis

FTIR studies and analysis was done using the Agilent Technology Cary 630 FTIR, basically to electrochemically augment the laboratory findings. Hence, the graphical presentation of the interaction between PS and the mild steel surface and blends of PS, sodium alginate, KI and the mild steel surface are presented in Figure 4.24(a-i).

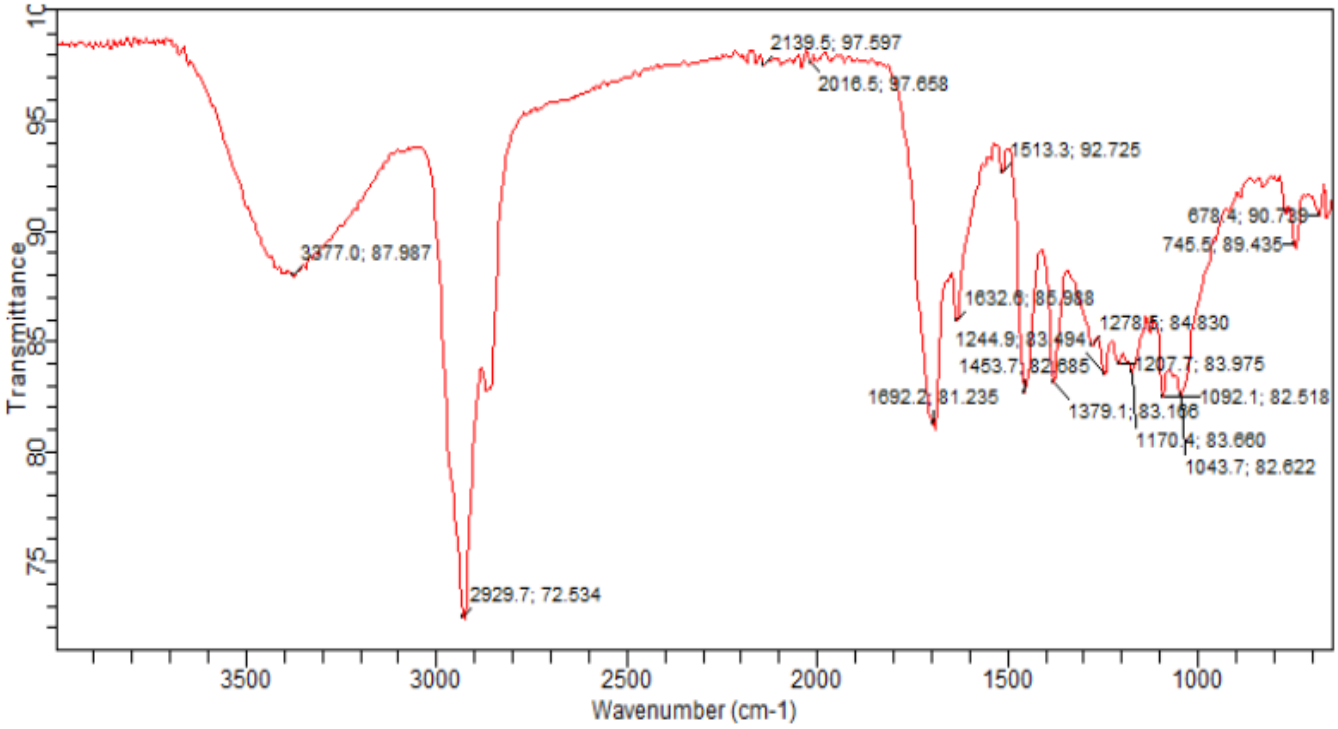

Fig 4.24a FTIR spectrum of ethanol extract of PS

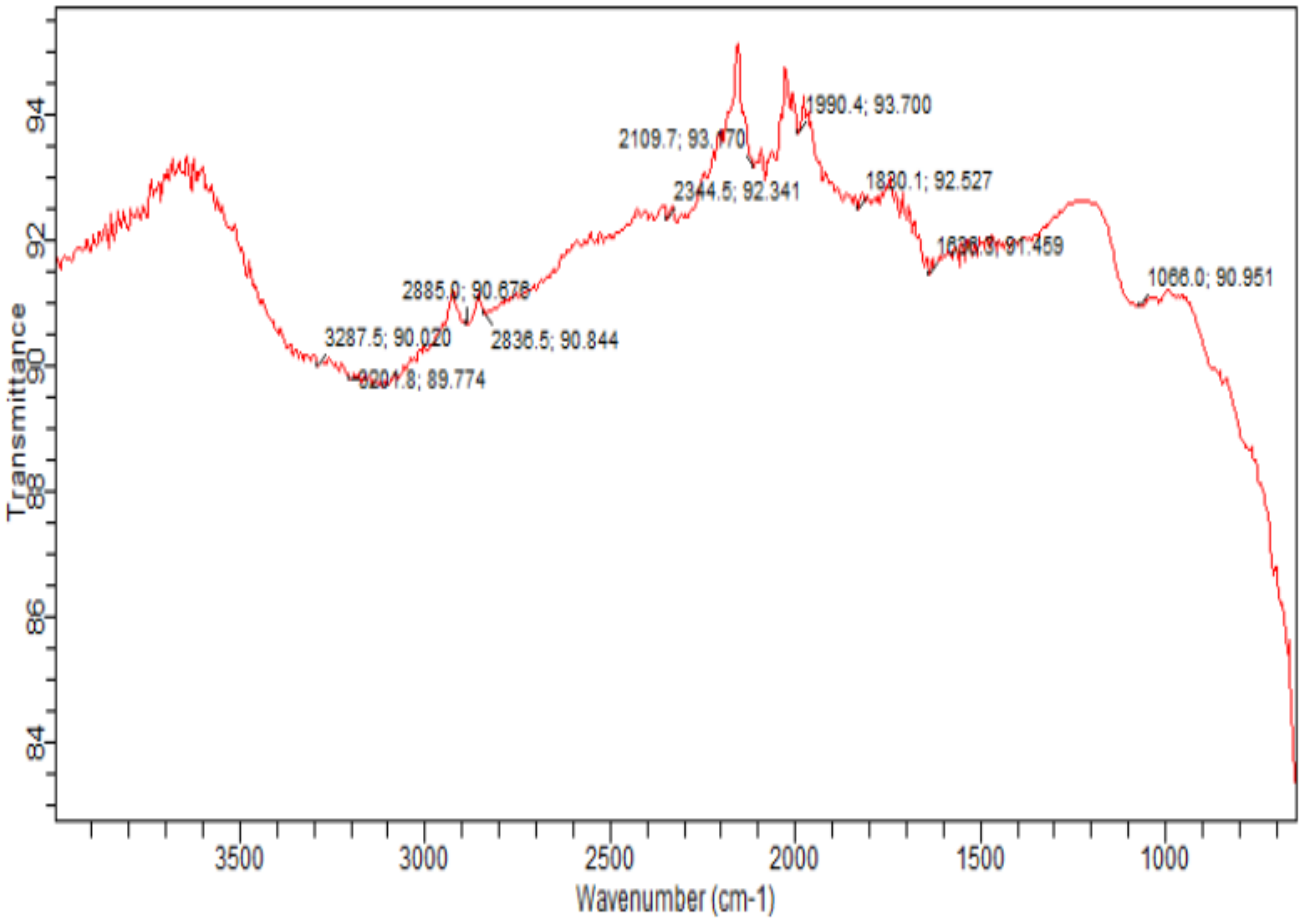

Fig 4.24b FTIR spectrum of mild steel in 0.25 M H_2SO_4 containing 1000 mg/L of PS

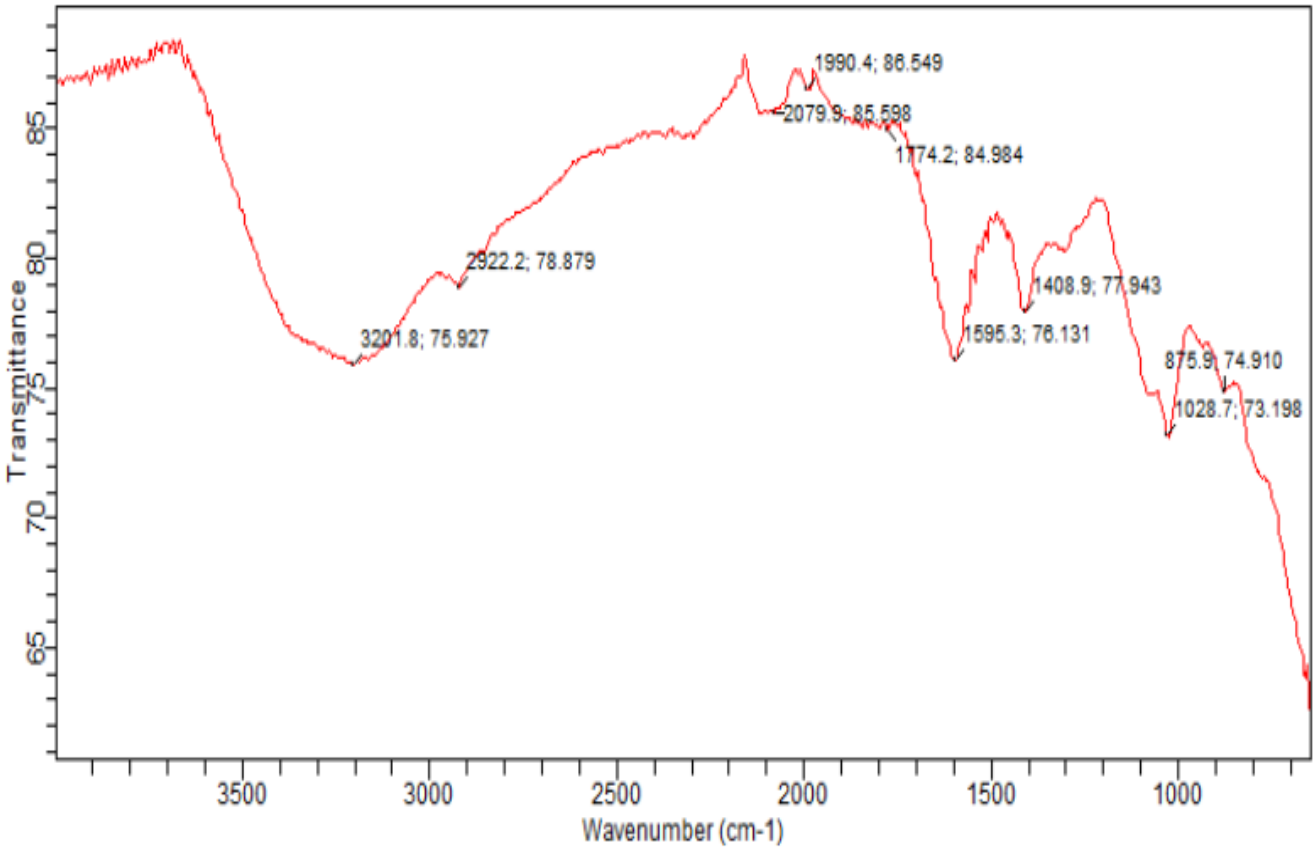

Fig 4.24c FTIR spectrum of mild steel in 0.25 M H_2SO_4 containing 500 mg/L of PS, 500 mg/L of sodium alginate and 0.025 M of KI

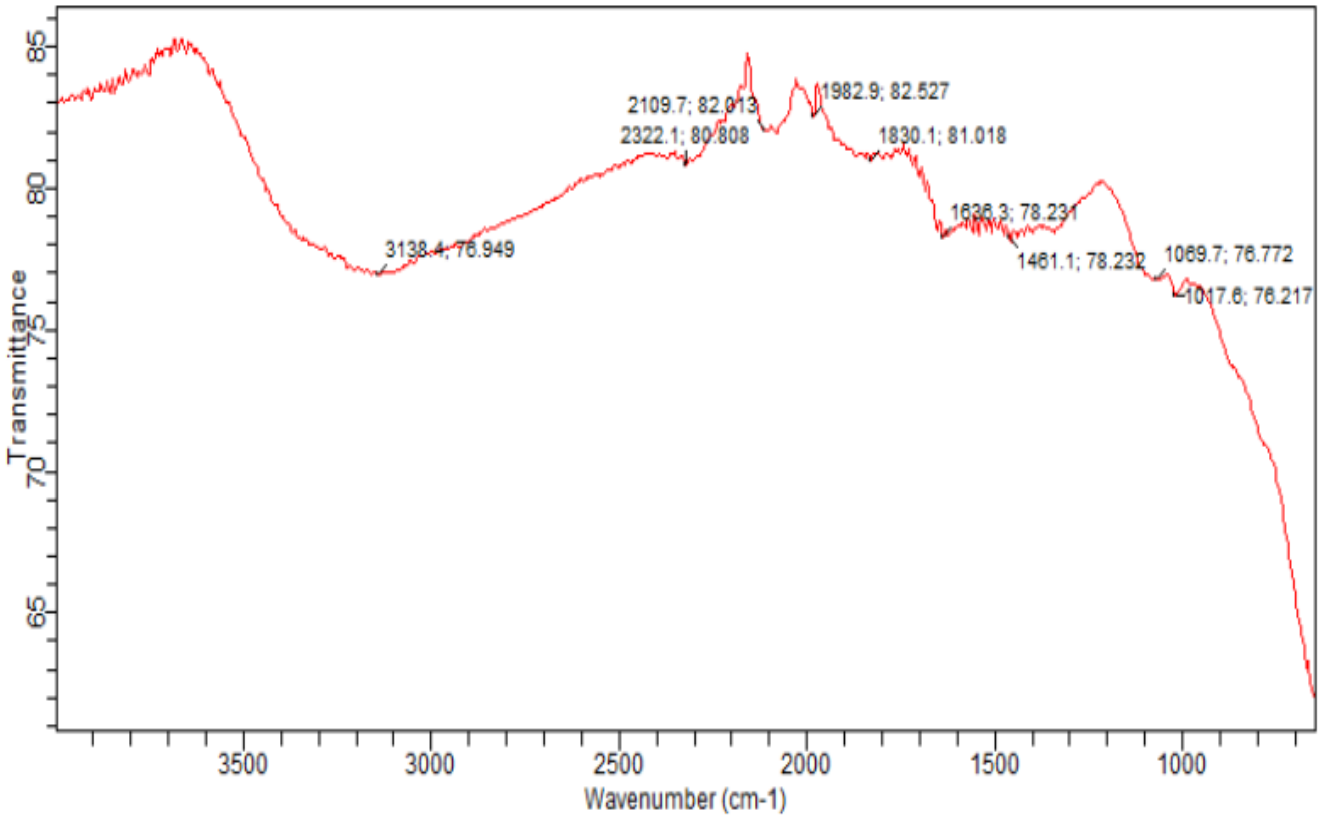

Fig 4.24d FTIR spectrum of mild steel in 0.25 M H_2SO_4 containing 1000 mg/L of PS and 0.025 M of KI

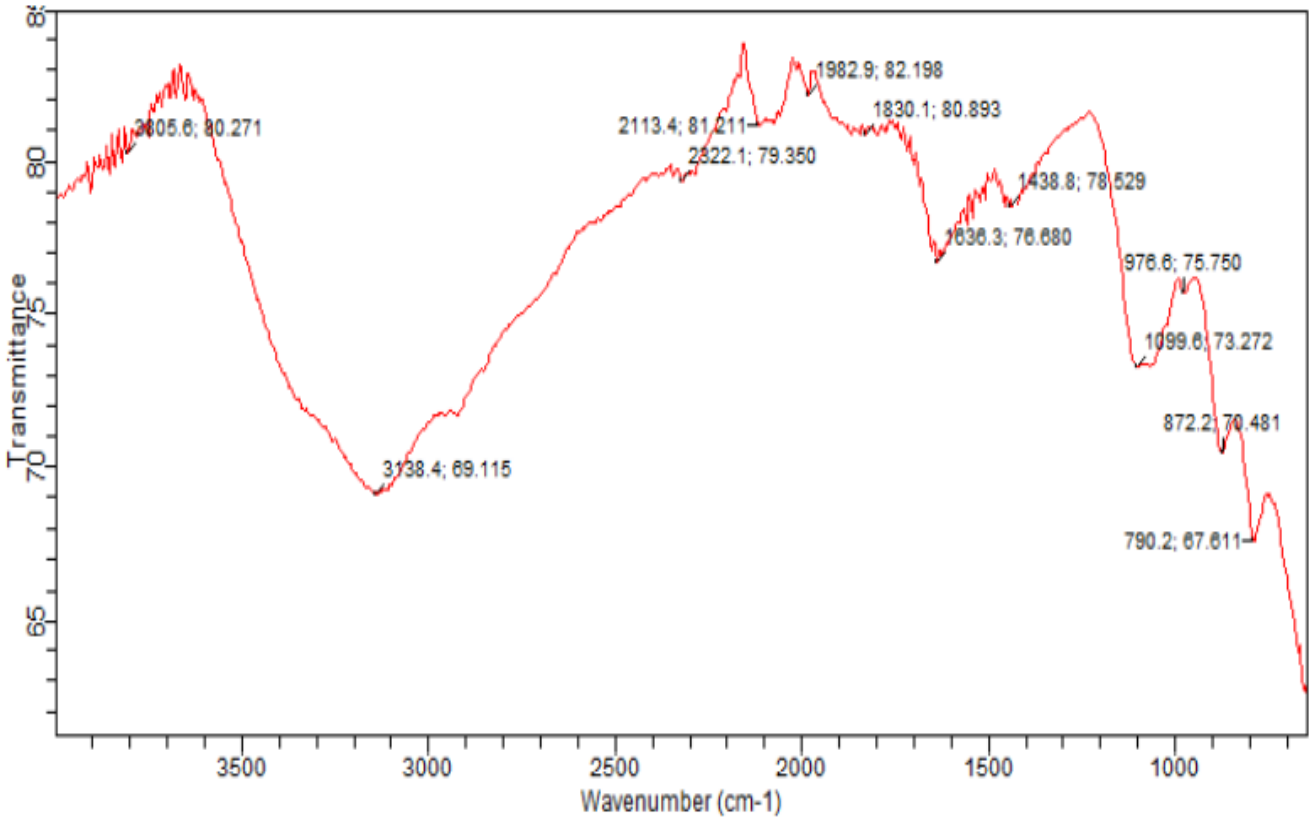

Fig 4.24e FTIR spectrum of mild steel in 0.25 M H_2SO_4 containing 500 mg/L of PS and 500 mg/L of sodium alginate

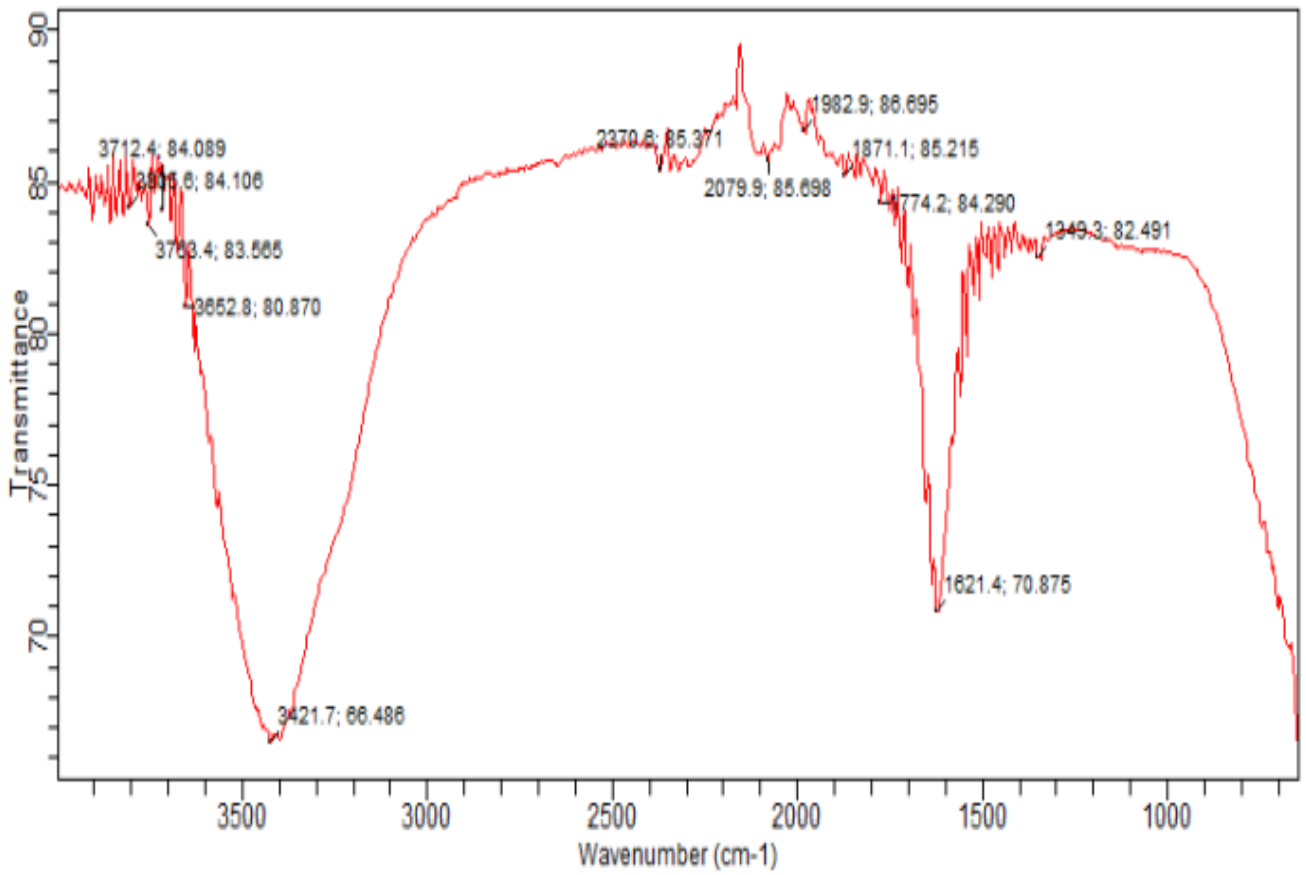

Fig 4.24f FTIR spectrum of mild steel in 0.25 M H_2SO_4 containing 0.025 M of KI

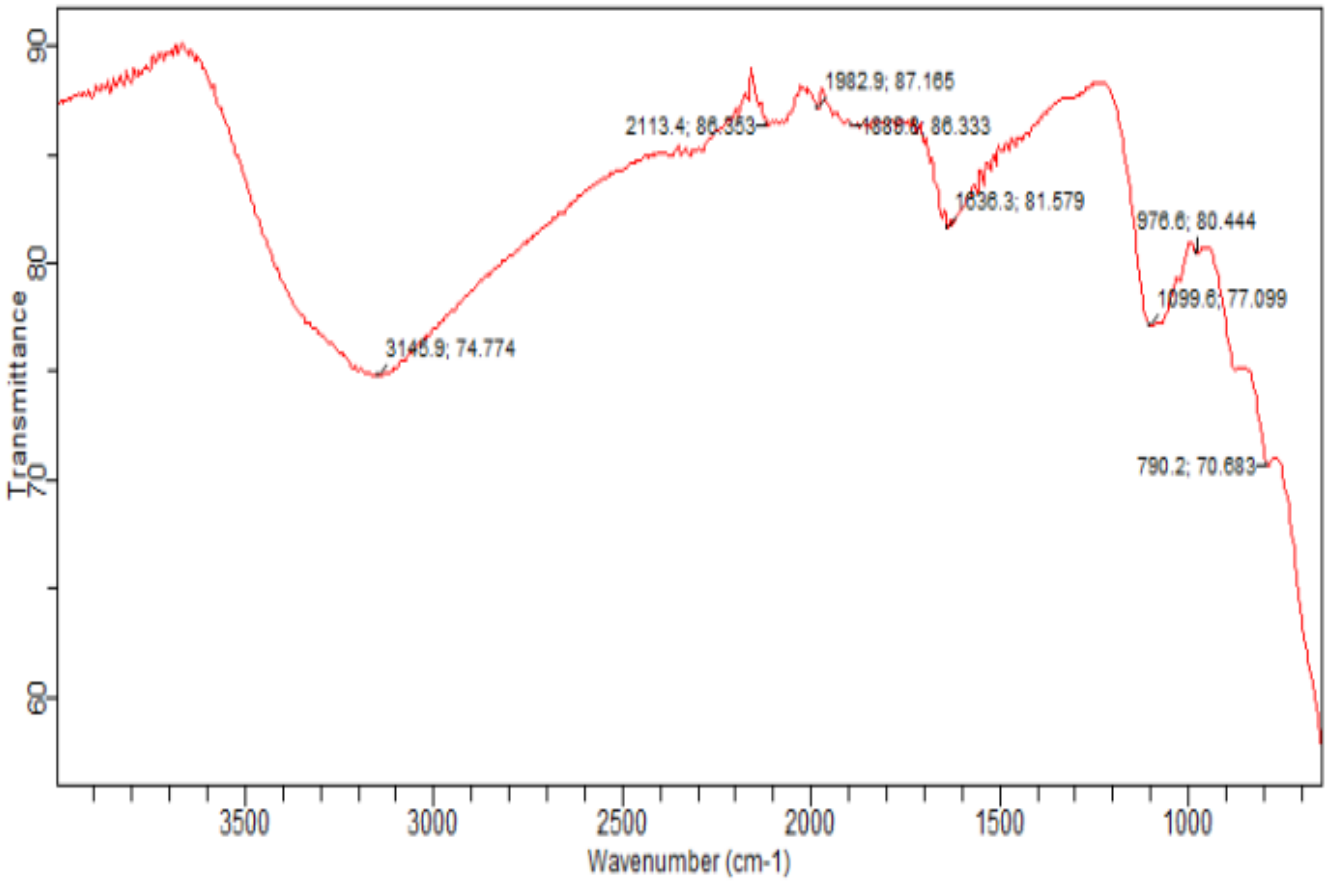

Fig 4.24g FTIR spectrum of mild steel in 0.25 M H_2SO_4 containing 1000 mg/L of sodium alginate

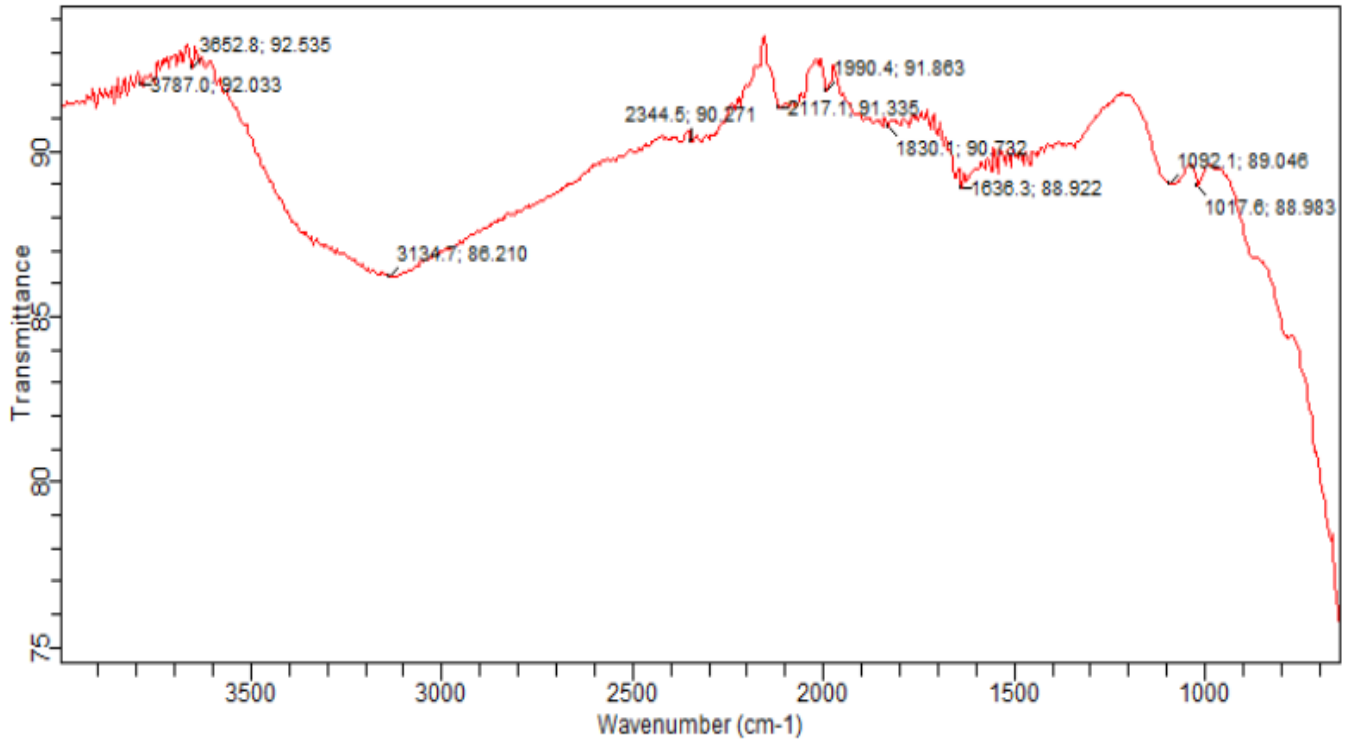

Fig 4.24h FTIR spectrum of KI

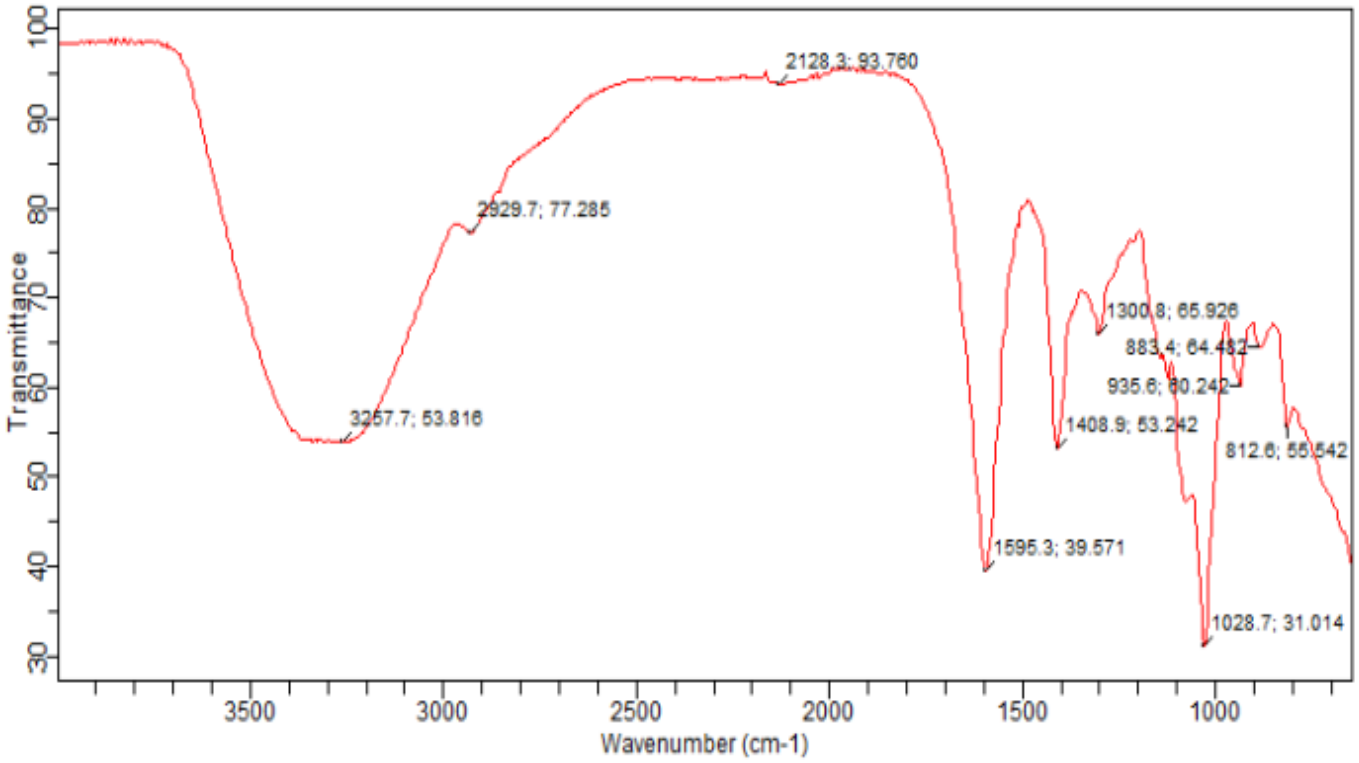

Fig 4.24i FTIR spectrum of sodium alginate

4.1.6 Adsorption Isotherm and Thermodynamic Parameters

The interaction between PS molecules as inhibitor and the active locations of the surface of mild steel is possibly defined by adsorption isotherms, hence, to better evaluate and analyze the inhibition mechanism, the adsorption isotherm was performed. Furthermore, Langmuir isotherm, as widely accepted and most conventional model (Golchinvafa *et al*., 2020; Matad *et al*., 2014) was employed, hence Table 4.20 was generated.

To also determine if the adsorption of PS as an inhibitor on the surface of the mild steel was of physical or chemical type (Golchinvafa *et al*., 2020; Matad *et al*., 2014), the thermodynamic parameter of ΔG^{o}_{ads} was evaluated and analyzed to reveal required information as shown in Table 4.21

Table 4.20 Calculated Langmuir isotherm properties values

S/N	C/Θ (g/L)	C (g/L)
1	0.1681	0.1000
2	0.3157	0.2500
3	0.5727	0.5000
4	1.1312	1.0000

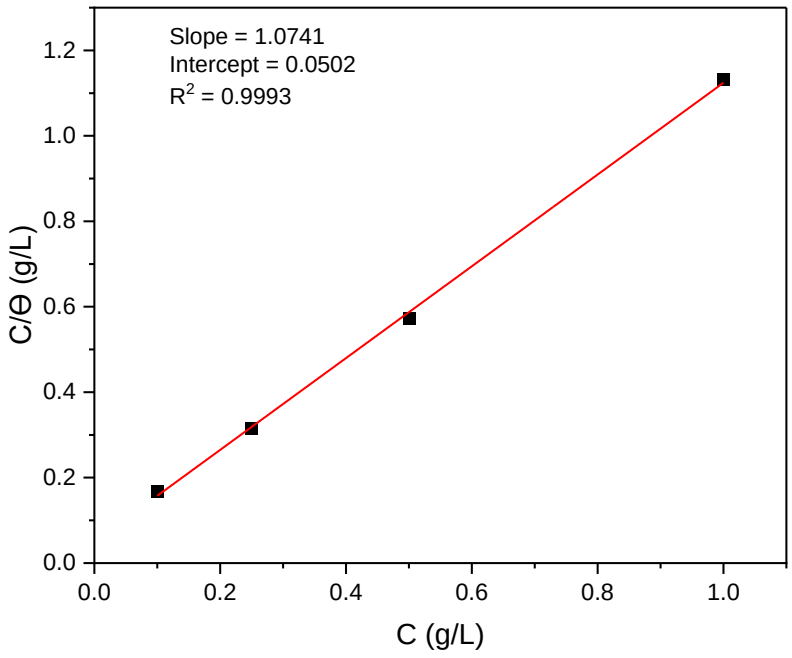

Fig 4.25 Langmuir adsorption isotherm for the adsorption of PS on the surface of the mild steel at room temperature

Table 4.21 Calculated thermodynamic parameters of ΔG^{o}_{ads}

Temperature ºC	**± 28**
K_{ads}	19.9200
ΔG^{0}_{ads} (KJ/mol)	-42.0800

4.1.7 Synergistic Index (SI)

The calculated SI parameter was obtained using the inhibition efficiency from gravimetric analysis. Hence, the SI values of 1000 mg/L: 0.025 M (PS: KI) and 500 mg/L: 500 mg/L (PS: sodium alginate) are presented in Table 4.22

Table 4.22 Calculated SI values

Time (h)	SI of PS:KI	SI of PS: sodium alginate
24	1.7631	1.1919
48	1.6914	0.9460
72	1.4801	0.6354
96	1.3144	0.3067
120	1.1508	0.0438

4.2 DISCUSSION

4.2.1 Gravimetric Data

Pterocarpus santalinoides (PS), *Piper guineense (PG)*, *Picrilima nitida* (PN) extracts reduced the weight loss of mild steel coupons immersed in HCl and H_2SO_4. Hence, the inhibition efficiency (IE) of the extracts were notably good in HCl environment but excellent in H_2SO_4 environment.

(a) Ethanol extract of *Pterocarpus santalinoides*, PS

The inhibition efficiency of ethanol extract of PS was proved in HCl and H_2SO_4 using gravimetric analysis (Ahanotu *et al*., 2020). Experimentally, the maximum corrosion inhibition efficiency of 1000 mg/L concentration of PS in 0.25 M H_2SO_4 environment in 24 h is 88%, also the maximum corrosion inhibition efficiency of 1000 mg/L concentration of PS in 0.5 M HCl environment in 24h is 80%, hence, PS inhibition efficiency was more pronounced in 0.25 M H_2SO_4 environment compared to 0.5 M HCl environment. Although inhibition efficiency of PS in these systems reduced with increasing immersion time. For instance, the efficiency at 24 h of immersion at 1000 mg/L concentration in 0.25 M H_2SO_4 was 88%, by 48 h it reduced

to 80%, this reduction in inhibition efficiency was noticed in 0.5 M HCl. This implies that the concentration of the acid environment is significantly influencing the performance of the extract. The reason for this is not very clear, but could be related to the degree of protonation of relevant organic phytoconstituents of the extract, which would improve their adsorption on the mild steel surface.

Hence, in order to maintain prolonged inhibition efficiency (IE), potassium iodide, KI and sodium alginate was combined with PS as a blend to experimentally observe their performance in 0.25 M H_2SO_4. Resultantly, the blend of these compounds shows positive results. Conclusively, these compounds as a blend significantly maintained efficiency above 96% up to 120 h in 0.25 M H_2SO_4, this could be as a result of the excellent adsorption properties of the inhibitor's blend on the surface of the mild steel in 0.25 M H_2SO_4. Results obtained from gravimetric analysis correlate with results obtained by (Njoku *et al*., 2021; Ahanotu *et al*., 2020).

The corrosion rate of mild steel in HCl without an inhibitor was 3.8166 (mm/yr) in 24 hours period, the corrosion rate dropped to 0.7822 (mm/yr) with the addition of 1000mg/L PS as inhibitor to the acidic environment in 24 hours period (Table 4.1). By 120 h, the corrosion rate dropped again from 1.3726 (mm/yr) to 0.4955 (mm/yr). This is as a result of good inhibition efficiency of PS. Also, the corrosion rate of mild steel in H_2SO_4 was 17.2619 (mm/yr) without PS in Table 4.2, the corrosion rate dropped to 2.0052 (mm/yr) after 24 h with 1000mg/L of PS as inhibitor, by 120 h, the corrosion rate dropped again from 4.9577 (mm/yr) to 2.7840 (mm/yr). This is also as a result of good inhibition efficiency of PS. The corrosion rate of mild steel in H_2SO_4 was 18.1628 (mm/yr) without an inhibitor, but the corrosion rate dropped to 0.5594 (mm/yr) after 24 h with the introduction of the optimum blend (Table 4.7) as inhibitor, by 120 h, the corrosion rate dropped again from 12.4708 (mm/yr) to 0.2364 (mm/yr). This is as a result of excellent inhibition efficiency of the blend (Ayoola *et al*., 2018).

Higher degree of surface coverage promotes inhibition efficiency, hence an inhibitor with high degree of surface coverage could be attributed to reason for high inhibition efficiency (Ayoola *et al*., 2018). The blend of PS, KI and sodium alginate (Table 4.7) shows excellent degree of surface coverage which directly promoted the inhibition efficiency.

(b) Ethanol extract of *Piper guineense*, PG

The ethanol extract of PG was also effective in 0.5 M HCl, just like PS, it is more effective in 0.25 M H_2SO_4 with maximum efficiency of about 90% at 1000 mg/L concentration and 93% at 1000 mg/L concentration respectively in 24 h but the inhibition efficiency of PG in these systems reduced with increasing immersion time. For instance, the efficiency at 24 h of immersion at 1000 mg/L concentration in 0.25 M H_2SO_4 was 93% but by 48 h it reduced to 92%, this reduction in inhibition efficiency was noticed also in 0.5 M HCl. This implies that the concentration of the acid environment is significantly affecting the performance of PG. The reason for this is not very clear as indicated earlier. Hence, for excellent and prolonged inhibition efficiency (IE), more research work is required. Results obtained from gravimetric analysis correlate with results obtained by Njoku *et al*., (2021) and Ahanotu *et al*., (2020).

(c) Ethanol extract of *Picrilima nitida*, PN

The ethanol extract of PN was also effective in 0.5 M HCl, it is notably more effective in 0.25 M H_2SO_4 with maximum IE of about 83% at 1000 mg/L concentration and 89% at 1000 mg/L concentration respectively in 24 h. it was also noted that the inhibition efficiency of PN in these systems reduced with increasing immersion time. For instance, IE of 1000 mg/LPN in 0.25 M H_2SO_4 was 89% after 24 h however, by 48 h it reduced to 84%, this reduction in inhibition efficiency was observed also in 0.5 M HCl. This implies that 0.25 M H_2SO_4 concentration of the

acid environment is significantly influencing the performance of PN. The reason for this is not very clear. Hence, for excellent and prolonged IE, more research work is required. Results obtained from gravimetric analysis correlate with results obtained by Njoku *et al*., 2021 and Ahanotu *et al*., 2020.

4.2.2 Gas Chromatography Mass Spectrometry Results of *Pterocarpus santalinoides*

From the GC/MS data represented in Appendix (1) and spectrum represented in Figure 4.18, the extract contained 36.54% Methylene chloride, 8.99% Hexadecanoic acid ethyl ester, 8.19% Linoleic acid ethyl ester, 6.19% Benzeneseleninic anhydride, 5.52% Neophytadiene, 4.86% squalene, 4.72% Ethyl 9,12,15-octadecatrienoate, 4.23% Octadecanoic acid ethyl ester while the remaining 20.76% belong to the other constituent as can been seen clearly in Appendix (1). More than 28 phytoconstituents were detected by the equipment with the presence of many small peaks indicating that there are more phytocomponents far more than the number detected as can be seen in Figure 4.18. It is important to note that the constituents were identified after comparison with those available in the computer library attached to the instrument and reported. Therefore, the structural assignment is based on spectral matching with NIST library (National Institute of standards and Technology 2014). Similar approach has been recorded by (Rosli *et al*., 2019; Vasyliev & Vorobiova, 2019).

4.2.3 UV-Visible Spectra Results

The UV-visible spectrophotometric analysis of the ethanol extract of *Pterocarpus santalinoides* (PS), *Picrilima nitida* (PN) and *Piper guineense* (PG) was undertaken in order to attempt possible visualization of the number of peaks for each extract, which could be related to the chromophoric units involved in the corrosion inhibition process, also the UV-visible spectrophotometric analysis was carried out to

investigate the reason why inhibition efficiency decline within short period of time. Figure 4.12 – 4.14 illustrate by comparing the UV-visible spectra graph for the new extract of the various natural materials and one month old of the same natural materials.

Note:

- Dilution of *Pterocarpus santalinoides* (PS): ratio of extract to ethanol (1ml:1ml).
- Dilution of *Piper guineense* (PG): ratio of extract to ethanol (1ml:0.25ml).
- Dilution of *Picrilima nitida* (PN): ratio of extract to ethanol (1ml:1ml).

The UV-visible spectrophotometer characterization was performed to identify the compounds containing σ-bonds, π-bonds and lone pair of electrons, chromophores and aromatic rings. The qualitative UV-VIS profile of ethanolic extract of PS, PG, and PN was taken at the wavelength of 500 nm to 800 nm, 500 nm to 800 nm, 450 nm to 800 nm respectively due to the sharpness of the peaks and proper baseline. The profile showed the peaks at (535nm, 611.5nm, 666nm) & (537nm, 608.5nm, 666.5nm) for old and new extract of PS respectively, the profile also showed the peaks at (606nm, 665nm, 758nm) and (606.5nm, 665.5nm, 725nm, 784.5nm, 796nm) for old and new extract of PG respectively, finally the profile showed the peaks at (532nm, 609.5nm, 664nm, 793nm) & (536.5nm, 6635nm) for old and new extract of PN respectively.

The appearance of one or more peaks in the graph in the UV-VIS spectrum is a blatant sign that unsaturated groups and heteroatoms like S, N, and O are present (Karpagasundari & Kulothungan, 2014). Furthermore, the presence of organic chromophores inside the extracts of PS, PG, and PN is confirmed by the peaks that were detected. Nevertheless, the inherent challenges in tagging the absorption peaks to any specific system constituents place a limit on the application of UV-visible spectrophotometer in the investigation of complex media. To enable proper extract characterization and constituents identification using UV-visible spectrophotometer

(Keerthana & Ashraf, 2020; Galvão *et al*., 2016), other analytical techniques such as GC/MS, etc., must be added to UV-VIS findings.

Figure 4.12, 4.13and 4.14 respectively are UV-visible spectrophotometer graph of one month old and new ethanol extract of PS, PG, and PN respectively. A careful observation of the graph will reveal that these extracts have higher value of absorbance (Abs.) when freshly extracted compared to the aged extract. The value of Abs of each extract is observed to vary with time. An aged extract could affect inhibition performance with time, hence aged extract could be attributed to the poor IE. Furthermore, UV-visible spectrophotometer was utilized to analysis and investigate the number of peaks an inhibitor will generate Keerthana & Ashraf, (2020); Galvão *et al*., (2016) in an acidic environment for day 1 and day 5. Thus, Figure 4.15 to 4.17 present graphs showing inhibitors peaks overtime in the various acidic environments. Progressively, Figure 4.15 and 4.16 respectively showed the extent of peak reduction with time. Furthermore, the maintained IE effect of the blend of PS, KI and Sodium alginate in 0.25 M H_2SO_4 is presented in Figure 4.17, hence the number of peaks observed in the graph for day-1 is insignificantly the same in day-5 (peak was maintained) up to 120 h.

4.2.4 Theoretical (Computational) Studies

Overtime, computational studies (Quantum Chemical methods) have been applied and results obtained has also proven to be very useful in elucidating the electronic structures and hence predict the adsorption characteristics of the selected constituents of the extract in view (Njoku *et al*., 2021; Rouifi *et al*., 2019). Hence, recent studies have also shown that it is important to carry out quantum chemical calculations in corrosion inhibition studies.

Calculations have been carried out to model the adsorption structures of some selected conformational chemical constituent of PS extracts. The selected chemical

constituents from PS extract are: Benzene acetaldehyde (BA), 2(5H)-Furanone (FUR), Ethyl 9,12,15-octadecatrienoate (EOD), Linoleic acid ethyl ester (LAEE), Squalene (SQU).

The drive and major reason for theoretical (computational) studies is to provide some insight by simulating and predicting the nature of these extract's individual constituents and their interaction with the metal surface which could give us insight on their individual possible contributions to the overall inhibition effect observed experimentally.

The theoretical calculation was done in the frame work of density functional theory (DFT) using DMol^3 and Forcite module tools respectively as contained in material studio (BIOVIA) 2017 version. Hence, the structures of the selected phytoconstituents for PS extract and the calculated quantum properties (E_{HOMO}, E_{LUMO}, ΔE energy etc.) are contained in Table 4.19. The regions of highest occupied electron molecular orbitals (HOMO) and lowest unoccupied molecular orbitals (LUMO) in the selected organic constituents of the extracts were calculated and are very important parameters that determine the reactivity, softness and corrosion inhibition capabilities of compounds (Njoku *et al*., 2021).

The tendency of a molecule to donate electrons to the vacant d orbitals within the Fe atom is reflected by high values of E_{HOMO}. In the same way, low values of the energy of the gap ($\Delta E = E_{LUMO-HOMO}$) means that the energy required to remove an electron from the last occupied orbital will be minimized, resulting in improved inhibition efficiencies. Hence, smaller energy gaps correspond to better stability (Rouifi *et al*., 2019).

The LUMO orbital can absorb electrons from the orbitals of the metals employing anti-bonding orbitals to establish feedback bonds, whereas the HOMO orbitals are the locations at which electrophiles attack and represent the active centers with the greatest ability to attach to the metal by donating electrons. Organic compounds that

not only take free electrons from the metals but also offer electrons to empty orbitals of the metals make excellent corrosion inhibitors (Obi-Egbedi *et al*., 2012) such as caffeine and nicotine. It has long been known in the literature that the more effective the corrosion inhibitor is at offering electrons to the metal's empty orbitals, the higher its HOMO energy must be. In addition, the energy gap between LUMO and HOMO would be smaller and the inhibitor's ability to inhibit would be more effective the lower the LUMO energy made the acceptance of electrons from metal surfaces easier.

Ionization potential and the molecules' propensity to be attacked by electrophiles have a direct impact on the energy of HOMO (Njoku *et al*., 2021). On the other hand, the energy of LUMO is also influenced by the molecule's ability to withstand nucleophilic attack and its affinity for electrons. Another crucial metric that provides details on the reactive behavior of inhibitor molecules is the energy gap, or ΔE, given by the equation $\Delta E = E_{HOMO}-E_{LUMO}$. Since a smaller energy gap typically results in simpler polarization of the molecules, the qualitative meaning of ΔE is directly related to polarizability. Because less energy is required to remove an electron from the final occupied orbital, low values of ΔE will result in good inhibition efficiencies. ΔN has been reported to correlate remarkably with adsorption energy for metal−inhibitor interactions, with larger ΔN values corresponding to stronger adsorption. Hence, χ and η are related to A and I as expressed above.

(a) Computational results of PS leaves extract's phytoconstituents

Calculated quantum chemical properties were possible with the use of the material studio software. The geometry optimization was without any symmetry constraints. From the PS phytoconstituents selected, HOMO orbital is saturated around the oxygen atoms and the aromatic nucleus in BA, carbon and oxygen atoms in FUR, carbon –carbon atoms bond in EOD, carbon –carbon atoms bond in LAEE, carbon

–carbon atoms bond in SQU, these carbon –carbon atoms bond can accept the electrons from the d – orbital of the metals. While the LUMO density is saturated around oxygen atoms and the aromatic nucleus in BA, carbon and oxygen atoms in FUR, oxygen and carbon atoms in EOD, oxygen and carbon atoms in LAEE, carbon –carbon atoms bond in SQU, this can be seen from Figure 4.19a to Figure 4.23a.

Nucleophile by definition is a chemical specie that forms bonds by donating an electron pair while electrophiles are electron-deficient species that are attracted to an electron-rich center. Clearly, from Figure 4.19a to Figure 4.23a, it is observed that the electrophilic site and nucleophilic site of the phytoconstituents are positioned to promote adsorption resulting from their readiness to interact with Fe (mild steel). Each molecule has a saturated electron density (Mulliken charge centers). Therefore, it should be anticipated that all of the chosen elements will have flat-lying adsorption orientation as demonstrated by the electron density. A typical diagram representative of the molecular dynamics model of biomass adsorption of plant extract is given in Figure 4.19b to Figure 4.23b.

The obtained values from the quantum parameter values in Table 4.19 do not exhibit any clearly defined and cut correlation, which was not unexpected given that the compounds' individual inhibition efficiencies are unknown and that their chemical structures differ significantly from one another. Nevertheless, some characteristics suggest that each molecule's ability to suppress corrosion is present. These characteristics are discussed below.

SQU had the highest HOMO, indicating that it was highly polarizable or would donate electrons more quickly than other materials, while FUR had the lowest LUMO, indicating that it was easier to take an electron from the metal to establish a feedback bond. This was plainly seen in Table 4.19 E_{HOMO} values tended to decline in the following order: SQU > EOD > LAEE > BA > FUR, whereas E_{LUMO} values tended to decline in the following order: SQU > EOD > LAEE > BA > FUR. The

energy gap ΔE values grew in the following order: BA, FUR, EOD, LAEE, and SQU. Hence, the value of the energy gap (ΔE) correlates to inhibitor stability.

The tendency of a molecule to donate electrons to the vacant d orbitals within the Fe atom is reflected by high values of E_{HOMO}. In the same way, low values of the energy gap ($\Delta E = E_{LUMO-HOMO}$) means that the energy required to remove an electron from the last occupied orbital will be minimized, resulting in improved inhibition efficiencies (Njoku *et al*., 2021; Rouifi *et al*., 2019).

The molecules might ensure stability, more readily donate electrons to the metal surface, and so play a significant part in the chemisorptions of the PS extract on the metal surface when taking into account the locations of BA in the ΔE values and SQU in the E_{HOMO} values.

SQU> LAEE > EOD > BA > FUR is the sequence of the selected compounds from GC-MS results of PS, this is the declining trend of molecular size, which reflects the tendency of the molecule to function by a geometric blocking effect. This suggests that while BA and FUR should be much more strongly adsorbed based on the sequence's electronic structure, SQU and LAEE should be more strongly adsorbed based on molecule size considerations.

Computational simulation done with Forcite quench molecular dynamics showed that the molecules maintained a flat lying adsorption orientation on the Fe (1 1 0) surface slab. This could be attributed to the delocalization of the electron density all around the molecules (Figure 4.19a to Figure 4.23a). In order to clearly evaluate each molecules interaction with Fe (1 1 0) surface extensively, the binding energy was estimated and reported in Table 4.19 molecules with negative binding energy values in kJ/mol could be a potential inhibitor capable of interacting favorably with Fe (1 1 0) surface(Njoku *et al*., 2021). From Table 4.19, the trend of E_{bind} for PS extract selected constituent is in the order: SQU < LAEE < EOD < BA < FUR. On clear observation, there is a relationship with the trend of molecular surface coverage

or size discussed earlier and energy gap (ΔE). Also, molecules possessing low energy gap (ΔE) have the potential of stable interaction energies.

Proper observation of the Fe – inhibitor interaction (Figure 4.19b to Figure 4.23b), the polarizable atoms (C, N, O, F) found along the chain of the selected phytoconstituents are noted to have been preferentially accommodated in the characteristic epitaxial groves on the Fe (1 1 0) metal slab surface, hence, avoiding contact with the Fe atoms on the surface (the larger spheres on Fe (1 1 0) slab). The recorded binding energy values could be said to be a function of the molecular arrangements resulting in excellent corrosion inhibiting effect of the plant extract (PS).

4.2.5 Fourier Transform Infrared (FTIR) Spectroscopy Analysis

Figure 4.24a to 4.24i shows the comparative FTIR spectra of ethanol extract of PS, KI sample, sodium alginate sample, and the film extracted from the mild steel specimen surface after immersion in 0.25 M H_2SO_4 solution containing PS, KI, sodium alginate (blend of 500 mg/L PS, 500 mg/L sodium alginate and 0.025 M KI), (blend of 1000 mg/L PS and 0.025 M KI), (blend of 500 mg/L PS and 500 mg/L sodium alginate) separately for 48 h at room temperature. The graphs aforementioned revealed existence of numerous peaks depicting presence of active functional groups which could result in good corrosion inhibition of the extract and the blend. Furthermore, the full details of the phytoconstituents recorded by GC-MS analysis of PS are given in appendix (1). Hence, Table 4.22 is a summary of the presence of active functional groups which is responsible for the excellent corrosion inhibition of the extract and its blend.

Table 4.23 Summary of FTIR Peak Values (cm^{-1}) and Possible Groups

FTIR Peak Values (cm^{-1})			
Plant Extract (Ethanol Extract of PS)	**Mild Steel in 0.25 M H_2SO_4 with Ethanol Extract of PS**	**Mild Steel in 0.25 M H_2SO_4 with Blend of PS, KI and sodium alginate**	**Possible functional groups presence**
3377.0000			Stretching mode of OH from plant extract
2929.7000		2922.2000	Aromatic C-H stretching vibration
		1774.2000	C=O stretch
1692.2000			C-O stretching vibration of amide
1632.6000	1636.3000		C=C stretching band for aromatic ring
1207.7000		1595.3000	-NO_2 Group Amines

Table 4.22 represent some peaks identified and their possible groups (Mohammed *et al*., 2020; Anbarasi & Vasudha, 2014). These summary reveal the possibility of adsorption and interaction of nitrogen, oxygen and other active elements heteroatoms as PS phytoconstituents with the mild steel surface (Mohammed *et al*., 2020), hence, the reason for the good corrosion inhibition of PS and the blend.

4.2.6 Adsorption Isotherm and Thermodynamic Parameters

The mode of adsorption of organic inhibitors on the metal surface in acidic environment at room temperature can be investigated by correlating with experimental data using several adsorption isotherms (Golchinvafa *et al*., 2020; Matad *et al*., 2014). In this study, the mode of adsorption of PS in 0.25 M H_2SO_4 environment was investigated using obtained data and thermodynamic parameters calculated.

Langmuir adsorption isotherm resulting from PS on the surface of mild steel in the solution of 0.25 M H_2SO_4 was investigated at room temperature. Figure 4.25 is a result of the Langmuir adsorption isotherm lines with the presence of 0.1, 0.25, 0.5

and 1.0 g/L PS as an inhibitor. The slope is 1.07 which is an indication that there is no interaction between the adsorbed molecules of the PS (Golchinvafa *et al*., 2020) Furthermore, the surface of the mild steel has a fixed number of adsorption locations and each molecule of PS covers one adsorption opportunity existing on the surface of this steel (Golchinvafa *et al*., 2020). On proper observation of the Langmuir adsorption isotherm curves, it is clearly noticed that the amount of R^2 in the Langmuir adsorption isotherm curves (Figure 4.25) is very close to 1 ($R^2 = 0.9993$). Conclusively from the plot, the adsorbed PS on the surface of the steel in this research study follows the Langmuir adsorption isotherm.

Extensively, thermodynamic parameter of ΔG^o_{ads} as calculated and shown in Table 4.21 was used to determine if the adsorption of PS as an inhibitor on the surface of the investigated mild steel was of physical type or chemical type. Hence, the calculated parameter indicated that ΔG^o_{ads} has a negative value. The negative value indicates that the adsorption process of PS on the surface of the mild steel is spontaneous in nature. The negative value of ΔG^o_{ads} could also suggest a strong and stable interaction of the adsorbent layers on the surface of the steel (Golchinvafa *et al*., 2020; Matad *et al*., 2014).

Value of ΔG^o_{ads} higher than -20 KJ/mol is indicative of the electrostatic interaction between PS molecules and the surface of the steel (which could be said to be physical adsorption type). Also, ΔG^o_{ads} values between -40 KJ/mol and -400 KJ/mol are suggesting chemical adsorption type as well as the formation of coordinating bond. Finally, physical-chemical adsorption of the PS molecules on the surface of the steels are deduced at ΔG^o_{ads} values between -20 KJ/mol and -40 KJ/mol (Golchinvafa *et al*., 2020; Matad *et al*., 2014).

From the calculated ΔG^o_{ads} value shown in Table 4.21, ΔG^o_{ads} has a value between -40 KJ/mol and -400 KJ/mol, hence the adsorption of PS on the surface of the mild steel is in the form of chemical adsorption type as well as the formation of

coordinating bond. As already mentioned, ΔG^{o}_{ads} has a negative value, therefore, spontaneous adsorption of the PS occurred on the surface of the mild steel (Golchinvafa *et al*., 2020; Matad *et al*., 2014).

4.2.7 Synergistic Index (SI)

The SI values of 1000 mg/L: 0.025 M (PS : KI) after 24 h, 48 h, 72 h, 96 h and 120 h of immersion are more than unity as presented in Table 4.22 hence, this indicates good synergistic behavior (Chidiebere *et al*., 2014) of 1000 mg/L:0.025 M (PS: KI). Also, the SI values of 500 mg/L: 500 mg/L (PS: sodium alginate) after 24 h, 48 h, 72 h, 96 h and 120 h of immersion are within unity. Hence SI of 1000 mg/L : 0.025 M (PS : KI) shows a co-operative synergistic effect (Chidiebere *et al*., 2014; Dehghani *et al*., 2020; Ramezanzadeh *et al*., 2018).

CHAPTER FIVE

Conclusion and Recommendations

5.1 Conclusion

The corrosion inhibition behavior of mild steel is improved when extracts of *Pterocarpus santalinoides* (PS), *Piper guineense* (PG), and *Picrilima nitida* (PN) are added to the acidic environment. Hence, the addition of these plant extracts also reduced corrosion rate. these extracts are found to be good corrosion inhibitor of mild steel in H_2SO_4 and HCl solution. It is important to note that the inhibition efficiency of the blend of PS, KI and sodium alginate was pronounced in H_2SO_4 solution as the IE was 96.9 % after 24 h, by 48 h the IE increased to 98.4 %, this value was maintained up to 120 h, hence, the corrosion rate was also greatly reduced. According to the findings of the gravimetric experiment, ethanol extracts of these natural materials are effective corrosion inhibitors for mild steel in acidic media.

The phytoconstituent analysis of the plant extracts performed using GC-MS and UV-vis revealed the presence of several phytochemical components. The plant extracts comprise a combination of distinct compounds with various chromophores that absorb in the UV-vis region, according to UV-visible spectra.

Theoretical quantum chemical calculations (DFT; $DMol^3$ and Forcite module tools) were used to theoretically confirm the corrosion inhibition potentials of some of the organic components from the plant extracts. The results of the theoretical modeling demonstrate that the compounds' ability to limit corrosion was based on their ability to bind to the surfaces of corroding metals and geometric blocking by some molecules due to their flat lying adsorption orientation on the Fe-surface slab, all these information were possible with Material Studio (BIOVIA).

FTIR spectra analysis revealed the possibility of adsorption and interaction of nitrogen, oxygen and other active elements heteroatoms (Table 4.22) as PS phytoconstituents with the mild steel surface (Mohammed *et al*., 2020), the analysis

conclusively proved the reason for the good corrosion inhibition ability of PS and the blend.

The Langmuir adsorption isotherm plot of PS on the surface of mild steel in the solution of 0.25 M H_2SO_4 investigated at room temperature proved the corrosion inhibition ability of PS on the surface of the steel, hence, the Langmuir adsorption isotherm is followed.

Conclusively, SI of 1000 mg/L : 0.025 M (PS : KI) shows a co-operative synergistic effect (Chidiebere *et al*., 2014; Dehghani *et al*., 2020; Ramezanzadeh *et al*., 2018) as the SI values are above unity. Also, the SI values of 500 mg/L: 500 mg/L (PS: sodium alginate) after 24 h, 48 h, 72 h, 96 h and 120 h of immersion are within unity.

Generally, ethanol extract of PS, PG and PN as mild steel corrosion inhibitors in 0.5 M HCl and 0.25 M H_2SO_4 environment are confirmed to be good, furthermore, the blends of ethanol extract of PS, KI and sodium alginate as mild steel corrosion inhibitor in 0.25 M H_2SO_4 environment is confirmed as an excellent inhibitor.

5.2 Recommendations

Further research work is recommended to improve and stabilize the corrosion inhibition potential of *Piper guineense* and *Picrilima nitida.*

Also, attempts should be made to identify and theoretically evaluate the individual phytochemical constituents contained in the extracts which are responsible for the mild steel corrosion inhibition, including the chemisorption's energies of the extract's components (molecules).

5.3 Research Gap

Overtime, corrosion inhibitors applied to mitigate the rate of mild steel corrosion losses stability and efficiency with time especially in acidic environment, hence the need for further studies.

5.4 Contribution to Knowledge

This study discovered eco-friendly inhibitor that possessed high inhibition efficiency, prolonged corrosion inhibition stability with time.

REFERENCE

Abdallah, M. (2002). Rhodanine azosulpha drugs as corrosion inhibitors for corrosion of 304 stainless steel in hydrochloric acid solution. Corrosion science, 44(4), 717-728.

Abdallah, M., Altass, H. M., AL Jahdaly, B. A., & Salem, M. M. (2018). Some natural aqueous extracts of plants as green inhibitor for carbon steel corrosion in 0.5 M sulfuric acid. *Green Chemistry Letters and Reviews*, *11*(3), 189–196. https://doi.org/10.1080/17518253.2018.1458161

Abuthahir, S. S. S., Jamal, A., Nasser, A., & Rajendran, S. (2013). Highly effective inorganic corrosion inhibitor for mild steel in sodium chloride solution. *European Chemical Bulletin*, *2*(12), 1041–1044.

Ahanotu, C. C., Onyeachu, I. B., Solomon, M. M., Chikwe, I. S., Chikwe, O. B., & Eziukwu, C. A. (2020). *Pterocarpus santalinoides* leaves extract as a sustainable and potent inhibitor for low carbon steel in a simulated pickling medium. *Sustainable Chemistry and Pharmacy*, *15*(December 2019), 100196. https://doi.org/10.1016/j.scp.2019.100196

AlBeladi, M. I., Riadi, Y., Geesi, M. H., Ouerghi, O., Anouar, elhassane, Kaiba, A., Alamri, A. H., & Aljohani, T. A. (2022). Benzalkonium chloride/titanium dioxide as an effective corrosion inhibitor for carbon steel in a sulfuric acid solution. *Journal of Saudi Chemical Society*, *26*(3), 101481. https://doi.org/10.1016/J.JSCS.2022.101481

Alibakhshi, E., Ramezanzadeh, M., Bahlakeh, G., Ramezanzadeh, B., Mahdavian, M., & Motamedi, M. (2018). *Glycyrrhiza glabra* leaves extract as a green corrosion inhibitor for mild steel in 1 M hydrochloric acid solution: Experimental, molecular dynamics, Monte Carlo and quantum mechanics study. *Journal of Molecular Liquids*, *255*, 185–198. https://doi.org/10.1016/j.molliq.2018.01.144

Anbarasi, K., & Vasudha, V. G. (2014). Corrosion Inhibition Potential of *Cucurbita Maxima* Plant Extract on Mild Steel in Acid Media. *Chemical Science Review and Letters*, *3*(9), 45–51.

Asadi, N., Ramezanzadeh, M., Bahlakeh, G., & Ramezanzadeh, B. (2019). Utilizing *Lemon Balm* extract as an effective green corrosion inhibitor for mild steel in 1M HCl solution: A detailed experimental, molecular dynamics, Monte Carlo and quantum mechanics study. *Journal of the Taiwan Institute of Chemical Engineers*, *95*, 252–272. https://doi.org/10.1016/j.jtice.2018.07.011

Atmani, F., Lahem, D., Poelman, M., Buess-Herman, C., & Olivier, M. G. (2013). Mild steel corrosion in chloride environment: Effect of surface preparation and influence of inorganic inhibitors. *Corrosion Engineering Science and Technology*, *48*(1), 9–18. https://doi.org/10.1179/1743278212Y.0000000037

Ayoola, A. A., Fayomi, O. S. I., & Ogunkanmbi, S. O. (2018). Data on inhibitive performance of chloraphenicol drug on A315 mild steel in acidic medium. *Data in Brief*, *19*, 804–809. https://doi.org/10.1016/j.dib.2018.05.108

Benabdellah, M., Yahyi, A., Dafali, A., Aouniti, A., Hammouti, B., & Ettouhami, A. (2011). Corrosion inhibition of steel in molar HCl by triphenyltin2-thiophene carboxylate. *Arabian Journal of Chemistry*, *4*(3), 243–247. https://doi.org/10.1016/j.arabjc.2010.06.055

Camila, G. (2016). Corrosion inhibitors: Principles, mechanisms and applications. *Corrosion Inhibitors: Principles, Mechanisms and Applications*, 1–161. https://doi.org/10.5772/57255

Chidiebere, M. A., Oguzie, E. E., Liu, L., Li, Y., & Wang, F. (2014). Corrosion inhibition of Q235 mild steel in 0.5 M H2SO 4 solution by phytic acid and synergistic iodide additives. *Industrial and Engineering Chemistry Research*, *53*(18), 7670–7679. https://doi.org/10.1021/ie404382v

Dang, N., Wei, Y. H., Hou, L. F., Li, Y. G., & Guo, C. L. (2015). Investigation of the inhibition effect of the environmentally friendly inhibitor sodium alginate on magnesium alloy in sodium chloride solution. *Materials and Corrosion*, *66*(11), 1354–1362. https://doi.org/10.1002/maco.201408141

Dehghani, A., Bahlakeh, G., Ramezanzadeh, B., & Ramezanzadeh, M. (2019). Potential of Borage fl ower aqueous extract as an environmentally sustainable corrosion inhibitor for acid corrosion of mild steel : Electrochemical and theoretical studies. *Journal of Molecular Liquids*, *277*, 895–911. https://doi.org/10.1016/j.molliq.2019.01.008

Dehghani, A., Mostafatabar, A. H., Bahlakeh, G., & Ramezanzadeh, B. (2020). A detailed study on the synergistic corrosion inhibition impact of the Quercetin molecules and trivalent europium salt on mild steel; electrochemical/surface studies, DFT modeling, and MC/MD computer simulation. *Journal of Molecular Liquids*, *316*, 113914. https://doi.org/10.1016/j.molliq.2020.113914

Deyab, M. A., Eddahaoui, K., Essehli, R., Rhadfi, T., Benmokhtar, S., & Mele, G. (2016). Experimental evaluation of new inorganic phosphites as corrosion inhibitors for carbon steel in saline water from oil source wells. *Desalination*, *383*, 38–45. https://doi.org/10.1016/j.desal.2016.01.019.

Dillmann, P., Mazaudier, F., & Hœrlé, S. (2004). Advances in understanding atmospheric corrosion of iron. I. Rust characterisation of ancient ferrous artefacts exposed to indoor atmospheric corrosion. Corrosion science, 46(6), 1401-1429.

Ezeugo, J. N. O. & Onukwuli, M. O. (2017). *Optimization of corrosion inhibition of Picralima nitida leaves extract as green corrosion inhibitor for zinc in 1.0 M HCl*. *2*(1), 139–161.

Ezeugo, J. N. O. & Omotioma, M. (2018). Adsorption kinetics of *picralima nitida* seed extract as a green corrosion inhibitor for zinc in 0.5 M H_2SO_4. 2(1)

Farag, A. A., & Hegazy, M. A. (2013). Synergistic inhibition effect of potassium iodide and novel Schiff bases on X65 steel corrosion in 0.5M H2SO4. *Corrosion Science*, *74*, 168–177. https://doi.org/10.1016/j.corsci.2013.04.039

Ferraa, S., Ouakki, M., Barebita, H., Nimour, A., Cherkaoui, M., & Guedira, T. (2021). Corrosion inhibition potentials of some phosphovanadate-based glasses on mild steel in 1 M HCl. *Inorganic Chemistry Communications*, *132*(April). https://doi.org/10.1016/j.inoche.2021.108806

Finšgar, M., & Jackson, J. (2014). Application of corrosion inhibitors for steels in acidic media for the oil and gas industry: A review. *Corrosion Science*, *86*, 17–41. https://doi.org/10.1016/j.corsci.2014.04.044

Finšgar, M., & Merl, D. K. (2014). 2-Mercaptobenzoxazole as a copper corrosion inhibitor in chloride solution: Electrochemistry, 3D-profilometry, and XPS surface analysis. *Corrosion Science*, *80*, 82–95. https://doi.org/10.1016/j.corsci.2013.11.022

Fouda, A. S., Attia, A. M., & Rashed, A. M. (2017). Corrosion inhibition of mild steel in aqueous solutions using nonionic surfactants. *Protection of Metals and Physical Chemistry of Surfaces*, *53*(4), 743–752. https://doi.org/10.1134/S2070205117040062

Frenier, W. W., Growcock, F. B., & Lopp, V. R. (1988). alpha -alkenylphenones-a new class of acid corrosion inhibitors. *Corrosion*, *44*(9), 590–598. https://doi.org/10.5006/1.3584970

Galvão, T. L. P., Kuznetsova, A., Gomes, J. R. B., Zheludkevich, M. L., Tedim, J., & Ferreira, M. G. S. (2016). A computational UV–Vis spectroscopic study of the chemical speciation of 2-mercaptobenzothiazole corrosion inhibitor in aqueous solution. *Theoretical Chemistry Accounts*, *135*(3). https://doi.org/10.1007/s00214-016-1839-3

Gao, B., Zhang, X., & Sheng, Y. (2008). Studies on preparing and corrosion inhibition behaviour of quaternized polyethyleneimine for low carbon steel in sulfuric acid. *Materials Chemistry and Physics*, *108*(2–3), 375–381. https://doi.org/10.1016/j.matchemphys.2007.10.033

Golchinvafa, A., Anijdan, S. H. M., Sabzi, M., & Sadeghi, M. (2020). The effect of natural inhibitor concentration of Fumaria officinalis and temperature on corrosion protection mechanism in API X80 pipeline steel in 1 M H2SO4 solution. *International Journal of Pressure Vessels and Piping*, 104241. https://doi.org/10.1016/j.ijpvp.2020.104241

Haldhar, R., Prasad, D., & Bhardwaj, N. (2019). Extraction and experimental studies of Citrus aurantifolia as an economical and green corrosion inhibitor for mild steel in acidic media. *Journal of Adhesion Science and Technology*, *33*(11), 1169–1183. https://doi.org/10.1080/01694243.2019.1585030

Haldhar, R., Prasad, D., Saxena, A., & Kumar, R. (2018). Experimental and theoretical studies of Ficus religiosa as green corrosion inhibitor for mild steel in 0.5 M H2SO4 solution. *Sustainable Chemistry and Pharmacy*, *9*(July), 95–105. https://doi.org/10.1016/j.scp.2018.07.002

Hassannejad, H., & Nouri, A. (2018). Sunflower seed hull extract as a novel green corrosion inhibitor for mild steel in HCl solution. *Journal of Molecular Liquids*, *254*, 377–382. https://doi.org/10.1016/j.molliq.2018.01.142

Hemlata, V., Sudershan, K., Indra, B., & Gurmeet, S. (2013). *Evaluation of (2-Hydroxyethyl) Triphenyl Phosphonium Bromide as Corrosion Inhibitor for Mild Steel in Sulphuric Acid | Request PDF | ResearchGate*. https://www.researchgate.net/publication/286169534_Evaluation_of_2-Hydroxyethyl_Triphenyl_Phosphonium_Bromide_as_Corrosion_Inhibitor_for_Mild_Steel_in_Sulphuric_Acid

Ituen, E., Mkpenie, V., & Ekemini, E. (2019). Corrosion inhibition of X80 steel in simulated acid wash solution using glutathione and its blends: Experimental and theoretical studies. *Colloids and Surfaces A: Physicochemical and Engineering Aspects*, *578*(June), 123597. https://doi.org/10.1016/j.colsurfa.2019.123597

Jeyaprabha, C., Sathiyanarayanan, S., Phani, K. L. N., & Venkatachari, G. (2005). Influence of poly(aminoquinone) on corrosion inhibition of iron in acid media. *Applied Surface Science*, *252*(4), 966–975. https://doi.org/10.1016/j.apsusc.2005.01.098

Kamali Ardakani, E., Kowsari, E., & Ehsani, A. (2020). Imidazolium-derived polymeric ionic liquid as a green inhibitor for corrosion inhibition of mild steel

in 1.0 M HCl: Experimental and computational study. *Colloids and Surfaces A: Physicochemical and Engineering Aspects*, *586*, 124195. https://doi.org/10.1016/j.colsurfa.2019.124195

Kapor, F. (2002). *Corrosion inhibition of carbon steel in the near neutral media by blends of tannin and calcium gluconate*. *268*, 264–268.

Karpagasundari, C., & Kulothungan, S. (2014). *Analysis of bioactive compounds in Physalis minima leaves using GC MS , HPLC , UV-VIS and FTIR techniques*. *3*(May), 196–201.

Kausalya, T., & Hazlina, H. (2020). *VGVG applied sciences Review on Corrosion Inhibitors for Oil and Gas Corrosion Issues*.

Keerthana, A. K., & Ashraf, P. M. (2020). Carbon nanodots synthesized from chitosan and its application as a corrosion inhibitor in boat-building carbon steel BIS2062. *Applied Nanoscience (Switzerland)*, *10*(4), 1061–1071. https://doi.org/10.1007/s13204-019-01177-0

Khadom, A. A., & Farhan, S. N. (2018). Corrosion inhibition of steel in phosphoric acid. *Corrosion Reviews*, *36*(3), 267–280. https://doi.org/10.1515/corrrev-2017-0104

Khan, M. A. A., Irfan, O. M., Djavanroodi, F., & Asad, M. (2022). Development of Sustainable Inhibitors for Corrosion Control. Sustainability, 14(15), 9502.

Kobzar, Y. L., & Fatyeyeva, K. (2021). Ionic liquids as green and sustainable steel corrosion inhibitors: Recent developments. Chemical Engineering Journal, 425, 131480.

Kokalj, A., Kovačević, N., Peljhan, S., Finšgar, M., Lesar, A., & Milošev, I. (2011). Triazole, benzotriazole, and naphthotriazole as copper corrosion inhibitors: I. Molecular electronic and adsorption properties. *ChemPhysChem*, *12*(18), 3547–3555. https://doi.org/10.1002/cphc.201100537

Li, Y., Zhi Xin Ba, Yong Liang Li, Yan Ge, X. C. Z. (2017). Influence of sodium alginate inhibitor addition on the corrosion protection performance of AZ91D magnesium alloy in NaCl solution. *Anti-Corrosion Methods and Materials*.

Lin, B., Tang, J., Wang, Y., Wang, H., & Zuo, Y. (2020). Study on Synergistic Corrosion Inhibition Effect between Calcium Lignosulfonate (CLS) and Inorganic Inhibitors on Q235 Carbon Steel in Alkaline Environment with Cl−. *Molecules*, *25*(18). https://doi.org/10.3390/molecules25184200

Matad, P. B., Mokshanatha, P. B., Hebbar, N., Venkatesha, V. T., & Tandon, H. C.

(2014). Ketosulfone drug as a green corrosion inhibitor for mild steel in acidic medium. *Industrial and Engineering Chemistry Research*, *53*(20), 8436–8444. https://doi.org/10.1021/ie500232g

Mohamad, A. B., Kadhum, A. A. H., Al-Amiery, A. A., Ying, L. C., & Musa, A. Y. (2014). Synergistic of a coumarin derivative with potassium iodide on the corrosion inhibition of aluminum alloy in 1.0 M H2SO4. *Metals and Materials International*, *20*(3), 459–467. https://doi.org/10.1007/s12540-014-3008-3

Mohammed, A. R. I., Solomon, M. M., Haruna, K., Umoren, S. A., & Saleh, T. A. (2020). Evaluation of the corrosion inhibition efficacy of Cola acuminata extract for low carbon steel in simulated acid pickling environment. *Environmental Science and Pollution Research*, *27*(27), 34270–34288. https://doi.org/10.1007/s11356-020-09636-w

Moussa, O. (2018). *Inorganic Compound (Apatite doped by Mg and Na) as a Corrosion Inhibitor for Mild Steel in Phosphoric Acidic Medium*. *10*(7), 943–960.

Musa, A. Y., Mohamad, A. B., Kadhum, A. A. H., Takriff, M. S., & Tien, L. T. (2011). Synergistic effect of potassium iodide with phthalazone on the corrosion inhibition of mild steel in 1.0M HCl. *Corrosion Science*, *53*(11), 3672–3677. https://doi.org/10.1016/j.corsci.2011.07.010

Njoku, D. I., Njoku, C. N., Lgaz, H., Okafor, P. C., Oguzie, E. E., & Li, Y. (2021). Corrosion protection of Q235 steel in acidic-chloride media using seed extracts of Piper guineense. *Journal of Molecular Liquids*, *330*, 115619. https://doi.org/10.1016/j.molliq.2021.115619

Nwosu, O. F., A, N. L., & S, A. C. (2014). Acidic Corrosion Inhibition of Piper guineense Seed Extract on Al Alloy. *American Journal of Materials Science*, *2014*(4), 178–183. https://doi.org/10.5923/j.materials.20140404.04

Obi-Egbedi, N. O., Obot, I. B., & Umoren, S. A. (2012). Spondias mombin L. as a green corrosion inhibitor for aluminium in sulphuric acid: Correlation between inhibitive effect and electronic properties of extracts major constituents using density functional theory. *Arabian Journal of Chemistry*, *5*(3), 361–373. https://doi.org/10.1016/j.arabjc.2010.09.002

Obot, I. B., Onyeachu, I. B., & Kumar, A. M. (2017). Sodium alginate: A promising biopolymer for corrosion protection of API X60 high strength carbon steel in saline medium. *Carbohydrate Polymers*, *178*, 200–208. https://doi.org/10.1016/j.carbpol.2017.09.049

Ofoma, E.O.; EKEMEZIE, P. N. (2018). *Mild Steel Deterioration Inhibition in 1 . 0M and 5 . 0M Tetraoxosulphate (VI) Acid using Leaf Extract of Pterocarpus santaliniodes DOI : https://dx.doi.org/10.4314/jasem.v22i8.32*.

Oguzie, E. E., Ogukwe, C. E., Ogbulie, J. N., Nwanebu, F. C., Adindu, C. B., Udeze, I. O., Oguzie, K. L., & Eze, F. C. (2011). Broad spectrum corrosion inhibition: Corrosion and microbial (SRB) growth inhibiting effects of Piper guineense extract. *Journal of Materials Science*, *47*(8), 3592–3601. https://doi.org/10.1007/s10853-011-6205-1

Oguzie, Emeka E., Adindu, C. B., Enenebeaku, C. K., Ogukwe, C. E., Chidiebere, M. A., & Oguzie, K. L. (2012). Natural products for materials protection: Mechanism of corrosion inhibition of mild steel by acid extracts of piper guineense. *Journal of Physical Chemistry C*, *116*(25), 13603–13615. https://doi.org/10.1021/jp300791s

Onukwuli, O. D., & Ezeugo, J. O. (2018). *Plant extract as biodegradable inhibitor for zinc in dilute solution of sulphuric acid*. *109*(August), 195–210.

Popoola, L. T. (2019). *Organic green corrosion inhibitors (OGCIs): a critical review*.

Qian, S., & Cheng, Y. F. (2019). Synergism of imidazoline and sodium dodecylbenzenesulphonate inhibitors on corrosion inhibition of X52 carbon steel in CO2-saturated chloride solutions. *Journal of Molecular Liquids*, *294*, 111674. https://doi.org/10.1016/j.molliq.2019.111674

Raja, P. B., Ismail, M., Ghoreishiamiri, S., Mirza, J., Ismail, M. C., Kakooei, S., & Rahim, A. A. (2016). Reviews on Corrosion Inhibitors: A Short View. *Chemical Engineering Communications*, *203*(9), 1145–1156. https://doi.org/10.1080/00986445.2016.1172485

Ramezanzadeh, M., Sanaei, Z., Bahlakeh, G., & Ramezanzadeh, B. (2018). Highly effective inhibition of mild steel corrosion in 3.5% NaCl solution by green Nettle leaves extract and synergistic effect of eco-friendly cerium nitrate additive: Experimental, MD simulation and QM investigations. In *Journal of Molecular Liquids* (Vol. 256, Issue 2017). Elsevier B.V. https://doi.org/10.1016/j.molliq.2018.02.021

Rosli, N. R., Yusuf, S. M., Sauki, A., & Razali, W. M. R. W. (2019). Musa sapientum (Banana) peels as green corrosion inhibitor for mild steel. *Key Engineering Materials*, *797*, 230–239. https://doi.org/10.4028/www.scientific.net/KEM.797.230

Rouifi, Z., Benhiba, F., Faydy, M. El, Laabaissi, T., About, H., Oudda, H., Warad, I., Guenbour, A., Lakhrissi, B., & Zarrouk, A. (2019). Performance and computational studies of new soluble triazole as corrosion inhibitor for carbon steel in HCl. *Chemical Data Collections*, *22*, 100242. https://doi.org/10.1016/j.cdc.2019.100242

Saei, E., Ramezanzadeh, B., Amini, R., & Kalajahi, M. S. (2017). Effects of combined organic and inorganic corrosion inhibitors on the nanostructure cerium based conversion coating performance on AZ31 magnesium alloy: Morphological and corrosion studies. *Corrosion Science*, *127*(August), 186–200. https://doi.org/10.1016/j.corsci.2017.08.017

Saxena, A., Prasad, D., Haldhar, R., Singh, G., & Kumar, A. (2018a). Use of Saraca ashoka extract as green corrosion inhibitor for mild steel in 0.5 M H2SO4. *Journal of Molecular Liquids*, *258*(2017), 89–97. https://doi.org/10.1016/j.molliq.2018.02.104

Saxena, A., Prasad, D., Haldhar, R., Singh, G., & Kumar, A. (2018b). Use of Sida cordifolia extract as green corrosion inhibitor for mild steel in 0.5 M H2SO4. *Journal of Environmental Chemical Engineering*, *6*(1), 694–700. https://doi.org/10.1016/j.jece.2017.12.064

Sitz, C., Frenier, W., & Vallejo, C. (2012). Acid corrosion inhibitors with improved environmental profiles. *Society of Petroleum Engineers - SPE International Conference and Exhibition on Oilfield Corrosion 2012*, *May*, 296–307. https://doi.org/10.2118/155966-ms

Srivastava, V., Haque, J., Verma, C., Singh, P., Lgaz, H., Salghi, R., & Quraishi, M. A. (2017). Amino acid based imidazolium zwitterions as novel and green corrosion inhibitors for mild steel: Experimental, DFT and MD studies. *Journal of Molecular Liquids*, *244*, 340–352. https://doi.org/10.1016/j.molliq.2017.08.049

Umoren, S. A., Eduok, U. M., & Solomon, M. M. (2014). Effect of polyvinylpyrrolidone-polyethylene glycol blends on the corrosion inhibition of aluminium in HCl solution. *Pigment and Resin Technology*, *43*(5), 299–313. https://doi.org/10.1108/PRT-09-2013-0079

Vasyliev, G., & Vorobiova, V. (2019). Rape grist extract (Brassica napus) as a green corrosion inhibitor for water systems. *Materials Today: Proceedings*, *6*, 178–186. https://doi.org/10.1016/j.matpr.2018.10.092

Verma, C., Ebenso, E. E., Bahadur, I., & Quraishi, M. A. (2018). An overview on plant extracts as environmental sustainable and green corrosion inhibitors for

metals and alloys in aggressive corrosive media. *Journal of Molecular Liquids*, #pagerange#. https://doi.org/10.1016/j.molliq.2018.06.110

Wang, D., Li, Y., Chen, B., & Zhang, L. (2020). Novel surfactants as green corrosion inhibitors for mild steel in 15% HCl: Experimental and theoretical studies. *Chemical Engineering Journal*, *402*(June), 126219. https://doi.org/10.1016/j.cej.2020.126219

Wei, H., Heidarshenas, B., Zhou, L., Hussain, G., Li, Q., & Ostrikov, K. (Ken). (2020). Green inhibitors for steel corrosion in acidic environment: state of art. *Materials Today Sustainability*, *10*, 100044. https://doi.org/10.1016/j.mtsust.2020.100044

Yadav, M., Behera, D., & Sharma, U. (2016). Nontoxic corrosion inhibitors for N80 steel in hydrochloric acid. *Arabian Journal of Chemistry*, *9*, S1487–S1495. https://doi.org/10.1016/j.arabjc.2012.03.011

Zhang, W., Nie, B., Li, H. J., Li, Q., Li, C., & Wu, Y. C. (2021). Inhibition of mild steel corrosion in 1 M HCl by chondroitin sulfate and its synergistic effect with sodium alginate. *Carbohydrate Polymers*, *260*(February). https://doi.org/10.1016/j.carbpol.2021.117842

Zhao, J., Duan, H., & Jiang, R. (2015). Synergistic corrosion inhibition effect of quinoline quaternary ammonium salt and Gemini surfactant in H2S and CO2 saturated brine solution. *Corrosion Science*, *91*, 108–119. https://doi.org/10.1016/j.corsci.2014.11.007

Znini, M., Majidi, L., Bouyanzer, A., Paolini, J., Desjobert, J. M., Costa, J., & Hammouti, B. (2012). Essential oil of Salvia aucheri mesatlantica as a green inhibitor for the corrosion of steel in 0.5M H 2SO 4. *Arabian Journal of Chemistry*, *5*(4), 467–474. https://doi.org/10.1016/j.arabjc.2010.09.017

Serdaroglu G., Kaya, S. (2021). Organic and Inorganic Corrosion Inhibitors. https://doi.org/10.1002/9781119794516.ch4

APPENDIX

Appendix I. The structures and details of the phytoconstituents identified in *Pterocarpus santalinoides* (PS) leaf extract from GC/MS.

S/N	Name	Formula	Structure	Retention Time	% Composition	MW (g/mol)
1	1H-3a,7-Methanoazulene, octahydro-1,4,9,9-tetramethyl-	$C_{15}H_{26}$		1.8620	1.9300	206.3700
2	Benzeneseleninic anhydride	$C_{12}H_{10}O_3Se_2$	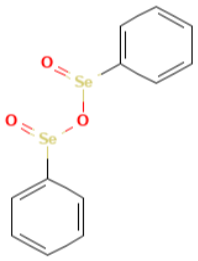	1.9070	6.1900	360.1000
3	Methylene chloride	CH_2Cl_2	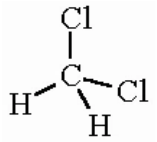	1.9420	36.5400	84.9300
4	2(5H)-Furanone	$C_4H_4O_2$	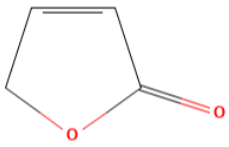	3.2450	1.7300	84.0700
5	Benzeneacetaldehyde	C_8H_8O	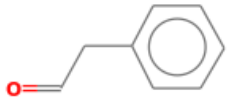	3.8450	0.6800	120.1500
6	3-Heptafluorobutyroxytridecane	$C_{17}H_{27}F_7O_2$	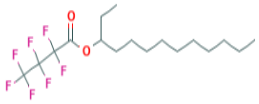	4.6050	0.9700	396.4000

7	Cyclohexane, 1,2,3-trimethyl-, (1.alpha.,2.alpha.,3.beta.)-	C_9H_{18}	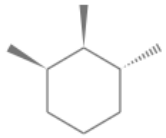	5.1880	0.4500	126.2400
8	2-Heptene, (E)-	C_7H_{14}		5.3990	1.8000	98.1900
9	cis-9,10-Epoxyoctadecan-1-ol	$C_{18}H_{36}O_2$	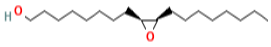	5.7480	0.8300	284.5000
10	5-Tetradecene, (E)-	$C_{14}H_{28}$	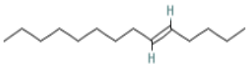	5.9140	1.1400	196.3700
11	Cyclohexane, 1,1,2-trimethyl-3,5-bis(1-methylethenyl)-, (2.alpha.,3.alpha.,5.beta.)-	$C_{15}H_{26}$	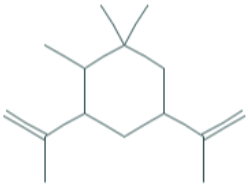	6.1020	0.4700	206.3700
12	3-Tetradecen-5-yne, (Z)-	$C_{14}H_{24}$	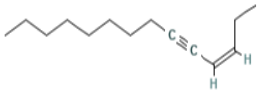	6.3540	0.4000	192.3400
13	Cyclopentanol, 1-(1-methylene-2-propenyl)-	$C_9H_{14}O$	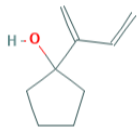	6.4280	0.3500	138.2100
14	Longifolene	$C_{15}H_{24}$	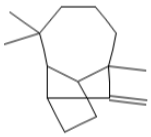	6.6970	0.3600	204.3600
15	.Beta.-Bisabolene	$C_{15}H_{24}$	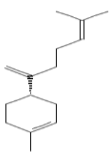	6.8280	1.1400	204.3500

16	(1R,5R)-4-Methylene-1-((R)-6-methylhept-5-en-2-yl)bicyclo[3.1.0]hexane, (relative configuration)	$C_{15}H_{24}$	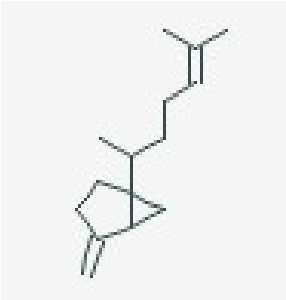	6.9480	0.8900	204.3500
17	5-Eicosene, (E)-	$C_{20}H_{40}$		7.2000	1.2200	280.5000
18	Cyclopropaneoctanal, 2-octyl-	$C_{19}H_{36}O$	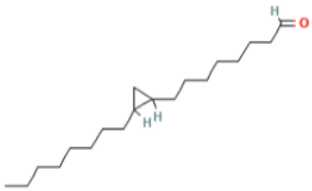	8.1430	0.4200	280.5000
19	1-Octadecene	$C_{18}H_{36}$		8.5770	0.6500	252.5000
20	Neophytadiene	$C_{20}H_{38}$	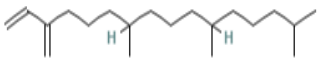	8.9490 & 9.1370	4.6600 + 0.8600 = 5.5200	278.5000
21	Bicyclo[3.1.1]heptane, 2,6,6-trimethyl-	$C_{10}H_{18}$	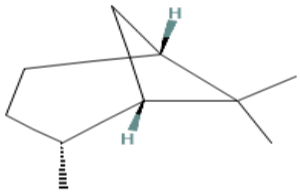	9.2740	2.4800	138.2500
22	Tricosyl trifluoroacetate	$C_{25}H_{47}F_3O_2$	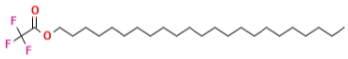	10.0460	0.9300	436.6000
23	Hexadecanoic acid, ethyl ester	$C_{18}H_{36}O_2$		10.1370	8.9900	284.4800

24	Phytol	$C_{20}H_{40}O$	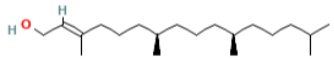	11.1660	1.4800	296.5000
25	Linoleic acid ethyl ester	$C_{20}H_{36}O_2$	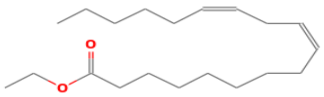	11.4980	8.1900	308.5000
26	Ethyl 9,12,15-octadecatrienoate	$C_{20}H_{34}O_2$	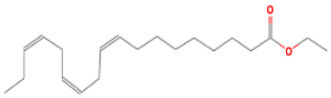	11.5780	4.7200	306.4800
27	Octadecanoic acid, ethyl ester	$C_{20}H_{40}O_2$		11.6520	4.2300	312.5300
28	(Z)-Tetradec-11-en-1-yl 2,2,3,3,3-pentafluoropropanoate	$C_{17}H_{27}F_5O_2$	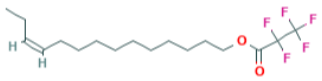	12.7490	0.4400	358.4000
29	Squalene	$C_{30}H_{50}$	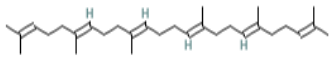	16.2300	4.8600	410.7300
					Total: 100 %	